NASA TECHNICAL NOTE

NASA TN D-6536

NASA TN D-6536

CALCULATED PRESSURE DISTRIBUTIONS AND COMPONENTS OF TOTAL-DRAG COEFFICIENTS FOR 18 CONSTANT-VOLUME, SLENDER BODIES OF REVOLUTION AT ZERO INCIDENCE FOR MACH NUMBERS FROM 2.0 TO 12.0, WITH EXPERIMENTAL AERODYNAMIC CHARACTERISTICS FOR THREE OF THE BODIES

by Louis S. Stivers, Jr.

Ames Research Center
Moffett Field, Calif. 94035

NATIONAL AERONAUTICS AND SPACE ADMINISTRATION • WASHINGTON, D. C. • OCTOBER 1971

1. Report No.	2. Government Accession No.	3. Recipient's
NASA TN D-6536		

4. Title and Subtitle
CALCULATED PRESSURE DISTRIBUTIONS AND COMPONENTS OF TOTAL-DRAG COEFFICIENTS FOR 18 CONSTANT-VOLUME, SLENDER BODIES OF REVOLUTION AT ZERO INCIDENCE FOR MACH NUMBERS FROM 2.0 TO 12.0, WITH EXPERIMENTAL AERODYNAMIC CHARACTERISTICS FOR THREE OF THE BODIES

5. Report Date: October 1971

6. Performing Organization Code:

7. Author(s)
Louis S. Stivers, Jr.

8. Performing Organization Report No.: A-4005

9. Performing Organization Name and Address
Ames Research Center
Moffett Field, Calif., 94035

10. Work Unit No.: 760-75-01-00-21

11. Contract or Grant No.:

12. Sponsoring Agency Name and Address
National Aeronautics and Space Administration
Washington, D. C., 20546

13. Type of Report and Period Covered: Technical Note

14. Sponsoring Agency Code:

15. Supplementary Notes

16. Abstract

The pressure distributions and drag coefficients of 18 constant length and volume, slender bodies of revolution at zero incidence have been calculated for Mach numbers 2.0 to 12.0. Four bodies were selected from each of four families of profiles: the Sears-Haack, the parabolic arc, the Von Kármán, and one of Miele's. A 3/4-power body and a cone body were included to complete the group. Experimental aerodynamic characteristics for two Sears-Haack bodies and the 3/4-power body were obtained from tests in the Ames 3.5-Foot Hypersonic Wind Tunnel at Mach numbers of 5.4, 7.4, and 10.5.

The calculations showed that the Sears-Haack bodies generally provided the least drag throughout the range of Mach numbers from 2.0 to 12.0. The experimental aerodynamic characteristics of the three bodies showed that the overall lift and drag characteristics did not differ markedly, but that the minimum-drag coefficients were the least for the Sears-Haack bodies. The centers of pressure for the three bodies were roughly approximated by the centers of projected plan area of the bodies.

17. Key Words (Suggested by Author(s))	18. Distribution Statement
Bodies of revolution Pressure distribution Supersonic Hypersonic Minimum drag	Unclassified – Unlimited

19. Security Classif. (of this report)	20. Security Classif. (of this page)	21. No. of Pages	22. Price*
Unclassified	Unclassified	100	$3.00

*For sale by the National Technical Information Service, Springfield, Virginia 22151

NOTATION

A_B base area of body

A_0 maximum cross-sectional area of body

C_D total-drag coefficient, $\frac{\text{total drag}}{q_\infty S}$

C_D' total-drag coefficient adjusted for free-stream static pressure at the base of the body, $\frac{\text{adjusted total drag}}{q_\infty S}$

C_{D_B} base-drag coefficient, $\frac{\text{base drag}}{q_\infty S}$

C_{D_F} skin-friction-drag coefficient, $\frac{\text{skin friction drag}}{q_\infty S}$

C_{D_W} wave-drag coefficient, $\frac{\text{wave drag}}{q_\infty S}$

C_L lift coefficient, $\frac{\text{lift}}{q_\infty S}$

C_m pitching-moment coefficient about a point on the body axis two-thirds of the body length downstream of the body nose and based on the body length, $\frac{\text{pitching moment}}{q_\infty S l}$

C_p pressure coefficient, $\frac{p - p_\infty}{q_\infty}$

d_0 maximum body diameter, $2r_0$

k body cutoff, $1 - \frac{l}{l_0}$, amount of afterbody portion of the fully closed body cut off to provide a body with a base; 0 for a fully closed body and 0.5 for a body with maximum diameter at the base

$\frac{L}{D'}$ lift-drag ratio, $\frac{C_L}{C_D'}$

l actual body length

l_0 length of fully closed body, virtual length

[l,d] body derived for a given length and diameter

[l,V] body derived for a given length and volume

M	Mach number
p	local static pressure
p_∞	free-stream static pressure
q_∞	free-stream dynamic pressure
R	Reynolds number based on body length, l
r	local body radius
r_0	maximum body radius
S	reference area for coefficients, $0.077\,l^2$ or $4.0\,V^{2/3}$
S_W	wetted surface area of body
$[S_W,d]$	body derived for a given wetted surface area and diameter
$[S_W,V]$	body derived for a given wetted surface area and volume
V	body volume, $0.002655l^3$
x	longitudinal distance along body axis
α	angle of attack, deg
η	dimensionless radial coordinate of body, $\frac{r}{r_0}$
ξ	dimensionless longitudinal coordinate of body, $\frac{x}{l_0}$

CALCULATED PRESSURE DISTRIBUTIONS AND COMPONENTS OF TOTAL–DRAG COEFFICIENTS FOR 18 CONSTANT-VOLUME, SLENDER BODIES OF REVOLUTION AT ZERO INCIDENCE FOR MACH NUMBERS FROM 2.0 TO 12.0, WITH EXPERIMENTAL AERODYNAMIC CHARACTERISTICS FOR THREE OF THE BODIES

Louis S. Stivers, Jr.

Ames Research Center

SUMMARY

The pressure distributions and drag coefficients of four families of slender, constant length and volume bodies of revolution at zero incidence have been calculated for Mach numbers 2.0 to 12.0. These drag coefficients are the sum of wave-drag, base-drag, and skin-friction-drag components of the families of Sears-Haack, parabolic arc, Von Kármán, and one of Miele's. Four bodies in each family were formed by cutting off various portions of the afterbodies of the closed contours. Corresponding calculations were also made for a 3/4-power body and a cone to make a total of 18 bodies in the study. Experimental aerodynamic characteristics of three of the bodies were obtained from tests in the Ames 3.5-Foot Hypersonic Wind Tunnel at Mach numbers of 5.4, 7.4, and 10.5.

The calculations showed that the Sears-Haack bodies provided the least drag throughout the range of Mach numbers from 2.0 to 12.0 for most values of body cutoff. The value of body cutoff associated with the lowest drag coefficients varied from about 0.05 for a Mach number of 2.0 to about 0.35 for a Mach number of 12.0. As the Mach number approached 12.0, the wave-drag component became the largest contributor to the total-drag coefficients for the smaller values of body cutoff, and the skin-friction component, the largest contributor for the larger values of body cutoff.

From the wind-tunnel tests of two Sears-Haack bodies and the 3/4-power body it was determined that the overall lift and drag characteristics for the bodies did not differ markedly, but that the minimum-drag coefficients were the least for the Sears-Haack bodies. The centers of pressure for each body were roughly approximated by the centers of projected plan area of the bodies.

A comparison of the calculated and experimental minimum-drag coefficients for the three bodies showed that the values for the Sears-Haack bodies were more nearly in agreement than those for the 3/4-power body.

INTRODUCTION

The technical feasibility of hypersonic-cruise aircraft has been demonstrated by initial studies, such as that reported in reference 1. Although many more recent and extensive investigations

further substantiate the feasibility of such aircraft, many additional very detailed studies must be made to provide designers with sufficiently reliable information to appraise specific geometrical proposals.

Very large volume bodies will be required for hypersonic-cruise aircraft, mainly to accommodate the necessary liquid-hydrogen fuel. Since such large bodies can be expected to be unattractive from the standpoint of drag, a body profile that provides minimum drag will be of particular interest to the designer. It is only logical that consideration should be given to the theoretical minimum wave-drag body profiles, which have been derived for use from low-supersonic to hypersonic Mach numbers (refs. 2 to 7). The use of such bodies, however, introduces questions concerning their merit when employed outside the range of Mach numbers or with different geometrical restraints than those for which the bodies were derived to apply or to be optimum.

Calculated pressure distributions and components of the total-drag coefficients of four families of slender bodies at zero incidence for Mach numbers from 2.0 to 12.0 are presented in this report. The bodies in each family were formed by cutting off various portions of the afterbodies of the closed contours. Pressure distributions and corresponding drag components of a 3/4-power body and a cone are also presented. Eighteen bodies were included in this study. The length and volume of each were held constant.

The purpose of this report is to compare the total drag characteristics of the various body shapes and to determine the effects of the various amounts of afterbody cutoff for Mach numbers from 2.0 to 12.0. In addition, to provide experimental data for some of the bodies, three were tested in the Ames 3.5–Foot Hypersonic Wind Tunnel and the data are presented here. A brief summary of the calculated total-drag data has already been reported (ref. 8).

ANALYSIS

Four families of slender optimum bodies were selected for this analysis. The volume and length of each of the bodies were held constant such that $V = 0.002655l^3$, which is the relationship between the volume and length of a fully closed Sears-Haack body of fineness ratio 13.2. Reference 1 has shown that fineness ratios of about this magnitude are the most favorable for hypersonic transport aircraft. Although the volume and length of each body is fixed, the fineness ratios of the four families of bodies range from about 12.5 to 14.0.

Body Families

Each family is composed of four bodies with various base areas formed by cutting off given amounts of the afterbody of a fully closed body. This is illustrated in figure 1. The fully closed body at the top of the figure has no cutoff and is designated $k = 0$. To form the other bodies, the same closed profile was adjusted in diameter and stretched to such an extent that when 0.1, 0.3, and 0.5 of the virtual lengths were cut off, each remaining body had the same length and volume as the original closed body with no cutoff, but each had different amounts of base area. The location of the maximum cross-sectional area for each body is given by

$$\left(\frac{x}{l}\right)_{\text{max section}} = \left(\frac{1}{2}\right)\left(\frac{1}{1-k}\right)$$

The four distinct optimum profiles selected to make up the different families under this arrangement of body cutoffs are:

1. The Sears-Haack profile [l,V] ; optimized for a given length and volume by slender-body theory (refs. 3 and 4), and defined by

$$\eta = [1 - (1 - 2\xi)^2]^{3/4}$$

2. A parabolic-arc profile; for slender bodies closely approximates the circular arc profile that has been shown by experiment to provide low drag at supersonic Mach numbers. The parabolic arc profile is defined by

$$\eta = 4\xi(1 - \xi)$$

3. A Miele profile [S_w,V] ; optimized for a given wetted surface area and volume by Newtonian theory with the slender body approximation to the pressure coefficient (ref. 6), and defined by

$$\eta = 1 - (1 - 2\xi)^{3/2}$$

This equation defines a forebody only, $0 \leqslant \xi \leqslant 0.5$.

4. The Von Karman profile [l,d] ; optimized for a given length and diameter by slender-body theory (ref. 2), and defined by

$$\eta = \pi^{-1/2}\left[\cos^{-1}(1 - 4\xi) - 2(1 - 4\xi)\sqrt{2\xi(1 - 2\xi)}\right]^{1/2}$$

or

$$\eta = \pi^{-1/2}\sqrt{\theta - (1/2)\sin 2\theta}$$

where

$$\xi = (1/4)(1 - \cos\theta)$$

These equations also define a forebody only, $0 \leqslant \xi \leqslant 0.5$. Since afterbodies of the last two profiles are undefined by the equations (i.e., for $0.5 < \xi \leqslant 1.0$), and zero profile slope is specified at $\xi = 0.5$, each profile was placed back-to-back to form a closed basic body. The Eggers-Resnikoff-Dennis body [l,V] derived by Newtonian theory (ref. 5) and the Miele body [l,V] derived by Newtonian theory with the slender-body approximation to the pressure coefficient (ref. 6) have essentially the same profiles as the Von Kármán body [l,d] derived by slender-body theory. Accordingly, aerodynamic characteristics for the latter body can be considered to be, for all practical purposes, those for either of the former bodies.

The contours for the $k = 0.5$ bodies of each family are shown in figure 2 in which the dimensionless radius is plotted to an expanded scale versus the dimensionless longitudinal distance. The Sears-Haack contour is the fullest over the forward portion of the body, and has the smallest radius at the base. A straight-line contour is also shown in this figure for a cone having the same

length and volume as the k = 0.5 bodies. This cone has a smaller radius over the forward portion and a greater radius at the base than any of the other bodies. The contours for the other bodies are generally distributed between the limits of the Sears-Haack and the cone profiles, and it is for this reason that these particular profiles were selected for the present study. A 3/4-power body [l,d], $\eta = \xi^{3/4}$, and a cone [S_W,d], $\eta = \xi$ (see ref. 6), both of which were restricted to the same length and volume as the other bodies, were selected for comparison with the k = 0.5 bodies of each family. Useful geometrical data for each body are given in table 1. Coordinates for the bodies are given in tables 2 to 19.

Drag Component Calculations

The calculated drag coefficients for all the bodies are based on an assumed wing area representative of that of several proposed hypersonic transport aircraft and equivalent to 0.077 l^2 or 4.0 $V^{2/3}$.

Wave drag– For the wave-drag calculations, surface-pressure coefficients on each body at zero incidence were calculated by a computer program for Mach numbers of 2, 3, 4, 6, 8, 10, and 12. This program, which uses the method of characteristics for perfect or real gas solutions, is described in reference 9, in which a blunt nose starting solution is combined with the method of characteristics. For the present solutions, however, a pointed conical starting solution was used as was done in the study in reference 10. Real air computations were made for some of the bodies for Mach numbers from 6 to 12. These computations required substantially more computing time than the perfect gas calculations and the resulting pressure coefficients differed from the perfect-gas coefficients by an amount less than the accuracy to which they could be plotted with standard scales. Consequently, only the perfect-gas pressure coefficients are used in this report. The wave drag was calculated for each body by integrating the drag component of the pressure force over the profile of the body and is expressed in coefficient form as

$$C_{D_W} = \frac{2\pi}{S} \oint C_p r \, dr$$

The displacement effects of a boundary layer have not been included in the wave-drag calculations.

Base pressure– The base-pressure coefficients were determined by the procedure of reference 11, which was extended to hypersonic Mach numbers for this study. The extended values of the effective two-dimensional flow convergence angle δ_e used in this procedure are presented in figure 3 for Mach numbers just ahead of the body base up to 14. This concept can be used to correct the base-pressure coefficients for body boattail angles other than zero at the base. The resulting base-pressure coefficients were assumed to apply over the full base area of each body.

Skin friction– For the skin-friction calculations, Reynolds numbers were determined for each Mach number based on an assumed body length of 300 feet and for standard atmospheric conditions at the altitudes from the assumed flight profile for hypersonic cruise aircraft presented in figure 4. This flight profile for Mach numbers up to 5.5 is essentially identical to the upper boundary of the flight profile shown in figure 4 of reference 1. Above this Mach number the present flight profile is constrained only by a 1000 psf dynamic pressure and not by duct pressure and lower surface skin temperature. Using the present flight profile resulted in Reynolds numbers for the skin-friction calculations that varied in magnitude from about 1×10^8 to 7×10^8. Estimated

lengths of laminar and transitional boundary-layer flows on the bodies were determined from the transition Reynolds number data of figure 5. The cone data of this figure are from reference 12. The curves for the bodies with significant pressure gradients are assumed, guided by a few experimental test points at low supersonic Mach numbers and the cone data at the higher Mach numbers. To simplify the skin-friction calculations, the estimated lengths of laminar and transitional boundary-layer flows were converted to an equivalent length of turbulent boundary-layer flow, thus providing a virtual origin for an equivalent all-turbulent boundary-layer flow on each body that was, in turn, associated with a corresponding virtual wetted area. The development of an equation for determining such equivalent lengths for bodies of revolution is given in the appendix. This analysis follows the procedure given in appendix A of reference 13 for computation of equivalent lengths on a flat surface, but is developed in this report for bodies of revolution and includes transitional boundary-layer flow that becomes more and more significant at Mach numbers above about 5. Ratios of the compressible and incompressible skin-friction coefficients were determined from the charts of reference 14 by the procedure of Spalding and Chi, and the flat-plate incompressible skin-friction coefficients were obtained from reference 15. A transverse-curvature correction factor to transform flat-plate skin-friction coefficients into equivalent coefficients for bodies of revolution was included in the analysis. The calculations of reference 16 and the experimental data of reference 17 indicate that the magnitude of this factor is near unity for a turbulent boundary layer on various types of bodies of revolution at low supersonic Mach numbers. The data of reference 18, however, indicate that the factor increases to a magnitude of about 2 for a turbulent boundary layer on a cylindrical body at a Mach number of 5.80. Furthermore, the calculations of reference 19 indicate that such a factor for a laminar boundary layer on cones and cylinders would increase in magnitude as the supersonic Mach number is increased. The transverse-curvature correction factors for the particular bodies of revolution of this report are unknown, but values of 1.155 and 1.020 have been assumed for laminar and turbulent flow, respectively, to apply over the entire Mach number range.

APPARATUS AND TESTS

Test Facility

The tests were conducted in the Ames 3.5–Foot Hypersonic Wind Tunnel. This is a blowdown type tunnel in which compressed air is heated in a pebble-bed heater prior to its expansion through one of several fixed interchangeable nozzles. The air can be compressed to as much as 1.241×10^7 newtons per square meter (1800 psi) and heated to 1166.7° K (2100° R).

Models and Equipment

Three bodies were selected for the tests: the Sears-Haack [l,V], k = 0.1; the Sears-Haack [l,V], k = 0.5; and the 3/4-power [l,d], k = 0.5. Models of each body, 0.6096 m (24 in.) long, were constructed of stainless steel. During the tests the models were mounted on a sting-supported strain-gage balance. A length of uniform-diameter sting of about 2.5 to 3.0 maximum body diameters extended between the model base and the sting flare. The sting, in turn, was mounted on a quick-insert, side-mounted strut to permit introduction and withdrawal of the model from established flow in the tunnel. Pressures within the balance cavity were measured by a differential-type pressure transducer.

Tests

Normal force, axial force, pitching moment, and balance-cavity pressure were measured for each model at angles of attack from about -6° to 13° for M = 5.4, 7.4, and 10.5. The minimum permissible stagnation temperatures to prevent condensation of the air for these Mach numbers were employed in conjunction with the maximum allowable stagnation pressures within the wind tunnel to provide Reynolds numbers of approximately 8, 13, and 3 million, respectively, for these same Mach numbers, based on the length of the models. Natural boundary-layer transition on the models was expected only for Mach numbers of 5.4 and 7.4 and the corresponding Reynolds numbers above (see fig. 5). The measured balance-cavity pressures were taken to be the model base pressures.

Shadowgraph and oil-flow visualization tests were made for the models at zero incidence for each test Mach number. These tests were made separately from the measurements of the forces and moments. The shadowgraphs were made of only the model base region and the forward portion of the sting support. The oil-flow technique is described in reference 20. A satisfactory oil mixture was prepared from light vacuum-pump oil and titanium dioxide pigment in the approximate proportions, by volume, of 5:4 for Mach numbers of 5.4 and 7.4 and 3:2 for the Mach number of 10.5. Oleic acid was added to this mixture as a dispersing agent. One drop of oleic acid was added for about every 10 ml (1/3 oz) of light vacuum-pump oil.

Reduction and Precision of Data

For the drag calculations a constant fictitious wing area of $0.077\,l^2$ or $4.0\,V^{2/3}$ as the reference area was used to reduce the force and moment data to standard aerodynamic coefficients. The pitching-moment coefficients have been determined with respect to a moment center located on the body axis two-thirds of the body length from the nose, and based on the body length. As is customary for wind-tunnel data, the measured axial forces have been adjusted to a condition of free-stream static pressure on the base of the models. Accordingly, the base-pressure force is not a component of the resolved experimental lift, drag, or pitching-moment coefficients. For comparison with computed drag data, the base-pressure component of the drag must be added to the experimental data.

No attempt has been made to correct the measured data for the effects of the sting support. Such effects are usually classified as either "length" or "diameter" effects. Evidence that the sting used in these tests was sufficiently long for the lower test Mach numbers is shown in the shadowgraphs of figure 6. The appearance of trailing waves in the wake just downstream of the base of each model for Mach numbers of 5.4 and 7.4 indicates that the flow closes on the sting very near the model base and that this flow is turbulent in the boundary layer. Such rapid closure of the flow on the sting behind the base with the formation of trailing waves associated with the recompression does not generally take place unless the boundary layer has become turbulent at or ahead of the body base. Furthermore, the test Reynolds numbers for each of the above Mach numbers correspond closely to those expected for the establishment of turbulent flow on the bodies (see fig. 5). Since the sting flare is at a substantial distance downstream of the flow closure, there should be no length effects on the measured data for these Mach numbers. Some of the photographs for M = 5.4 and 7.4 also show the oil mixture leaving the model surface at the base and being carried by the flow to the sting a short distance from the base. This, too, is evidence of flow closure

on the sting very near the base at these Mach numbers. For M = 10.5, however, there is no evidence of trailing waves in the photograph, nor of oil being carried to the sting close to the base. Accordingly, there are possible sting "length" effects in the data for this Mach number. The test Reynolds number for these data, although the highest permissible in the wind tunnel for this Mach number, is much lower than that expected for turbulent flow to be established on the body. As for the sting "diameter" effects, such are unknown for the present test Mach numbers. The meager amount of relevant information available for hypersonic Mach numbers indicates that the pressure on the base can be increased by the presence of the sting, even for a sting diameter that is small relative to the diameter of the body (e.g., ref. 21).

In addition to any systematic errors that might be introduced by the sting support, the test data are also subject to random errors of measurement that affect the reliability of the data. The uncertainties in the measurement of the forces, moments, pressures, and test conditions have been determined to be as follows:

	M = 5.4	M = 7.4	M = 10.5
C_L	±0.001	±0.001	±0.002
C_D	±.0003	±.0003	±.0004
C_m	±.0002	±.0003	±.0003
L/D′	±.1	±.1	±.1
$C_{p_{base}}$	±.002	±.002	±.002
M	±.05	±.05	±.05
R	$\pm.2\times10^6$	$\pm.7\times10^6$	$\pm.1\times10^6$
α	±.1°	±.1°	±.1°

RESULTS AND DISCUSSION

Pressure Distributions

The calculated pressures on each of the 18 bodies are presented in figure 7 as a function of longitudinal distance along the bodies, with free-stream Mach number as a parameter. The fine grid has been retained in this figure to facilitate reading values from the curves and interpolation for other free-stream Mach numbers. It is obvious from the data of this figure that the effects of Mach number on the surface pressure coefficients rapidly diminish as the Mach number is increased to 12. This characteristic should simplify any extrapolation of pressure coefficients on the bodies for Mach numbers greater than 12.

Calculated Drag

Wave drag– The effect of Mach number on the calculated wave-drag coefficients for each body type is shown in figure 8 with body cutoff as a parameter. A marked reduction in wave drag accompanies an increase in body cutoff because as the length and volume are held constant, the body nose becomes more pointed as the cutoff is increased. The wave-drag coefficients of the

several groups of bodies are compared in figure 9 for constant values of body cutoff. The Sears-Haack profile provides the least wave drag for a given body cutoff for M = 2 to 12. For increasing Mach number and body cutoff, the wave drag of the Von Kármán and parabolic-arc profiles approach that for the Sears-Haack profile. The wave-drag coefficients are essentially identical for the Von Kármán and Sears-Haack profiles for a cutoff of 0.5.

Base drag– The effect of Mach number on the calculated base-drag coefficients of the various body groups is shown in figure 10. It is obvious from this figure, when compared with the corresponding wave-drag data of figure 9, that although the base drag for the bodies with large bases is reduced markedly as the Mach number is increased to 6, it still contributes substantially to the total drag for M = 6 to 12.

Skin-friction drag– The variation of the calculated skin-friction-drag coefficients with Mach number is presented in figure 11. The skin-friction drag coefficients diminish significantly as the Mach number is increased from 2 to about 6 and gradually as the Mach number is increased still further. The wetted surface areas of all the bodies vary only a small amount when the lengths and volumes are held constant. Therefore, the skin-friction-drag coefficients, as calculated, are affected very little by the amount of body cutoff within a given body group or between groups.

Total drag– The effect of Mach number on the calculated total-drag coefficients of each body, with body cutoff as a parameter, is shown in figure 12. These total-drag coefficients are the sum of the wave-drag, base-drag, and skin-friction-drag coefficients. It is apparent in figure 12 that the smallest total-drag coefficients are not associated with a constant value of body cutoff over the range of Mach numbers shown. As the Mach number is increased above 2, the smallest drag is given first by the 0.1 body cutoff, then by the 0.3 body cutoff as the Mach number is increased to 12. To facilitate a comparison of the calculated total drag of the various bodies for a given cutoff, the data of figure 12 have been replotted as a function of Mach number in figure 13. Here it is evident that the Sears-Haack profile clearly provides the least total drag for most cutoffs for M = 2 to 12. For a body cutoff of 0.3, the total-drag coefficients for each body are approximately the same, differing at most by only three drag-coefficient counts (0.0003) over the entire range of Mach numbers shown. For each of the other body cutoffs shown in figure 13 the total-drag coefficients for the parabolic arc and Von Kármán bodies closely approach those for the Sears-Haack bodies as the Mach number is increased to 12.0. The Eggers-Resnikoff-Dennis body [*l*,V] (ref. 5), and the Miele body [*l*,V] (ref. 6), neither of which was included in this study, have essentially the same profiles as the Von Kármán body [*l*,d], and therefore, would be expected to have essentially the same aerodynamic characteristics.

The influence of body cutoff on the calculated total-drag coefficients of the bodies is shown most clearly in figure 14, where total-drag coefficient is plotted as a function of body cutoff, k, for constant Mach number. The lowest drag coefficient provided by the Sears-Haack profile for M = 2.0 occurs for $k \cong 0.05$. At M = 6.0 the cutoff for the lowest drag coefficient is ~ 0.175. Also at this Mach number the drag coefficients for each body except the 3/4-power and the cone are within a range of about seven drag coefficient counts (0.0007) for any body cutoff. Furthermore, the drag coefficients for the body with cutoff values of 0 and 0.5 are nearly equal. At a Mach number of 12.0 the lowest drag coefficients are given by the Sears-Haack body

with $k \cong 0.35$. The overall spread of drag coefficients for the body groups at this Mach number is within about three drag coefficient counts, or 10, if the 3/4-power and cone bodies are included.

To facilitate comparison of the relative magnitudes of the components of the total-drag coefficients, the components for the Sears-Haack and cone bodies have been plotted in figure 15 as a function of Mach number, for constant k. The vertical height of each shaded band corresponds to the magnitude of the specified component. The reduction of the wave drag and the increase of the base-drag components as the magnitude of the body cutoff is increased is readily apparent in the figure. Although the skin-friction drag remains essentially constant for the different values of k at Mach numbers approaching 12, it becomes the largest contributor to the total-drag coefficients for the larger values of k. The wave drag is the largest contributor for $k = 0$ and 0.1. The component data comparison for the cone has been included in figure 15(e) to show that such bodies with a large base have base-drag components at Mach numbers approaching 12 that are still a very large part of the total-drag coefficients, and are even greater than the components of wave drag.

Experimental Aerodynamic Characteristics

The lift, drag, lift-drag ratio, and pitching-moment characteristics of the Sears-Haack [*l*,V], $k = 0.1$ body; the Sears-Haack [*l*,V], $k = 0.5$ body; and the 3/4-power [*l*,d], $k = 0.5$ body are presented in figure 16 for $M = 5.4$, 7.4, and 10.5. The experimental base-pressure coefficients for the same bodies are shown in figure 17.

The base-pressure force has not been included in the resolution of the lift, drag, and pitching-moment coefficients of figure 16, since the measured axial forces have been adjusted to a condition of free-stream static pressure on the base of the models, as is customary for wind-tunnel data. If a comparison is to be made between these experimental data and corresponding calculated total force and moment data, the component forces associated with the base pressures should be added to the experimental data.

The lift, drag, and lift-drag ratio data of figure 16 do not differ appreciably for the three bodies. The lift coefficients at the higher angles of attack for each Mach number, however, are slightly greater for the 3/4-power, $k = 0.5$ body, and the least for the Sears-Haack, $k = 0.1$ body. The minimum-drag coefficients are the lowest for the Sears-Haack bodies. The drag due to lift for these bodies, however, is slightly greater than that for the 3/4-power, $k = 0.5$ body. The maximum lift-drag ratios for each body generally differ very little for a given Mach number.

The pitching-moment characteristics for the three bodies are very distinct and indicate that the centers of pressure differ substantially for each body. These locations were found to be essentially unaffected by Mach number, and to be roughly approximated by the centers of projected plan areas of the bodies. The average experimental centers of pressure for the test Mach numbers together with the calculated centers of projected areas for the bodies are given below for comparison:

Body	Average experimental center of pressure, x/l		Calculated center of projected plan area of the body, x/l
	$\alpha \cong -2°$ to $2°$	$\alpha \cong 7°$ to $11°$	
Sears-Haack, k = 0.1	0.32	0.41	0.53
Sears-Haack, k = 0.5	.48	.55	.60
3/4-power, k = 0.5	.62	.63	.64

It is apparent that the experimental centers of pressure are farther forward than the centers of projected areas for the bodies, especially for the low angles of attack. For the 3/4-power, k = 0.5 body, the most pointed of the bodies and with maximum diameter at the base, the centers of pressure are only slightly forward of the centers of projected area of the body. For the Sears-Haack, k = 0.1 body, the least pointed of the bodies and with a closing afterbody contour and a small base, the centers of pressure are the most forward of the centers of projected area for the body.

The experimental base-pressure coefficients of figure 17 are essentially unaffected by angle of attack for the range of angles shown. The coefficients associated with a turbulent boundary layer over the base (i.e., the data for M = 5.4 and 7.4), as discussed earlier in the "Reduction and Precision of the Data" section, are roughly approximated by the expression $-1/M^2$. On the other hand, the base-pressure coefficients for M = 10.5 are related to a laminar boundary layer and are positive instead of negative, as for the two lower Mach numbers. No method is known for estimating the magnitude of such base-pressure coefficients associated with a laminar boundary-layer flow over the base.

If the wind-tunnel data of figure 16 for M = 5.4 and 7.4 had been resolved to include the measured base-pressure acting on the full base area of the bodies, the lift and pitching-moment characteristics would be essentially unchanged. The minimum-drag coefficients, however, would be increased in proportion to the magnitude of the base areas, such that the Sears-Haack, k = 0.1 body would provide much lower minimum-drag coefficients and higher values of $(L/D)_{max}$ than either of the other bodies. The magnitude of such minimum-drag coefficients are presented in the next section of this report.

Comparison of Calculated and Experimental Minimum-Drag Coefficients

In an effort to evaluate the calculation methods described earlier in this report, a comparison is made between the experimental and calculated minimum-drag coefficients for the Sears-Haack [l,V], k = 0.1 body, the Sears-Haack [l,V], k = 0.5 body, and the 3/4-power [l,d], k = 0.5 body. The calculated drag coefficients of figures 12 through 14, however, are not appropriate for such a comparison because of the very large differences in the associated Reynolds numbers. The calculated drag data given in these figures are based on Reynolds numbers of the order of 1×10^8 to 7×10^8. Appropriate calculations of minimum-drag coefficients for the wind-tunnel Reynolds

numbers, nevertheless, involved a recalculation of only the skin-friction-drag components. The wave-drag components as computed are unaffected by Reynolds number, and the base-pressure components were assumed to correspond to turbulent boundary-layer flow over the base even though this did not correspond to the apparent situation for a test Mach number of 10.5. Accordingly, the calculated and experimental base-drag components will not be expected to agree for this Mach number.

The calculated minimum-drag coefficients for the three bodies together with the corresponding experimental values are given in the following table. Since the wave-drag and skin-friction components are inseparable in the experimental data, a combined value is given in the table as read directly from figure 16. These data do not include the base-drag components so such components, obtained from the experimental data-reduction computations, have also been included in the table for comparison with the calculated values.

Components	Sears-Haack, k = 0.1		Sears-Haack, k = 0.5		3/4-power, k = 0.5	
	Calculated	Experiment	Calculated	Experiment	Calculated	Experiment
	$M = 5.4$ $R = 8.7\times10^6$		$M = 5.4$ $R = 7.7\times10^6$		$M = 5.4$ $R = 7.7\times10^6$	
Wave drag	0.0015	0.0032	0.0004	0.0032	0.0006	0.0038
Skin friction	.0021		.0021		.0020	
Base drag	.0004	.0003	.0024	.0022	.0036	.0034
Total drag, C_D	.0040	.0035	.0049	.0054	.0062	.0072
	$M = 7.4$ $R = 13.2\times10^6$		$M = 7.4$ $R = 12.7\times10^6$		$M = 7.4$ $R = 12.9\times10^6$	
Wave drag	.0014	.0026	.0004	.0027	.0005	.0037
Skin friction	.0016		.0016		.0015	
Base drag	.0002	.0001	.0013	.0011	.0021	.0016
Total drag, C_D	.0032	.0027	.0033	.0038	.0041	.0053
	$M = 10.5$ $R = 3.3\times10^6$		$M = 10.5$ $R = 3.3\times10^6$		$M = 10.5$ $R = 3.5\times10^6$	
Wave drag	.0011	.0028	.0003	.0030	.0005	.0034
Skin friction	.0015		.0015		.0014	
Base drag	.0001	-.0001	.0007	-.0009	.0011	-.0011
Total drag, C_D	.0027	.0027	.0025	.0021	.0030	.0023

The calculated and experimental total-drag coefficients for the Sears-Haack bodies are more nearly in agreement than for the 3/4-power body. For M = 5.4 and 7.4, however, the experimental values are lower than those calculated for the Sears-Haack, k = 0.1 body and higher for the other bodies. These differences might be explained if the pressures on the rearward portions of the bodies were higher than anticipated, possibly attributable to substantial boundary-layer growth, that can be expected at hypersonic Mach numbers. Such pressures would act on the rearward facing slopes of the Sears-Haack, k = 0.1 body reducing the wave drag, and on the forward facing slopes of the 3/4-power, k = 0.5 body increasing the drag. For the Sears-Haack, k = 0.5 body with slightly forward-facing slopes ahead of the base and with zero slope at the base, the same higher pressures

would not be expected to increase the wave drag significantly, if at all. Including the displacement effects of the boundary layer in the wave-drag computations can be expected to improve the agreement between the calculated and experimental drag coefficients.

Another possible source of the differences between the calculated and experimental minimum drag coefficients is in the skin-friction calculations. The present method of calculation does not distinguish between the three types of bodies except for differences in the magnitude of wetted area, and this difference is small when the lengths and volumes of the bodies are held constant. As a result the calculated values of skin-friction drag for the three bodies are essentially the same. If the transverse-curvature effects (see ref. 18 or 19) were taken into account, better agreement between the calculated and experimental drag coefficients could be expected. Such effects are proportional to the ratio of the boundary-layer thickness and the local body radius. Different corrections for each body can be anticipated because of the differences in the pressure and radius distributions for each body type (see fig. 7).

The calculated and experimental base-drag components for $M = 5.4$ and 7.4 agree well, but the experimental values are always less than calculated possibly because of an increase in pressure in the base region due to the sting-support diameter (see ref. 21). As anticipated, the agreement is poor between the calculated and experimental values of the base-drag component for a Mach number of 10.5. The values are even opposite in sign.

If the agreement between the calculated and experimental minimum-drag coefficients of the body types chosen for this report can be improved at hypersonic speeds by including boundary-layer displacement and transverse-curvature effects, such effects must be determined experimentally for each body type. Determining these effects would involve comprehensive surface-pressure and boundary-layer measurements in a hypersonic tunnel over the range of Mach numbers of interest. For sting-supported models, the effects of sting-support diameter should also be determined for the same body types.

CONCLUDING REMARKS

In this study the Sears-Haack profile provided the least drag throughout the Mach number range of 2.0 to 12.0 for most values of body cutoff. As the Mach number was increased to about 12.0, however, the drag coefficients for the Von Kármán and parabolic arc bodies closely approached those for the Sears-Haack bodies. The value of body cutoff associated with the lowest drag coefficients of the Sears-Haack bodies varied from about 0.05 for a Mach number of 2.0 to about 0.35 for a Mach number of 12.0. For Mach numbers approaching 12.0, the wave-drag component became the largest contributor to the total-drag coefficients for the smaller values of body cutoff, and the skin-friction or base-drag components became the largest for the larger values of body cutoff.

The wind-tunnel tests of the Sears-Haack $[l,V]$, $k = 0.1$ body, the Sears-Haack $[l,V]$, $k = 0.5$ body, and the 3/4-power $[l,d]$, $k = 0.5$ body at $M = 5.4$, 7.4, and 10.5, with corresponding Reynolds numbers of approximately 8, 13, and 3 million, respectively, have shown several significant results. The overall lift and drag characteristics for the bodies did not differ markedly, but the minimum-drag coefficients were the least for the Sears-Haack bodies. The pitching-moment

characteristics of the bodies, however, were distinct and indicated significant differences in the corresponding centers of pressure for each body. These locations were essentially unaffected by the test Mach number and could be roughly approximated by the center of projected plan area of the bodies.

The comparison of the calculated and experimental minimum-drag coefficients for the three bodies showed that the values for the Sears-Haack bodies were more nearly in agreement than those for the 3/4-power body. For Mach numbers of 5.4 and 7.4, however, the experimental values were lower than those calculated for the Sears-Haack, $k = 0.1$ body (with boattail), and higher for the other bodies, especially the 3/4-power, $k = 0.5$ body (with forward sloping surfaces and no boattail).

Ames Research Center
National Aeronautics and Space Administration
Moffett Field, Calif., 94035, June 3, 1971

APPENDIX

REDUCTION OF LENGTHS OF LAMINAR AND TRANSITIONAL BOUNDARY–LAYER FLOWS TO AN EQUIVALENT LENGTH OF TURBULENT BOUNDARY LAYER ON A BODY OF REVOLUTION

The calculation of skin-friction drag on a body of revolution is simplified if the skin-friction coefficients can be obtained from those for a flat plate having the same boundary-layer Reynolds numbers and adjusted by a lateral-correction factor for application to the body. It is further simplified if the skin friction resulting from laminar and transitional boundary-layer flows can be reduced to an equivalent length of turbulent boundary-layer flow, providing an effective virtual origin for the actual turbulent boundary-layer flow on the body. A method for reducing a length of laminar boundary-layer flow on a flat plate to an equivalent length of turbulent boundary-layer flow is given in appendix A of reference 13. The present analysis uses the same procedure but is developed for a body of revolution and includes transitional boundary-layer flow, a prominent feature of hypersonic flows.

For the present development the following illustration will be useful:

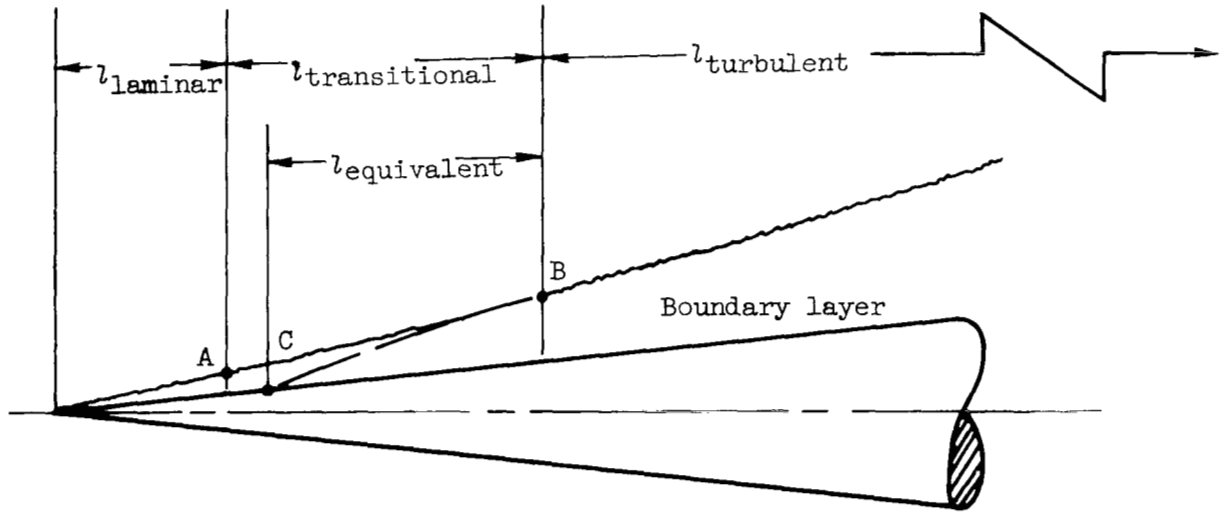

The skin-friction drag at station B per unit width of the flat plate corresponding to the body of revolution is the sum of the skin-friction drag in the laminar and transitional portions of the boundary-layer flow upstream of this station. This sum is set equal to the skin-friction drag due to a turbulent flow of length, $l_{equivalent}$, over the flat plate upstream of station B. Accordingly,

$$\overbrace{\left[C_{F_{lam}} \times q_\infty \times l_{lam} \times 1\right]}^{\text{laminar skin-friction drag}} + \overbrace{\left[C_{F_{trans}} \times q_\infty \times l_{trans} \times 1\right]}^{\text{transitional skin-friction drag}} = \overbrace{\left[C_{F_{turb}} \times q_\infty \times l_{eq} \times 1\right]}^{\text{equivalent turbulent skin-friction drag}} \quad (1)$$

where C_F is the average skin-friction coefficient. The skin-friction coefficient for the length of transitional flow, l_{trans}, between stations A and B is assumed to be given by the average of the laminar skin-friction coefficient at A and the turbulent skin-friction coefficient at B. Further, it is convenient to express the skin-friction coefficients as a product of an incompressible coefficient C_{F_i} and a compressibility correction factor C_F/C_{F_i}. A lateral-correction factor, F, is used to transform the flat-plate skin-friction coefficients into equivalent coefficients for bodies of revolution. If the flat-plate skin-friction coefficients are designated by primes, then equation (1) becomes

$$\overbrace{\left[C'_{F_{i_{lam}}} \times \left(\frac{C_F}{C_{F_i}}\right)_{lam} \times F_{lam} \times l_{lam}\right]}^{\text{laminar}} + \overbrace{\left[\frac{C'_{F_{i_{lam}}} \times (C_F/C_{F_i})_{lam} \times F_{lam} + C'_{F_{i_{turb}}} \times (C_F/C_{F_i})_{turb} \times F_{turb}}{2} \times l_{trans}\right]}^{\text{transitional}}$$

$$= \overbrace{\left[C'_{F_{i_{turb}}} \times \left(\frac{C_F}{C_{F_i}}\right)_{turb} \times F_{turb} \times l_{eq}\right]}^{\text{turbulent}} \qquad (2)$$

For determination of the equivalent length of turbulent flow, l_{eq}, it is believed that the laminar and turbulent flat-plate, average skin-friction coefficients will be adequately given by the Blasius and Prandtl-Von Kármán simple power function equations. Accordingly, equation (2) is then

$$\left[\frac{1.328}{\sqrt{R_{x_{lam}}}} \left(\frac{C_F}{C_{F_i}}\right)_{lam} \times F_{lam} \times l_{lam}\right] + \left[\frac{\frac{1.328}{\sqrt{R_{x_{lam}}}} \left(\frac{C_F}{C_{F_i}}\right)_{lam} \times F_{lam} + \frac{0.074}{R_{x_{turb}}^{1/5}} \left(\frac{C_F}{C_{F_i}}\right)_{turb} \times F_{turb}}{2} \times l_{trans}\right]$$

$$= \left[\frac{0.074}{R_{x_{turb}}^{1/5}} \left(\frac{C_F}{C_{F_i}}\right)_{turb} \times F_{turb} \times l_{eq}\right] \qquad (3)$$

Simplifying,

$$\frac{1.328}{(R_x/l)^{1/2} l_{lam}^{1/2}} \left(\frac{C_F}{C_{F_i}}\right)_{lam} F_{lam} \left(l_{lam} + \frac{l_{trans}}{2}\right) = \frac{0.074}{(R_x/l)^{1/5} l_{eq}^{1/5}} \left(\frac{C_F}{C_{F_i}}\right)_{turb} F_{turb} \left(l_{eq} - \frac{l_{trans}}{2}\right)$$

or

$$\frac{1.328}{(R_x/l)^{1/2}}\left(\frac{C_F}{C_{F_i}}\right)_{lam} F_{lam}\left(l_{lam}^{1/2} + \frac{l_{trans}}{2l_{lam}^{1/2}}\right) = \frac{0.074}{(R_x/l)^{1/5}}\left(\frac{C_F}{C_{F_i}}\right)_{turb} F_{turb}\left(l_{eq}^{4/5} - \frac{l_{trans}}{2l_{eq}^{1/5}}\right) \quad (4)$$

where (R_x/l) is the unit Reynolds number.

Solving for the factor $[l_{eq}^{4/5} - (l_{trans}/2l_{eq}^{1/5})]$

$$\left(l_{eq}^{4/5} - \frac{l_{trans}}{2l_{eq}^{1/5}}\right) = \frac{1.328}{0.074}\left[\frac{l_{lam}^{1/2} + (l_{trans}/2l_{lam}^{1/2})}{(R_x/l)^{0.3}}\right]\frac{(C_F/C_{F_i})_{lam} F_{lam}}{(C_F/C_{F_i})_{turb} F_{turb}}$$

$$= 17.946\left[\frac{l_{lam}^{1/2} + (l_{trans}/2l_{lam}^{1/2})}{(R_x/l)^{0.3}}\right]\frac{(C_F/C_{F_i})_{lam}}{(C_F/C_{F_i})_{turb}}\left(\frac{F_{lam}}{F_{turb}}\right) \quad (5)$$

Let $l_{trans}/2 = G$ and

$$17.946\left[\frac{l_{lam}^{1/2} + (l_{trans}/2l_{lam}^{1/2})}{(R_x/l)^{0.3}}\right]\frac{(C_F/C_{F_i})_{lam}}{(C_F/C_{F_i})_{turb}}\left(\frac{F_{lam}}{F_{turb}}\right) = H$$

Equation (5) then becomes

$$l_{eq}^{4/5} - \frac{G}{l_{eq}^{1/5}} = H$$

or

$$\left(l_{eq}^{4/5} - \frac{G}{l_{eq}^{1/5}}\right)^{5/4} = H^{5/4} \quad (6)$$

A binomial expansion of the left side of equation (6) gives, approximately,

$$l_{eq} - \frac{5}{4}G + \frac{5}{32}\frac{G^2}{l_{eq}} + \ldots \cong H^{5/4}$$

or, clearing of fractions and collecting like terms,

$$l_{eq}^2 - \left(\frac{5}{4}G + H^{5/4}\right) l_{eq} + \frac{5}{32}\,G^2 \cong 0 \tag{7}$$

then

$$l_{eq} \cong \frac{\left(\frac{5}{4}G + H^{5/4}\right) \pm \sqrt{\left(\frac{5}{4}G + H^{5/4}\right)^2 - \frac{5}{8}G^2}}{2} \tag{8}$$

In equation (7), however, the third term on the left side [$(5/32)G^2$] is small compared to the other two such that it can be neglected for most practical calculations; then

$$\begin{aligned} l_{eq} &\cong \frac{5}{4}G + H^{5/4} \\ &\cong \frac{5}{8}\,l_{trans} + \left\{ 17.946 \left[\frac{l_{lam}^{1/2} + (l_{trans}/2\, l_{lam}^{1/2})}{(R_x/l)^{0.3}} \right] \frac{(C_F/C_{F_i})_{lam}}{(C_F/C_{F_i})_{turb}} \left(\frac{F_{lam}}{F_{turb}}\right) \right\}^{5/4} \end{aligned} \tag{9}$$

This equivalent length l_{eq} provides a virtual origin of fully turbulent flow on a body of revolution, and should be associated, of course, with a corresponding virtual wetted area.

REFERENCES

1. Gregory, Thomas J.; Petersen, Richard H.; and Wyss, John A.: Performance Tradeoffs and Research Problems for Hypersonic Transports. AIAA Paper 64–605, Aug. 1964, and J. Aircraft, vol. 2, no. 4, July-Aug. 1965, pp. 266–271.

2. Von Kármán, Theodore: The Problem of Resistance in Compressible Fluids. GALCIT Pub. 75, 1936 (From Roma Reale Acad. D'Italia, vol. XIV, Roma, 1936).

3. Haack, W.: Geschossformen Kleinsten Wellenwiderstandes. Lilienthal-Gesellschaft fur Lüftfahrtforschung, Bericht 139, Teil 1, Oct. 9–10, 1941, pp. 14–28. (Translation: Douglas Aircraft Co., Inc., Rep. 288, 1946; also Projectile Shapes for Smallest Wave Drag. Brown University Graduate Division of Applied Mathematics, Translation No. A9–T–3, 1948).

4. Sears, William R.: On Projectiles of Minimum Wave Drag. Quart. Appl. Math., vol. IV, no. 4, Jan. 1947, pp. 361–366.

5. Eggers, A. J., Jr.; Resnikoff, Meyer M.; and Dennis, David H.: Bodies of Revolution Having Minimum Drag at High Supersonic Airspeeds. NACA Rep. 1306, 1958.

6. Miele, Angelo: Slender Shapes of Minimum Pressure Drag. Ch. 13 of Theory of Optimum Aerodynamic Shapes, A. Miele, ed., Academic Press, 1965, pp. 195–207.

7. Fink, Martin R.: Hypersonic Minimum-Drag Slender Bodies of Revolution. AIAA J., vol. 4, no. 10, Oct. 1966, pp. 1717–1724.

8. Stivers, Louis S., Jr.; and Spencer, Bernard, Jr.: Studies of Optimum Body Shapes at Hypersonic Speeds. NASA TN D–4191, 1967.

9. Inouye, Mamoru; Rakich, John V.; and Lomax, Harvard: A Description of Numerical Methods and Computer Programs for Two-Dimensional and Axisymmetric Supersonic Flow Over Blunt-Nosed and Flared Bodies. NASA TN D–2970, 1965.

10. Rakich, John V.: Numerical Calculation of Supersonic Flows of a Perfect Gas Over Bodies of Revolution at Small Angles of Yaw. NASA TN D–2390, 1964.

11. Love, Eugene S.: Base Pressure at Supersonic Speeds on Two-Dimensional Airfoils and on Bodies of Revolution With and Without Fins Having Turbulent Boundary Layers. NACA TN 3819, 1957.

12. Nagamatsu, H. T.; Sheer, R. E. Jr.; and Graber, B. C.: Hypersonic Laminar Boundary-Layer Transition on 8-Foot-Long, 10° Cone, $M_1 = 9.1–16$. AIAA J., vol. 5, no. 7, July 1967, pp. 1245–1252.

13. Hicks, Raymond, M.; and Hopkins, Edward J.: Effects of Spanwise Variation of Leading-Edge Sweep on the Lift, Drag, and Pitching Moment of a Wing-Body Combination at Mach Numbers From 0.7 to 2.94. NASA TN D–2236, 1964.

14. Neal, Luther, Jr.; and Bertram, Mitchel H.: Turbulent-Skin-Friction and Heat-Transfer Charts Adapted From the Spalding and Chi Method. NASA TN D–3969, 1967.

15. Locke, F. W. S., Jr.: Recommended Definition of Turbulent Friction in Incompressible Fluids. NAVAER DR Rep. 1415, June 1952.

16. Bertram, Mitchel H.: Calculations of Compressible Average Turbulent Skin Friction. NASA TR R–123, 1962.

17. Allen, Jerry M.; and Monta, William J.: Turbulent-Boundary-Layer Characteristics of Pointed Slender Bodies of Revolution at Supersonic Speeds. NASA TN D–4193, 1967.

18. Richmond, Ronald L.: Experimental Investigation of Thick Axially Symmetric Boundary Layers on Cylinders at Subsonic and Hypersonic Speeds. GALCIT Hypersonic Research Project Memorandum 39, June 1957.

19. Probstein, R. F.; and Elliott, D.: The Transverse Curvature Effect in Compressible Axially Symmetric Laminar Boundary-Layer Flow. Jour. Aero. Sci., vol. 23, no. 3, March 1956, pp. 208–224, 236.

20. Stanbrook, A.: The Surface Oil Flow Technique as Used in High Speed Wind Tunnels in the United Kingdom. British RAE–TN–Aero.-2712, 1960.

21. Hruby, Ronald J.; McDevitt, John B.; Coon, Grant W.; Harrison, Dean R.; and Kemp, Joseph H., Jr.: FM Telemetry and Free-Flight Techniques for Aerodynamic Measurements in Conventional Wind Tunnels. NASA TN D–3319, 1966.

TABLE 1.– GEOMETRICAL DATA FOR THE BODIES;
$V = 0.002655l^3$, $S = 0.077l^2 = 4.0V^{2/3}$

Body cutoff, k	Body type					
	Sears-Haack	Parabolic arc	Miele	Von Kármán	3/4 power	Cone
	Fineness ratio, l/d_0					
0	13.200	12.560	11.537	12.161	—	—
.1	13.807	13.183	12.124	12.745	—	—
.3	14.226	13.734	12.800	13.303	—	—
.5	13.200	12.560	11.537	12.161	10.877	9.930
	Maximum body radius, r_0/l					
0	0.037879	0.039808	0.043338	0.041114	—	—
.1	.036215	.037928	.041241	.039232	—	—
.3	.035147	.036407	.039062	.037586	—	—
.5	.037879	.039808	.043338	.041114	0.045967	0.050354
	Volume, $V/r_0^2 l$					
0	1.85055	1.67552	1.41372	1.57080	—	—
.1	2.02455	1.84575	1.56112	1.72506	—	—
.3	2.14937	2.00322	1.74010	1.87946	—	—
.5	1.85055	1.67552	1.41372	1.57080	1.25664	1.04720
	Surface area, $S_W/r_0 l$					
0	4.5169	4.1888	3.7699	4.1021	—	—
.1	4.8278	4.5239	4.0877	4.3779	—	—
.3	4.9488	4.6914	4.3063	4.5322	—	—
.5	4.5169	4.1888	3.7699	4.1021	3.5904	3.1495
	Surface area ratio, S_W/S					
0	2.2235	2.1671	2.1233	2.1918	—	—
.1	2.2722	2.2299	2.1909	2.2322	—	—
.3	2.2605	2.2197	2.1861	2.2139	—	—
.5	2.2235	2.1671	2.1233	2.1918	2.1449	2.0610
	Maximum cross-sectional area, $(A_0/l^2)\times 10^2$					
0	0.450757	0.497846	0.590039	0.531035	—	—
.1	.412017	.451929	.534328	.483546	—	—
.3	.388089	.416404	.479369	.443822	—	—
.5	.450757	.497846	.590039	.531035	0.663793	0.796552
	Ratio of base area to maximum cross-sectional area, A_B/A_0					
0	0	0	0	0	—	—
.1	.216001	.129598	.080916	.142387	—	—
.3	.769868	.705606	.558036	.626491	—	—
.5	1.000000	1.000000	1.000000	1.000000	1.000000	1.000000
	Base area ratio, A_B/S					
0	0	0	0	0	—	—
.1	.011566	.007612	.005619	.008948	—	—
.3	.038829	.038185	.034765	.036135	—	—
.5	.058580	.064700	.076681	.069013	0.086267	0.103520

TABLE 2.– COORDINATES FOR THE SEARS–HAACK BODIES [*l*,V]

x/*l*	k = 0	0.1	0.3	0.5
		η		
0	0	0	0	0
.01000	.08877	.08209	.06809	.05298
.01500	.11986	.11088	.09204	.07168
.02000	.14816	.13711	.11391	.08877
.02500	.17448	.16154	.13430	.10474
.03000	.19928	.18457	.15357	.11986
.04000	.24535	.22742	.18952	.14816
.05000	.28778	.26697	.22284	.17448
.06000	.32734	.30392	.25410	.19928
.07000	.36453	.33873	.28368	.22284
.08000	.39967	.37171	.31183	.24535
.09000	.43302	.40308	.33873	.26697
.10000	.46476	.43302	.36453	.28778
.11000	.49503	.46165	.38933	.30789
.12000	.52395	.48909	.41321	.32734
.13000	.55162	.51541	.43626	.34621
.14000	.57812	.54070	.45853	.36453
.15000	.60350	.56501	.48007	.38234
.16000	.62783	.58840	.50092	.39967
.17000	.65116	.61091	.52112	.41656
.18000	.67353	.63258	.54070	.43302
.19000	.69498	.65344	.55969	.44908
.20000	.71554	.67353	.57812	.46476
.22000	.75411	.71150	.61336	.49503
.24000	.78943	.74666	.64658	.52395
.26000	.82167	.77916	.67790	.55162
.28000	.85097	.80914	.70742	.57812
.30000	.87742	.83668	.73524	.60350
.32000	.90113	.86189	.76143	.62783
.34000	.92217	.88482	.78604	.65116
.36000	.94060	90555	.80914	.67353
.38000	.95648	.92413	.83077	.69498
.40000	.96985	.94060	.85097	.71554
.42000	.98074	.95501	.86978	.73524
.44000	.98918	.96737	.88723	.75411
.46000	.99520	.97773	.90336	.77216
.48000	.99880	.98610	.91818	.78943
.50000	1.00000	.99249	.93171	.80593
.54000	.99520	.99941	.95501	.83668
.58000	.98074	.99855	.97337	.86454
.62000	.95648	.98989	.98690	.88962
.66000	.92217	.97337	.99566	.91198
.70000	.87742	.94886	.99970	.93171
.74000	.82167	.91614	.99903	.94886
.78000	.75411	.87490	.99365	.96348
.82000	.67353	.82473	.98353	.97560
.86000	.57812	.76504	.96862	.98526
.90000	.46476	.69498	.94886	.99249
.95000	.28778	.59094	.91716	.99812
1.00000	0	.46476	.87742	1.00000

TABLE 3.– COORDINATES FOR THE PARABOLIC-ARC BODIES

	k = 0	0.1	0.3	0.5
x/l		η		
0	0	0	0	0
.01000	.03960	.03568	.02780	.01990
.01500	.05910	.05327	.04156	.02978
.02000	.07840	.07070	.05522	.03960
.02500	.09750	.08798	.06878	.04938
.03000	.11640	.10508	.08224	.05910
.04000	.15360	.13882	.10886	.07840
.05000	.19000	.17190	.13510	.09750
.06000	.22560	.20434	.16094	.11640
.07000	.26040	.23612	.18640	.13510
.08000	.29440	.26726	.21146	.15360
.09000	.32760	.29776	.23612	.17190
.10000	.36000	.32760	.26040	.19000
.11000	.39160	.35680	.28428	.20790
.12000	.42240	.38534	.30778	.22560
.13000	.45240	.41324	.33088	.24310
.14000	.48160	.44050	.35358	.26040
.15000	.51000	.46710	.37590	.27750
.16000	.53760	.49306	.39782	.29440
.17000	.56440	.51836	.41936	.31110
.18000	.59040	.54302	.44050	.32760
.19000	.61560	.56704	.46124	.34390
.20000	.64000	.59040	.48160	.36000
.22000	.68640	.63518	.52114	.39160
.24000	.72960	.67738	.55910	.42240
.26000	.76960	.71698	.59550	.45240
.28000	.80640	.75398	.63034	.48160
.30000	.84000	.78840	.66360	.51000
.32000	.87040	.82022	.69530	.53760
.34000	.89760	.84946	.72542	.56440
.36000	.92160	.87610	.75398	.59040
.38000	.94240	.90014	.78098	.61560
.40000	.96000	.92160	.80640	.64000
.42000	.97440	.94046	.83026	.66360
.44000	.98560	.95674	.85254	.68640
.46000	.99360	.97042	.87326	.70840
.48000	.99840	.98150	.89242	.72960
.50000	1.00000	.99000	.91000	.75000
.54000	.99360	.99922	.94046	.78840
.58000	.97440	.99806	.96466	.82360
.62000	.94240	.98654	.98258	.85560
.66000	.89760	.96466	.99422	.88440
.70000	.84000	.93240	.99960	.91000
.74000	.76960	.88978	.99870	.93240
.78000	.68640	.83678	.99154	.95160
.82000	.59040	.77342	.97810	.96760
.86000	.48160	.69970	.95838	.98040
.90000	.36000	.61560	.93240	.99000
.95000	.19000	.49590	.89110	.99750
1.00000	0	.36000	.84000	1.00000

TABLE 4.– COORDINATES FOR THE MIELE BODIES [S_W,V]

	k = 0	0.1	0.3	0.5
x/*l*			η	
0	0	0	0	0
.01000	.02985	.02688	.02093	.01496
.02000	.05940	.05351	.04170	.02985
.03000	.08864	.07990	.06233	.04466
.04000	.11757	.10603	.08281	.05940
.05000	.14619	.13192	.10314	.07405
.06000	.17449	.15754	.12332	.08864
.07000	.20247	.18292	.14334	.10314
.08000	.23013	.20803	.16320	.11757
.09000	.25746	.23288	.18292	.13192
.10000	.28446	.25746	.20247	.14619
.11000	.31112	.28177	.22186	.16038
.12000	.33745	.30582	.24110	.17449
.13000	.36343	.32959	.26017	.18852
.14000	.38906	.35308	.27909	.20247
.15000	.41434	.37629	.29783	.21634
.16000	.43926	.39921	.31642	.23013
.17000	.46381	.42185	.33483	.24383
.18000	.48800	.44420	.35308	.25746
.20000	.53524	.48800	.38906	.28446
.22000	.58093	.53059	.42435	.31112
.24000	.62502	.57192	.45893	.33745
.26000	.66745	.61197	.49279	.36343
.28000	.70814	.65068	.52592	.38906
.30000	.74702	.68801	.55829	.41434
.32000	.78400	.72391	.58988	.43926
.34000	.81898	.75832	.62069	.46381
.36000	.85184	.79116	.65068	.48800
.38000	.88242	.82236	.67984	.51181
.40000	.91056	.85184	.70814	.53524
.42000	.93600	.87947	.73555	.55829
.44000	.95843	.90514	.76204	.58093
.46000	.97737	.92867	.78759	.60318
.48000	.99200	.94985	.81215	.62502
.50000	1.00000	.96838	.83568	.64645
.52000	.99200	.98381	.85814	.66745
.54000	.97737	.99531	.87947	.68801
.56000	.95843	.99928	.89961	.70814
.60000	.91056	.97737	.93600	.74702
.64000	.85184	.94074	.96646	.78400
.68000	.78400	.89398	.98948	.81898
.72000	.70814	.83896	.99928	.85184
.76000	.62502	.77676	.98381	.88242
.80000	.53524	.70814	.95843	.91056
.84000	.43926	.63364	.92616	.93600
.88000	.33745	.55371	.88825	.95843
.92000	.23013	.46868	.84544	.97737
.96000	.11757	.37885	.79824	.99200
.98000	.05940	.33221	.77311	.99717
1.00000	0	.28446	.74702	1.00000

TABLE 5.– COORDINATES FOR THE VON KÁRMÁN BODIES* [l,d]

x/l	k = 0	0.1	0.3	0.5
			η	
0	0	0	0	0
.01000	.06909	.06386	.05292	.04114
.01500	.09350	.08643	.07165	.05572
.02000	.11583	.10710	.08881	.06909
.02500	.13672	.12643	.10487	.08161
.03000	.15651	.14476	.12011	.09350
.03500	.17542	.16227	.13469	.10487
.04000	.19359	.17911	.14871	.11583
.05000	.22813	.21114	.17542	.13672
.06000	.26072	.24138	.20068	.15651
.07000	.29171	.27017	.22478	.17542
.08000	.32137	.29774	.24789	.19359
.09000	.34986	.32426	.27017	.21114
.10000	.37733	.34986	.29171	.22813
.11000	.40388	.37463	.31260	.24464
.12000	.42959	.39864	.33289	.26072
.13000	.45453	.42196	.35265	.27639
.14000	.47876	.44464	.37191	.29171
.15000	.50231	.44673	.39072	.30669
.16000	.52523	.48826	.40909	.32137
.17000	.54755	.50925	.42706	.33575
.18000	.56930	.52974	.44465	.34986
.20000	.61117	.56930	.47876	.37733
.22000	.65099	.60708	.51155	.40388
.26000	.72488	.67771	.57358	.45453
.30000	.79150	.74221	.63133	.50231
.34000	.85096	.80088	.68517	.54755
.38000	.90302	.85374	.73533	.59050
.42000	.94696	.90060	.78196	.63133
.46000	.98108	.94093	.82509	.67017
.48000	.99327	.95834	.84534	.68887
.50000	1.00000	.97363	.86469	.70711
.52000	.99327	.98643	.88312	.72488
.54000	.98108	.99605	.90060	.74221
.56000	.96542	.99939	.91711	.75909
.58000	.94696	.99224	.93258	.77551
.60000	.92608	.98108	.94696	.79150
.64000	.87795	.95085	.97205	.82213
.68000	.82213	.91250	.99116	.85096
.70000	.79150	.89073	.99761	.86469
.72000	.75909	.86738	.99939	.87795
.74000	.72488	.84250	.99425	.89073
.76000	.68887	.81615	.98643	.90302
.80000	.61117	.75909	.96542	.92608
.84000	.52523	.69622	.93888	.94696
.88000	.42959	.62734	.90780	.96542
.92000	.32137	.55195	.87270	.98108
.96000	.19359	.46915	.83388	.99327
.98000	.11583	.42451	.81313	.99761
1.00000	0	.37733	.79150	1.00000

*The Eggers-Resnikoff-Dennis body [l,V] (ref. 5) and the Miele body [l,V] (ref. 6) have essentially the same coordinates as the Von Kármán body [l,d].

TABLE 6.– COORDINATES FOR THE 3/4–POWER BODY [l,d], k = 0.5

x/l	η
0	0
.01000	.03162
.01500	.04286
.02000	.05318
.02500	.06287
.03000	.07208
.03500	.08092
.04000	.08944
.05000	.10574
.06000	.12123
.07000	.13609
.08000	.15042
.09000	.16432
.10000	.17783
.11000	.19100
.12000	.20389
.13000	.21650
.14000	.22887
.15000	.24103
.16000	.25298
.17000	.26475
.18000	.27635
.20000	.29907
.22000	.32123
.24000	.34289
.26000	.36411
.28000	.38492
.30000	.40536
.32000	.42546
.34000	.44526
.36000	.46476
.38000	.48399
.40000	.50297
.42000	.52172
.44000	.54024
.46000	.55856
.48000	.47667
.50000	.59460
.54000	.62993
.58000	.66462
.62000	.69870
.66000	.73225
.70000	.76529
.74000	.79785
.78000	.82999
.82000	.86171
.86000	.89305
.90000	.92402
.95000	.96226
1.00000	1.00000

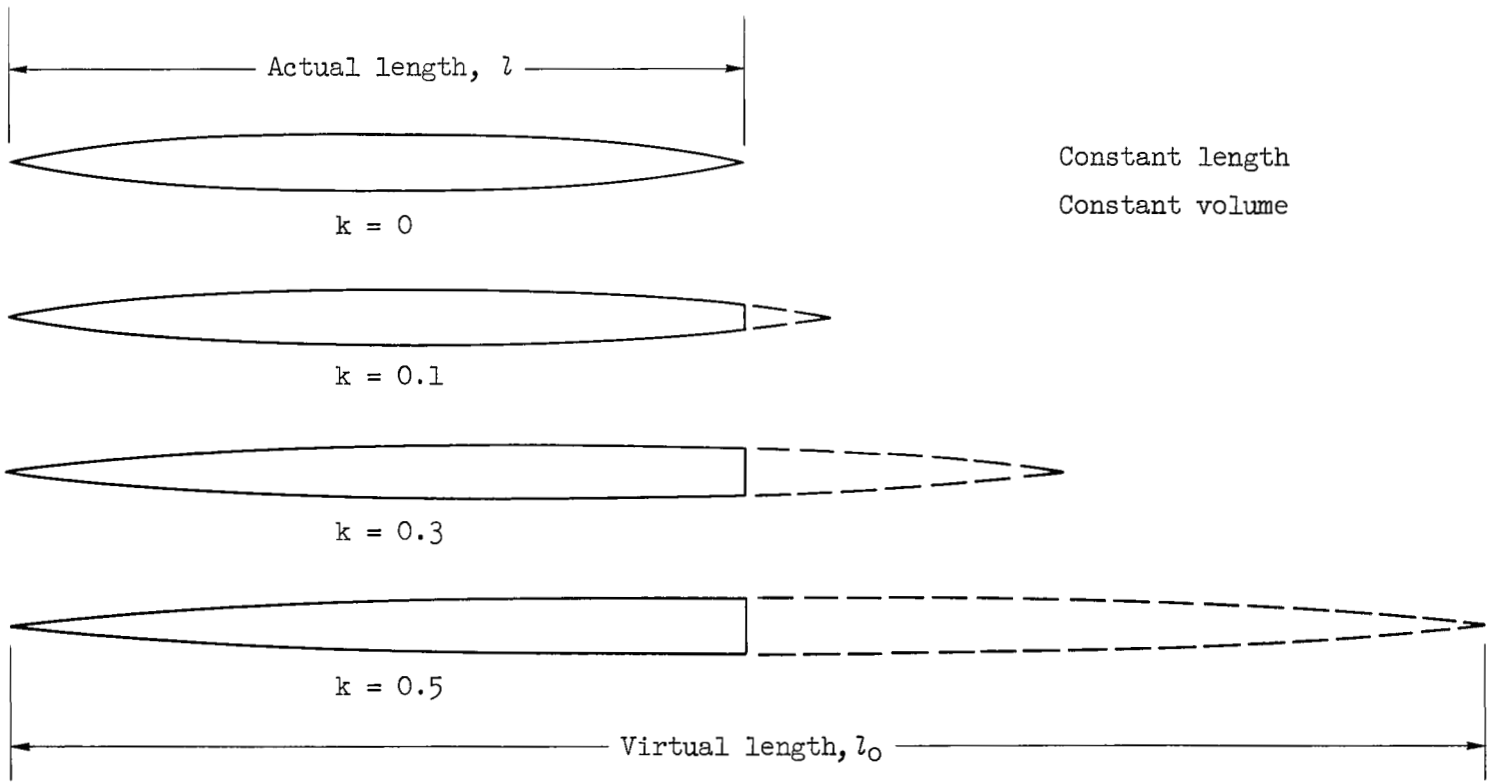

Figure 1.- Illustration of body cut offs for the Sears-Haack, parabolic-arc, Miele, and Von Kármán profiles.

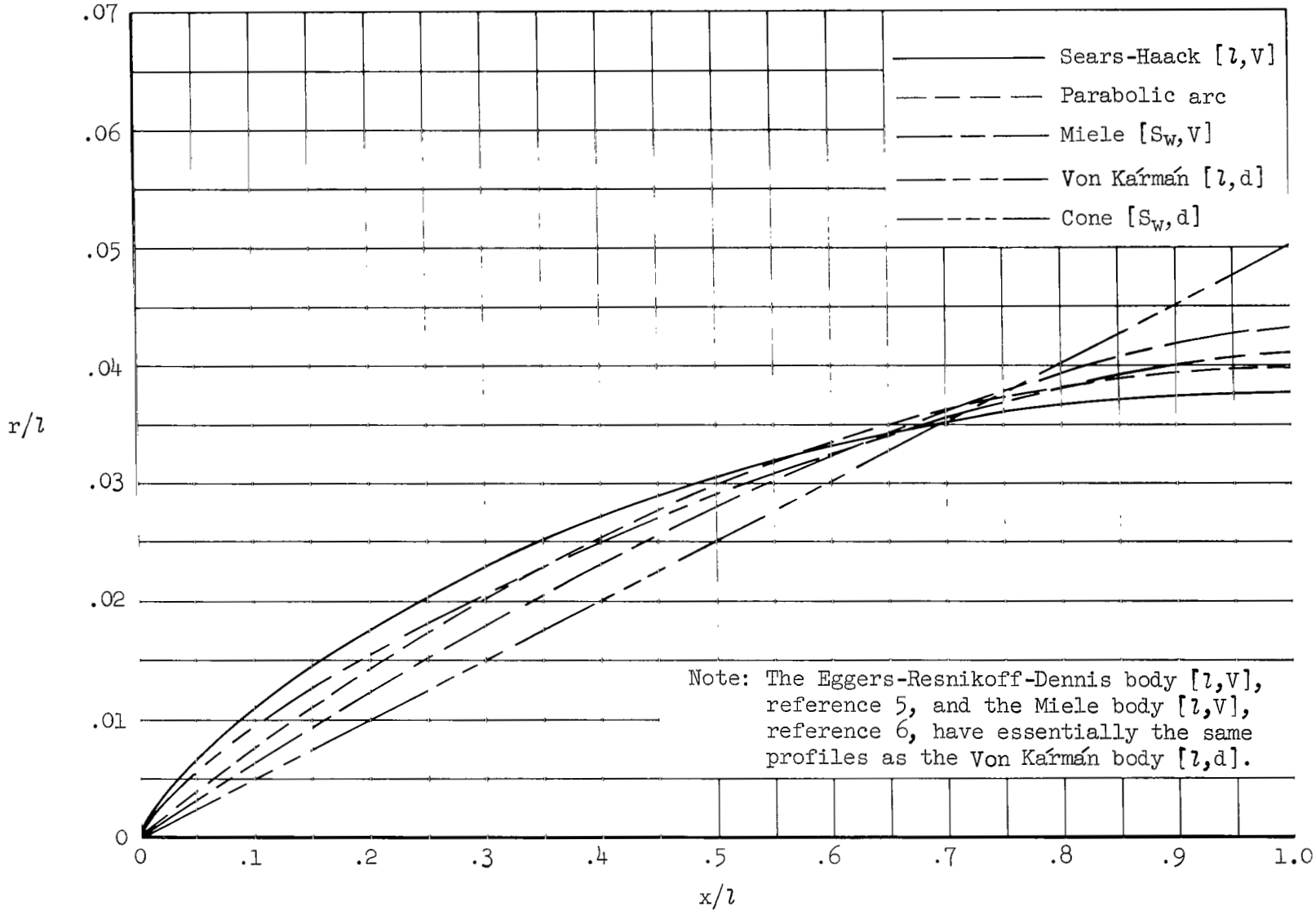

Figure 2.- Comparison of profiles for the k = 0.5 bodies.

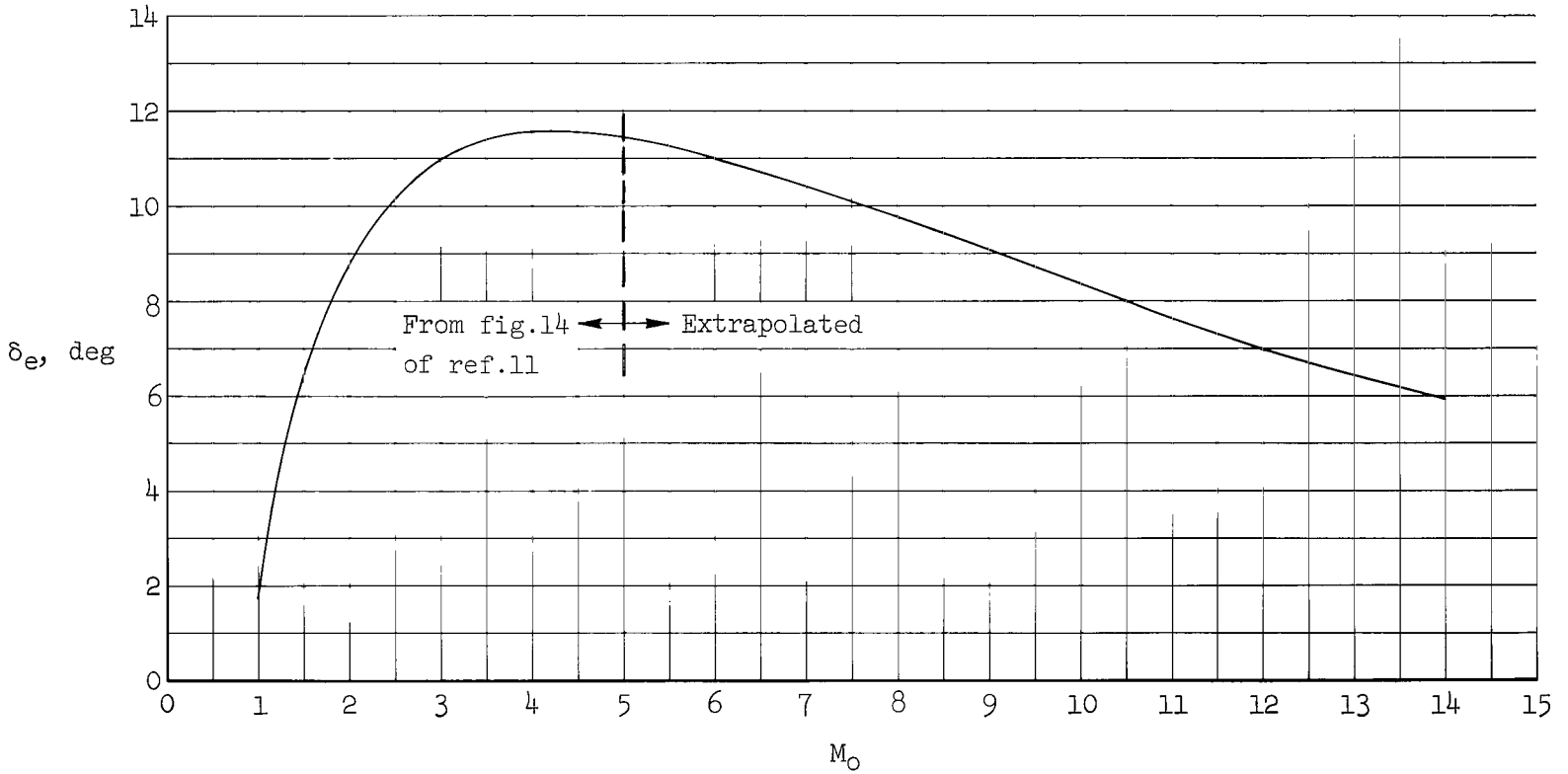

Figure 3.- Variation of the effective two-dimensional flow convergence angle over the base of a body of revolution as a function of Mach number just ahead of the base. For use in the calculation of the body base-pressure coefficient. Data for Mach numbers 1 to 5 are from NACA TN 3819.

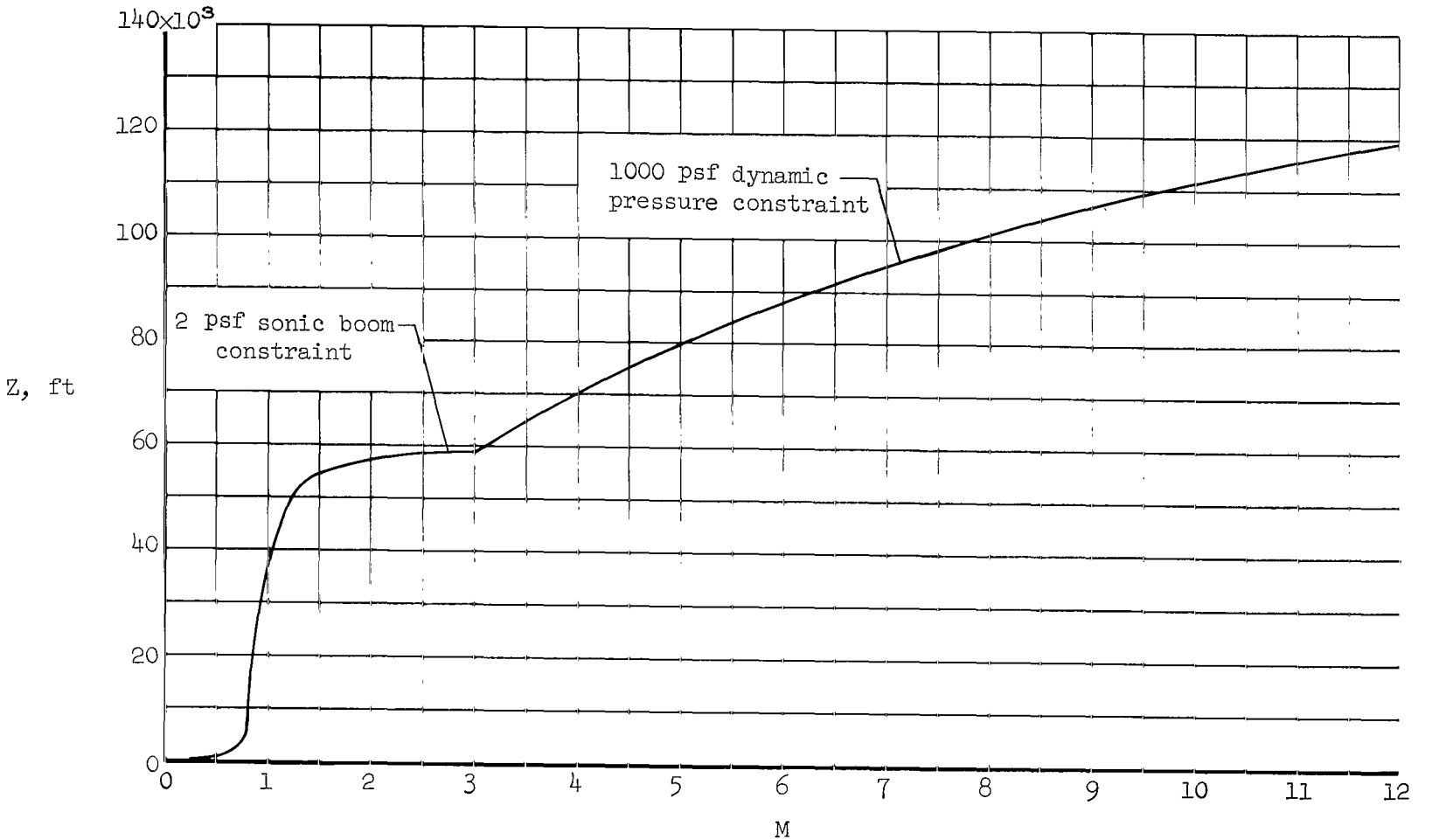

Figure 4.- Assumed flight profile used to specify Reynolds number of the skin-friction calculations.

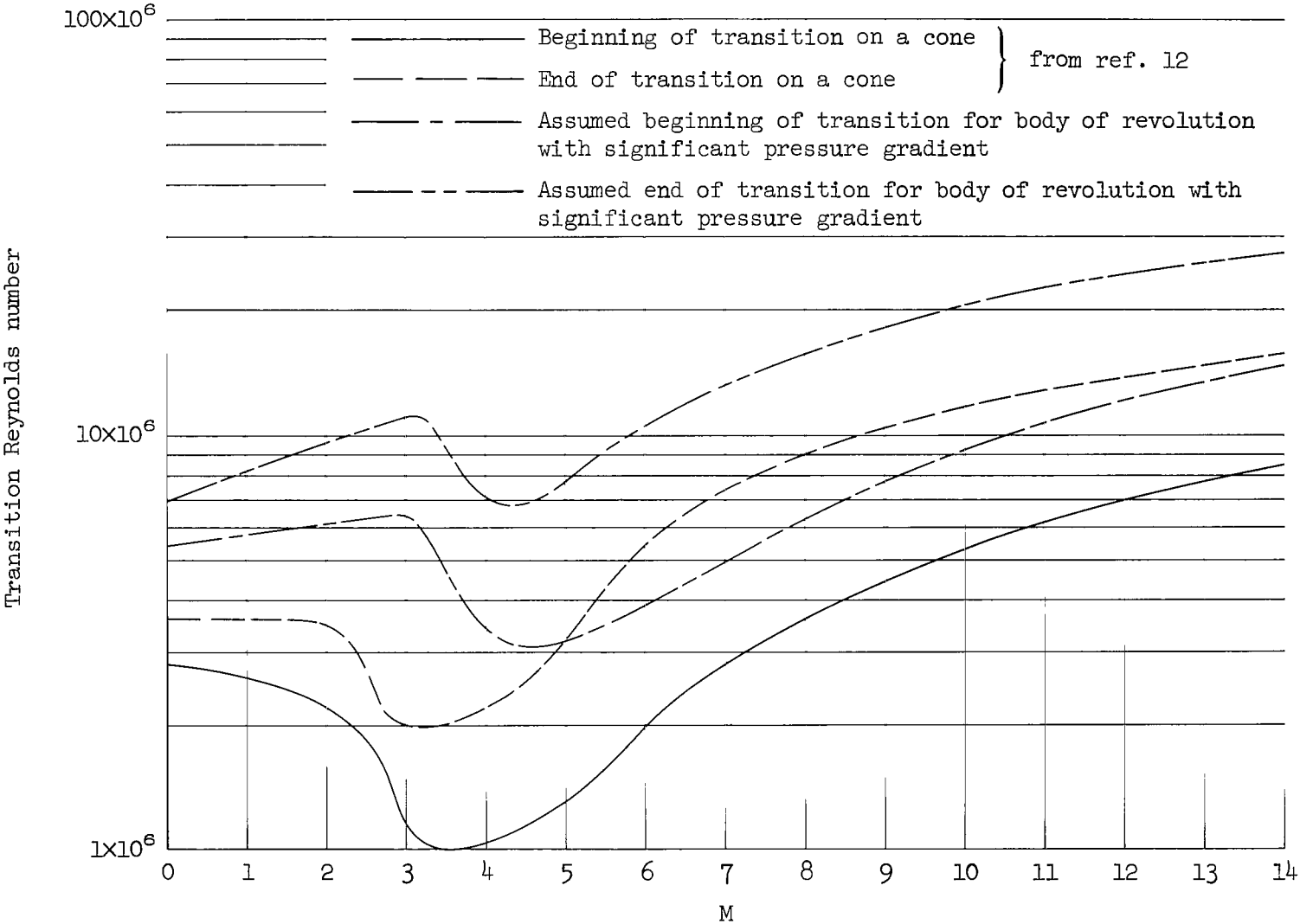

Figure 5.- Effect of Mach number on transition Reynolds number.

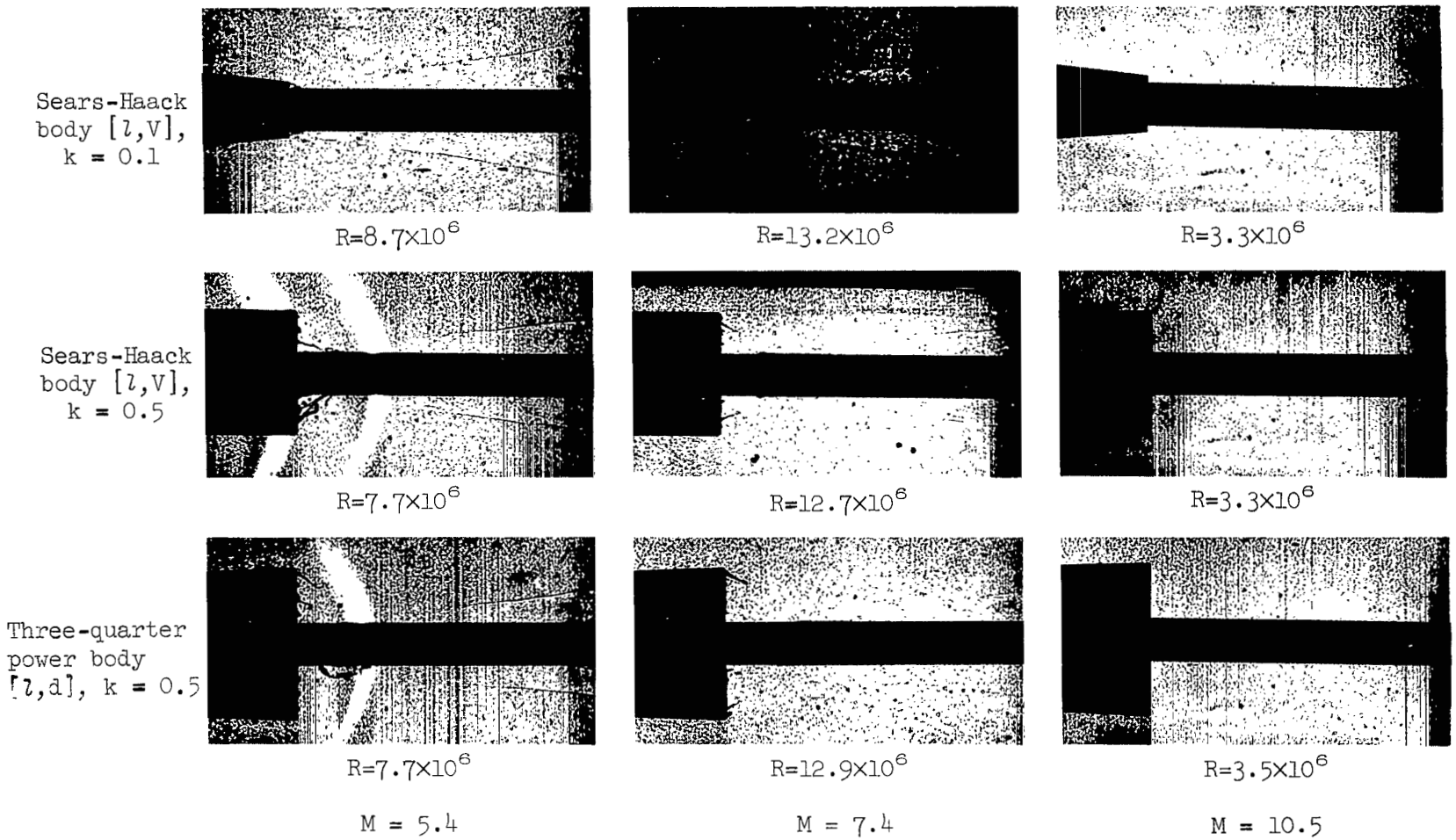

Figure 6.- Shadowgraph pictures of the base region of each model tested in the Ames 3.5-Foot Hypersonic Wind Tunnel.

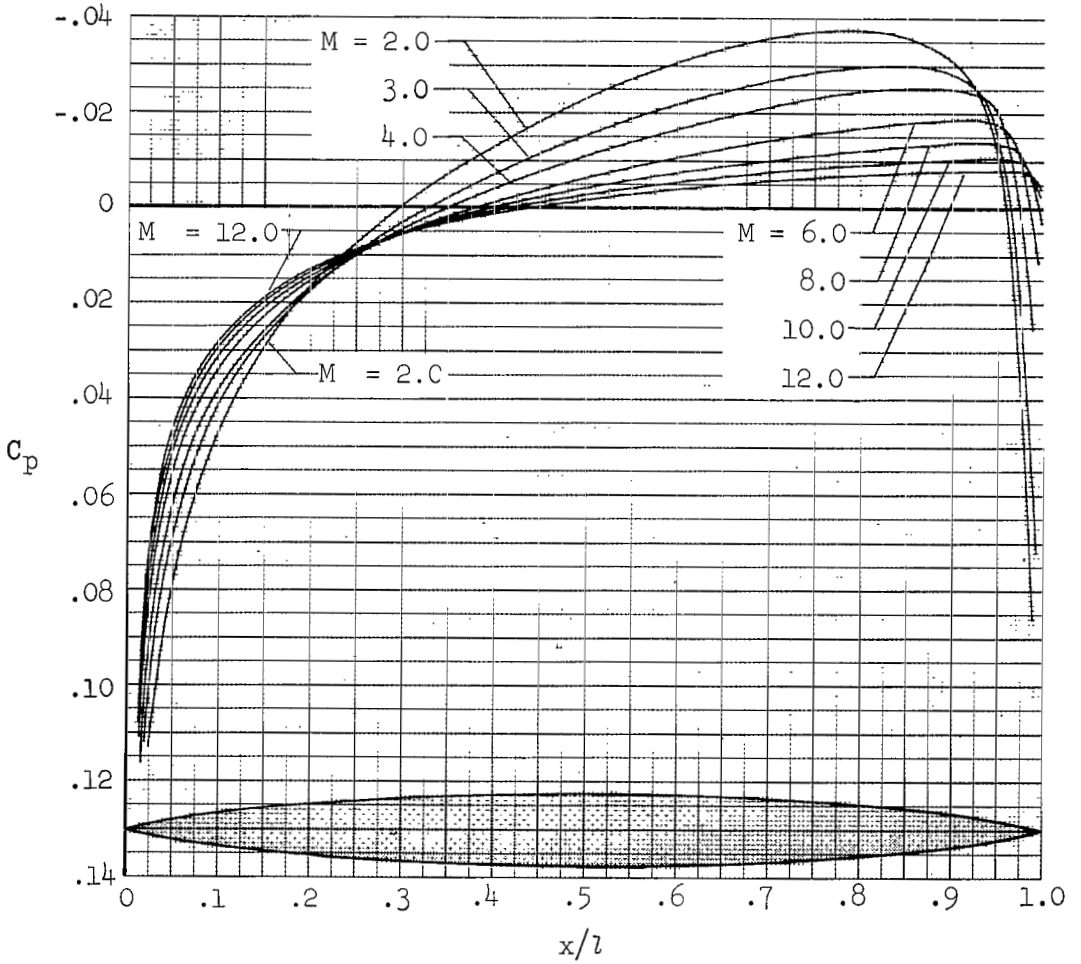

(a) Sears-Haack [l,V], k = 0

Figure 7.- Calculated pressure distributions for the bodies.

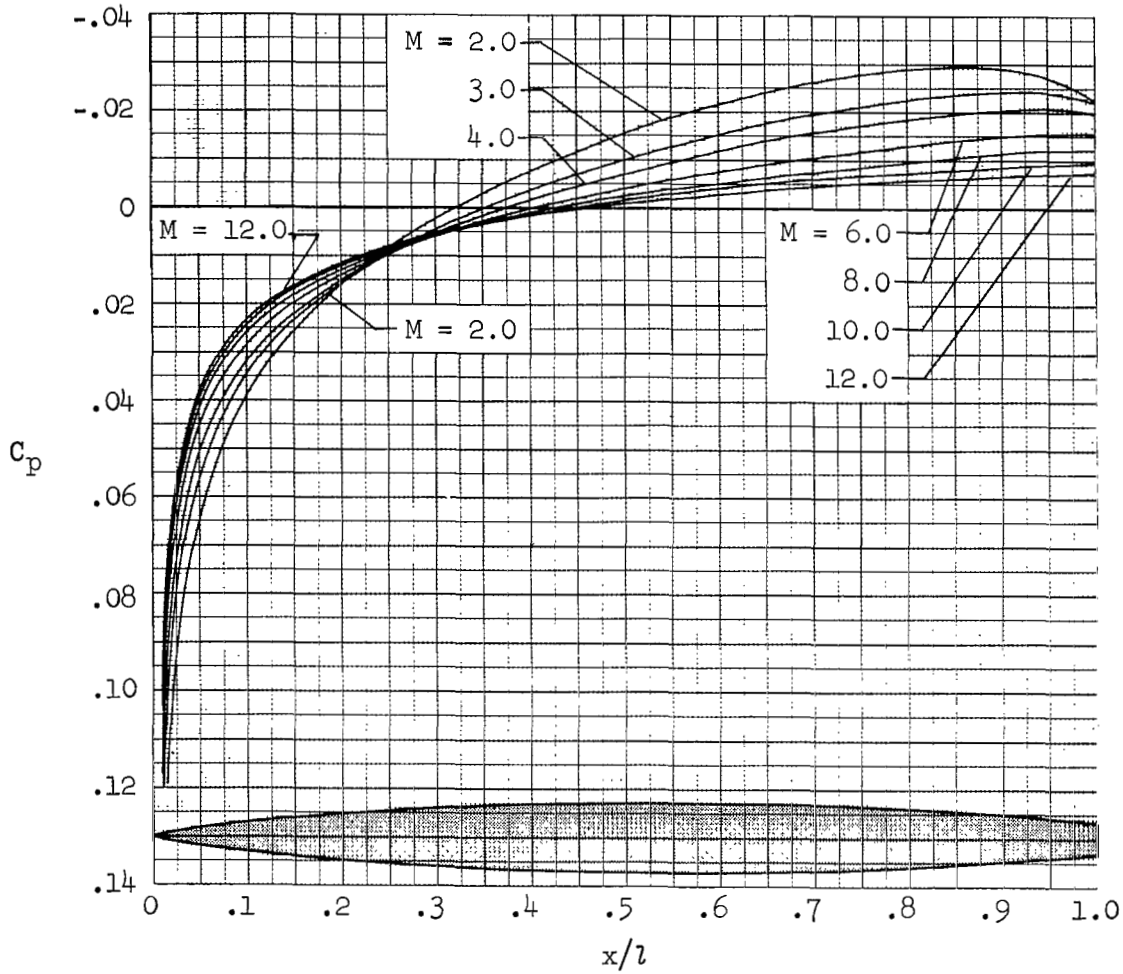

(b) Sears-Haack [l,V], k = 0.1

Figure 7.- Continued.

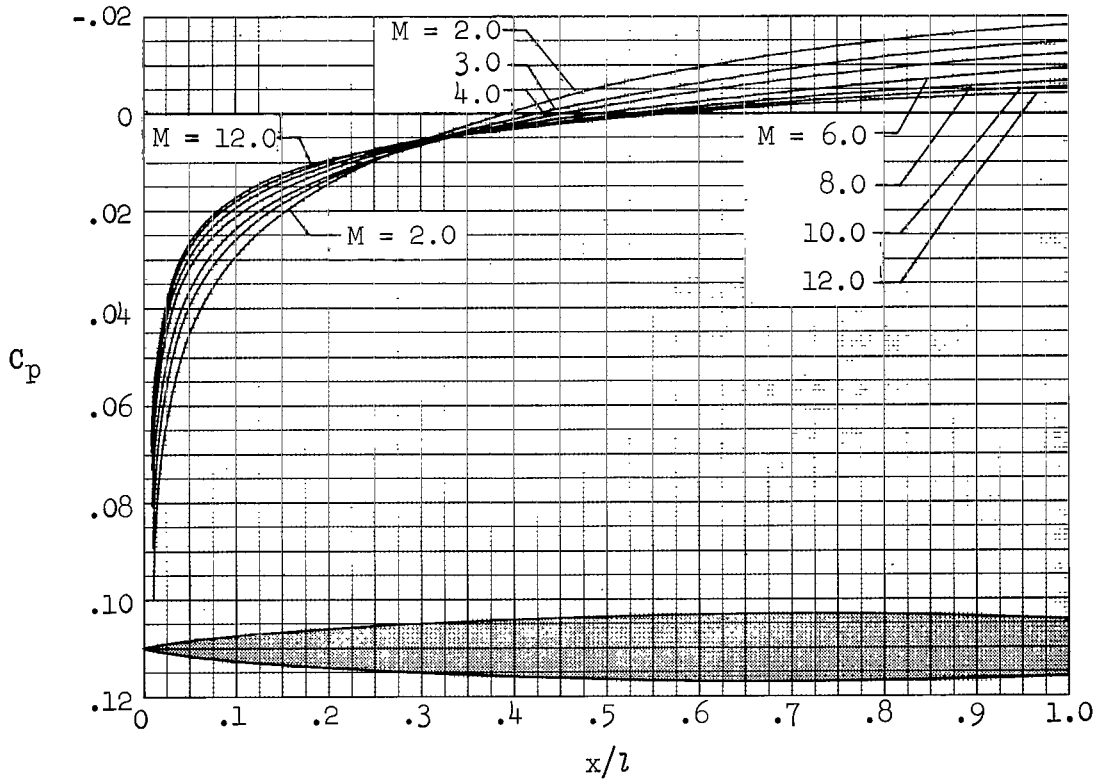

(c) Sears-Haack [l,V], k = 0.3

Figure 7.- Continued.

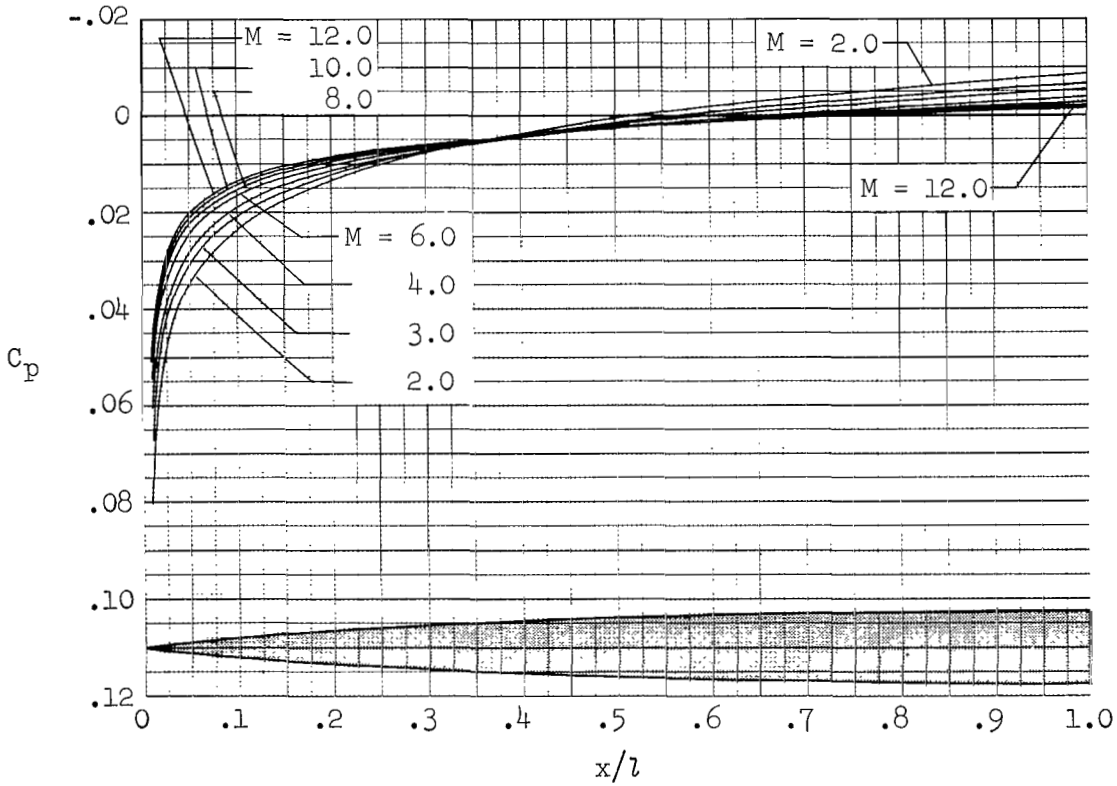

(d) Sears-Haack [l,V], k = 0.5

Figure 7.- Continued.

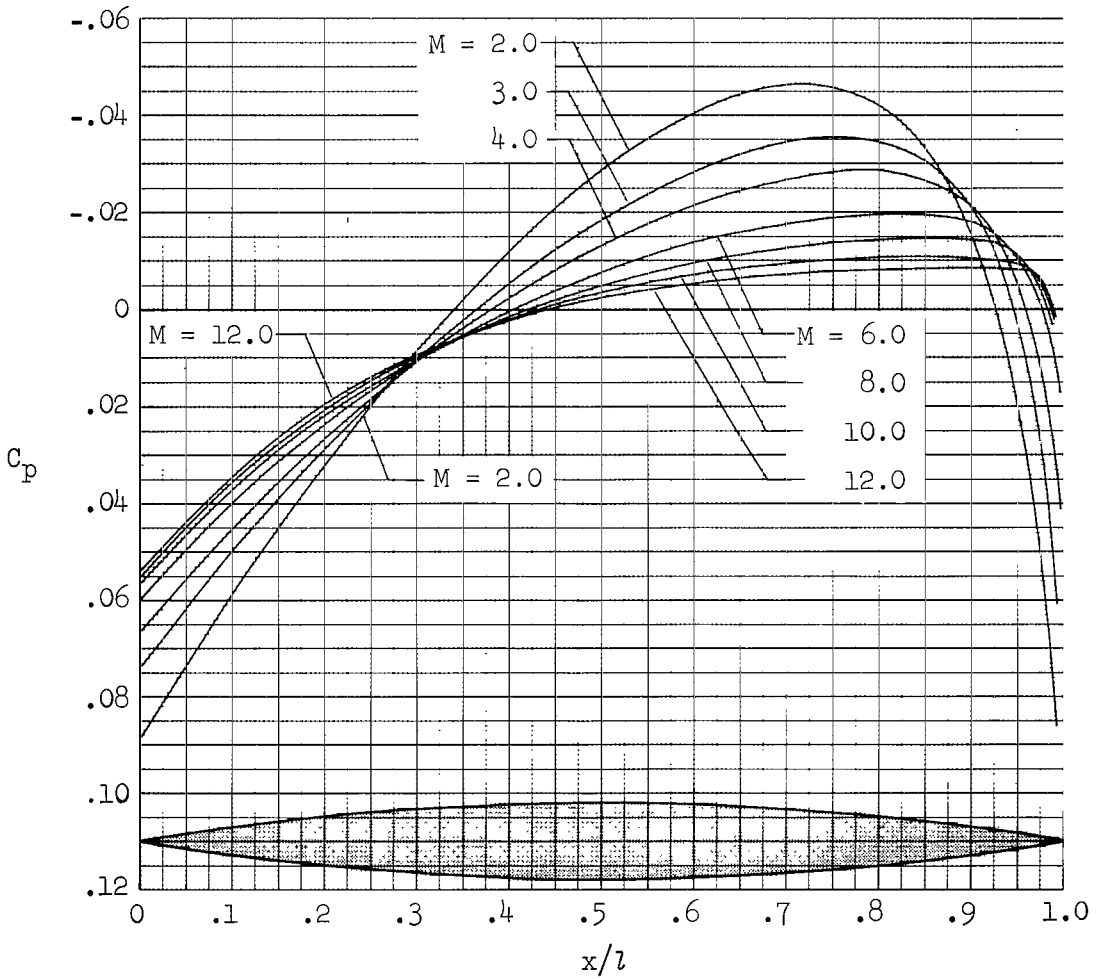

(e) Parabolic arc, k = 0

Figure 7.- Continued.

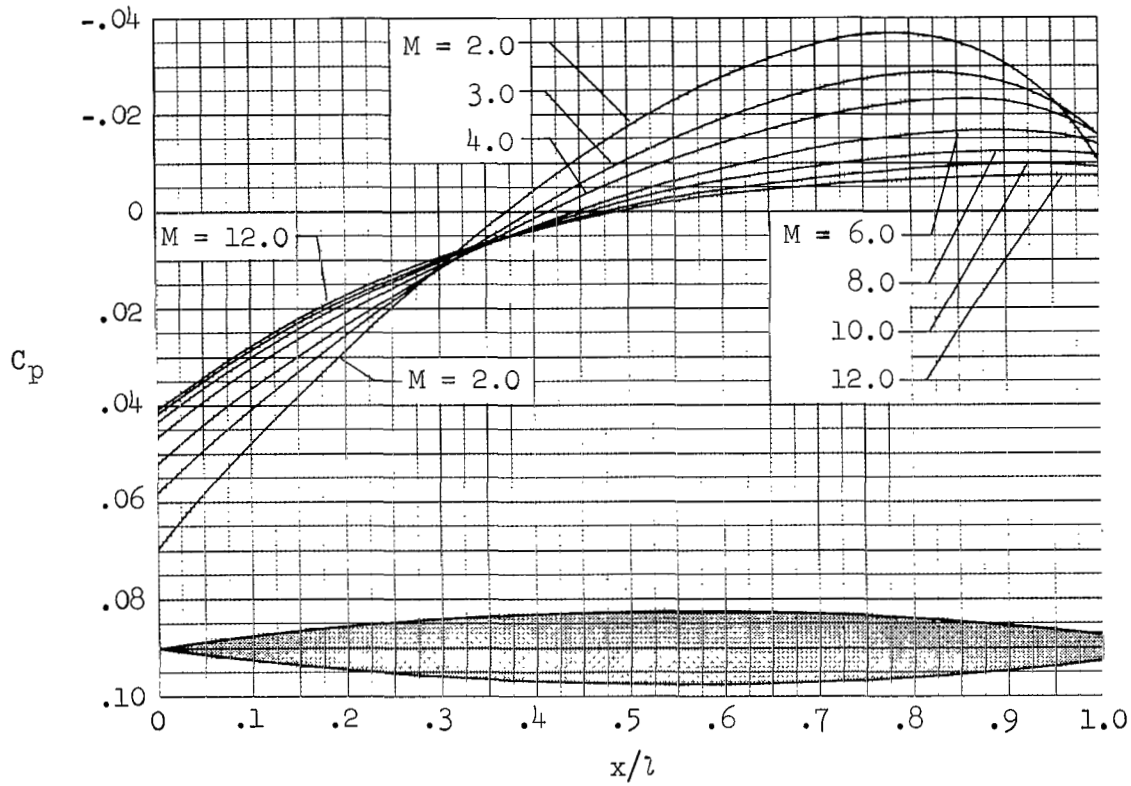

(f) Parabolic arc, k = 0.1

Figure 7.- Continued.

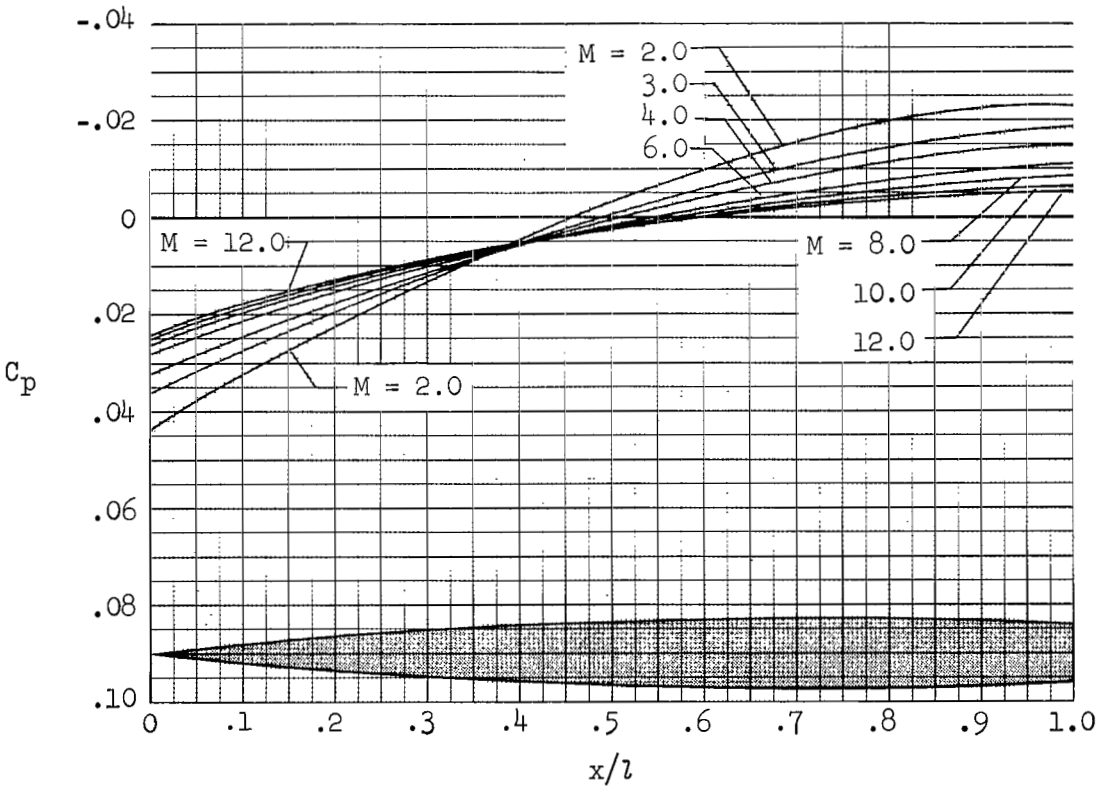

(g) Parabolic arc, k = 0.3

Figure 7.- Continued.

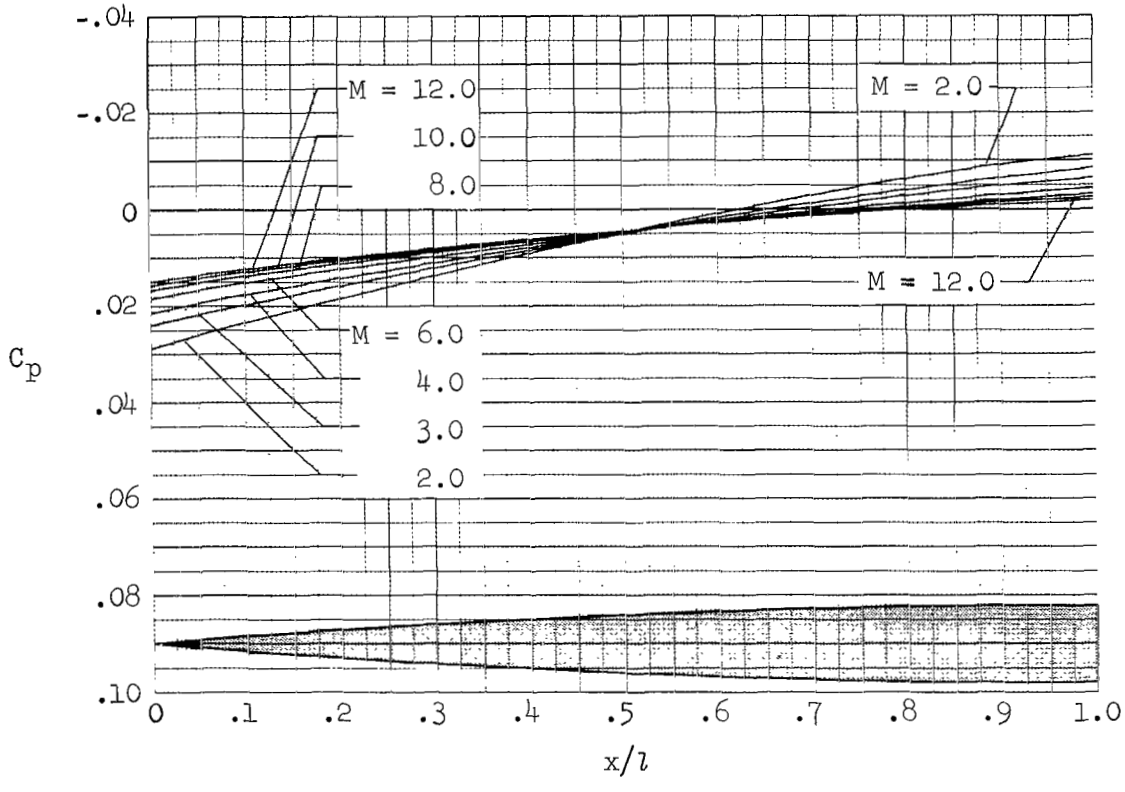

(h) Parabolic arc, k = 0.5

Figure 7.- Continued.

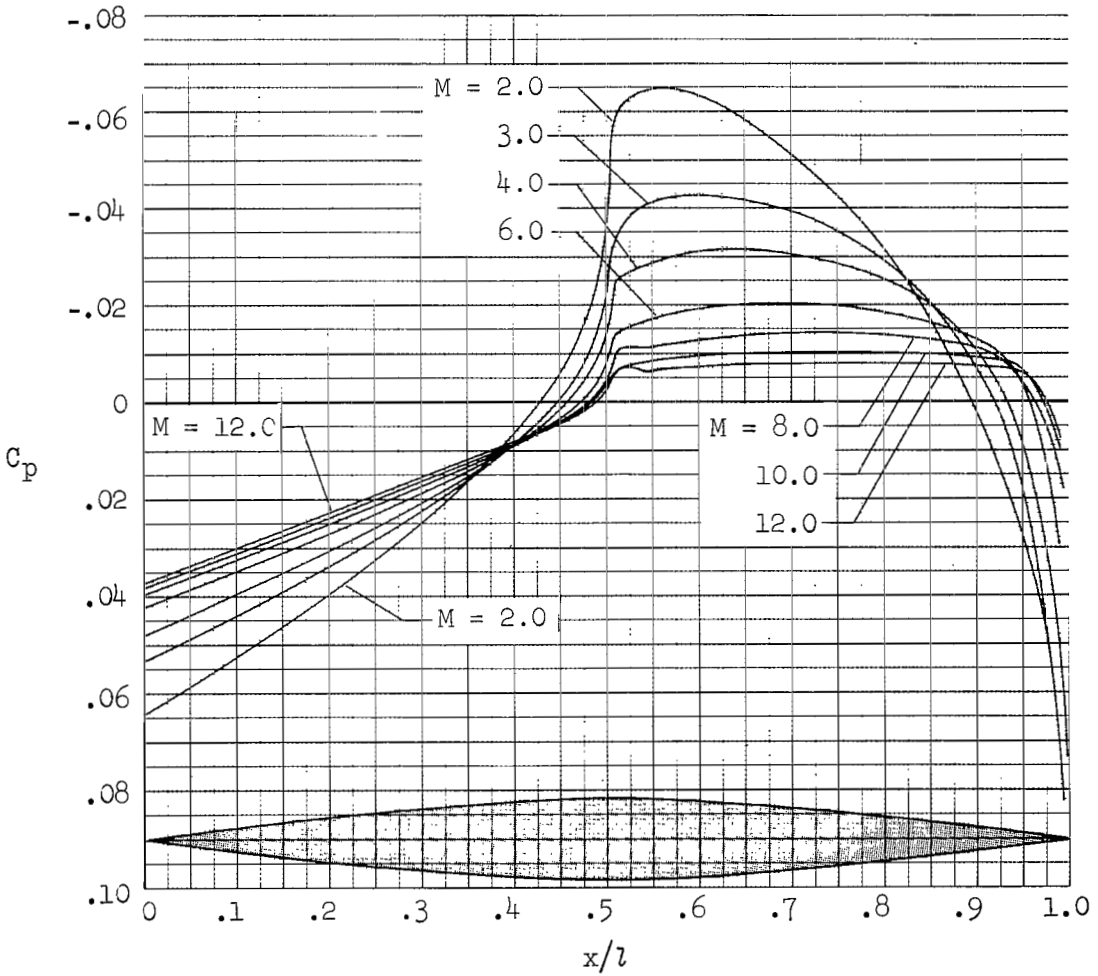

(i) Miele $[S_W,V]$, k = 0

Figure 7.- Continued.

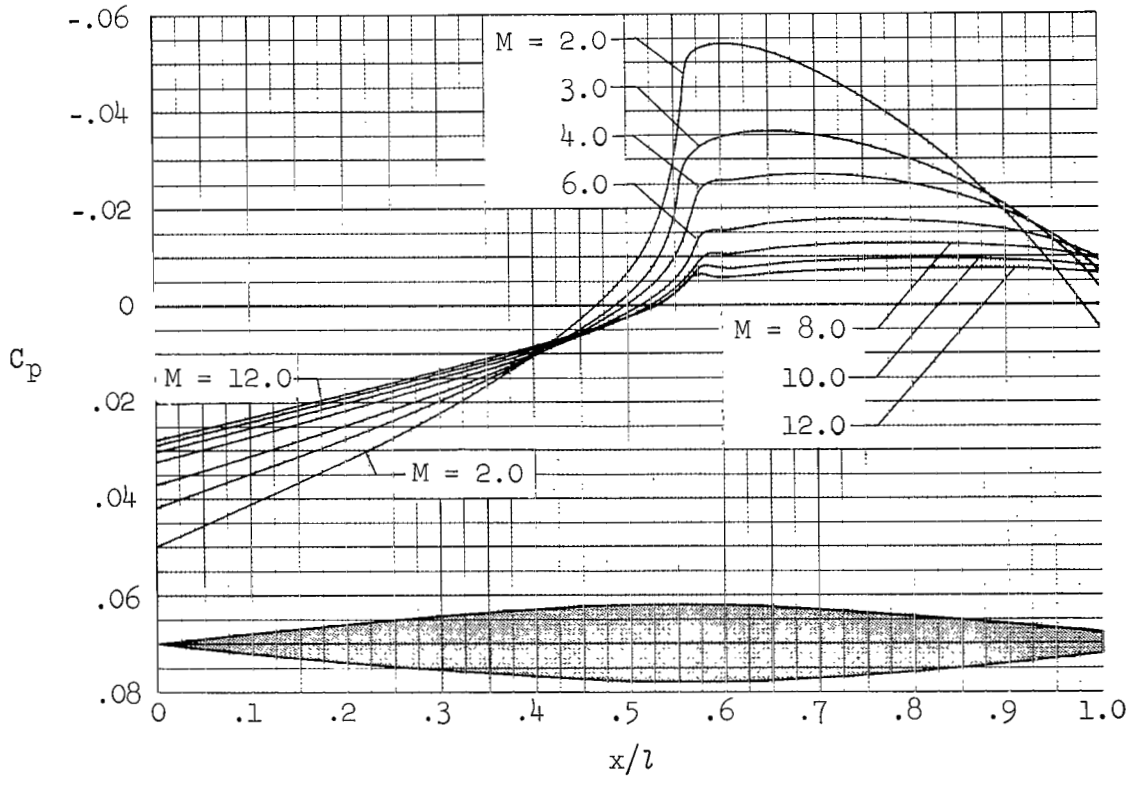

(j) Miele $[S_w,V]$, k = 0.1

Figure 7.- Continued.

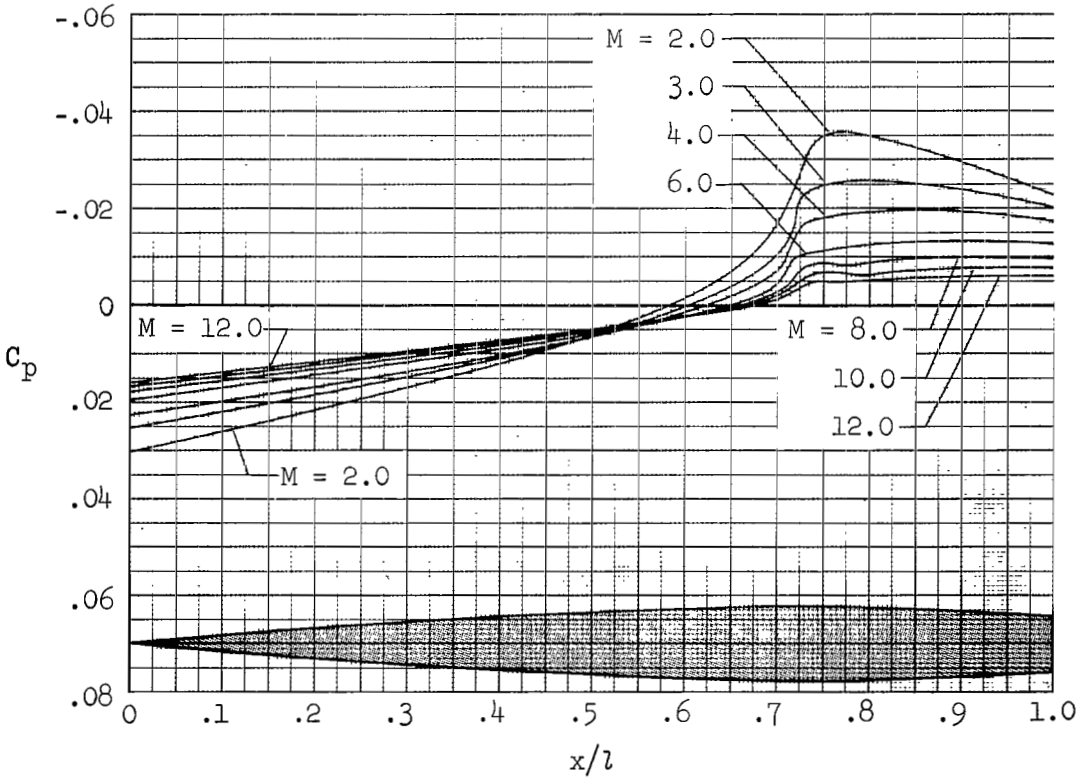

(k) Miele $[S_w,V]$, k = 0.3

Figure 7.- Continued.

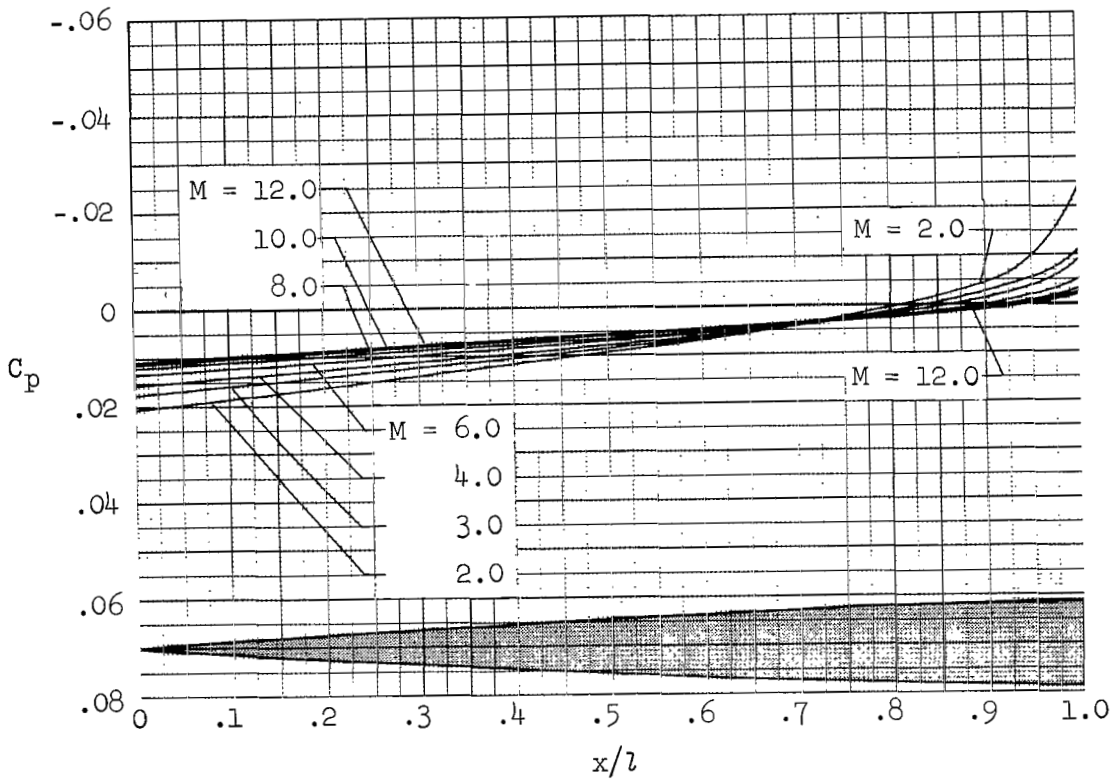

(1) Miele $[S_w,V]$, k = 0.5

Figure 7.- Continued.

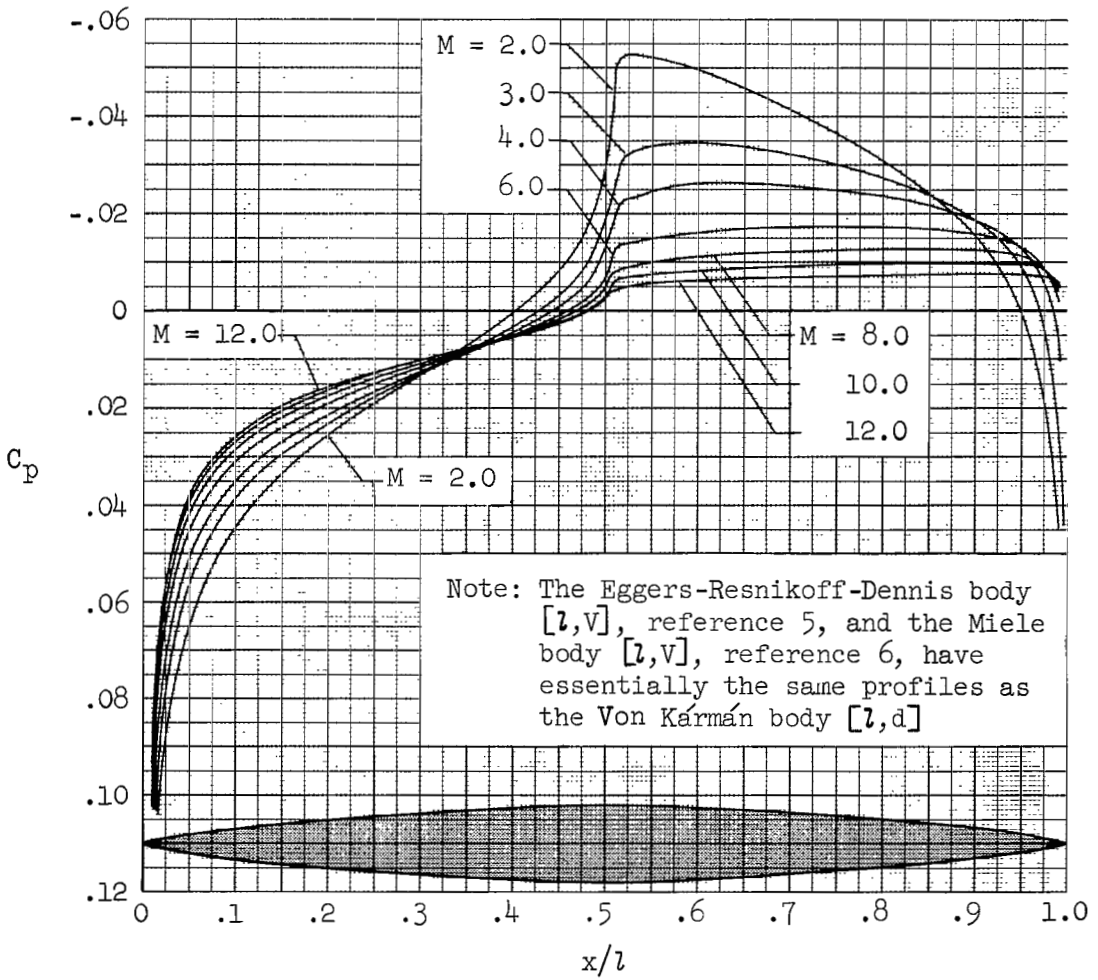

(m) Von Kármán [l,d], k = 0

Figure 7.- Continued.

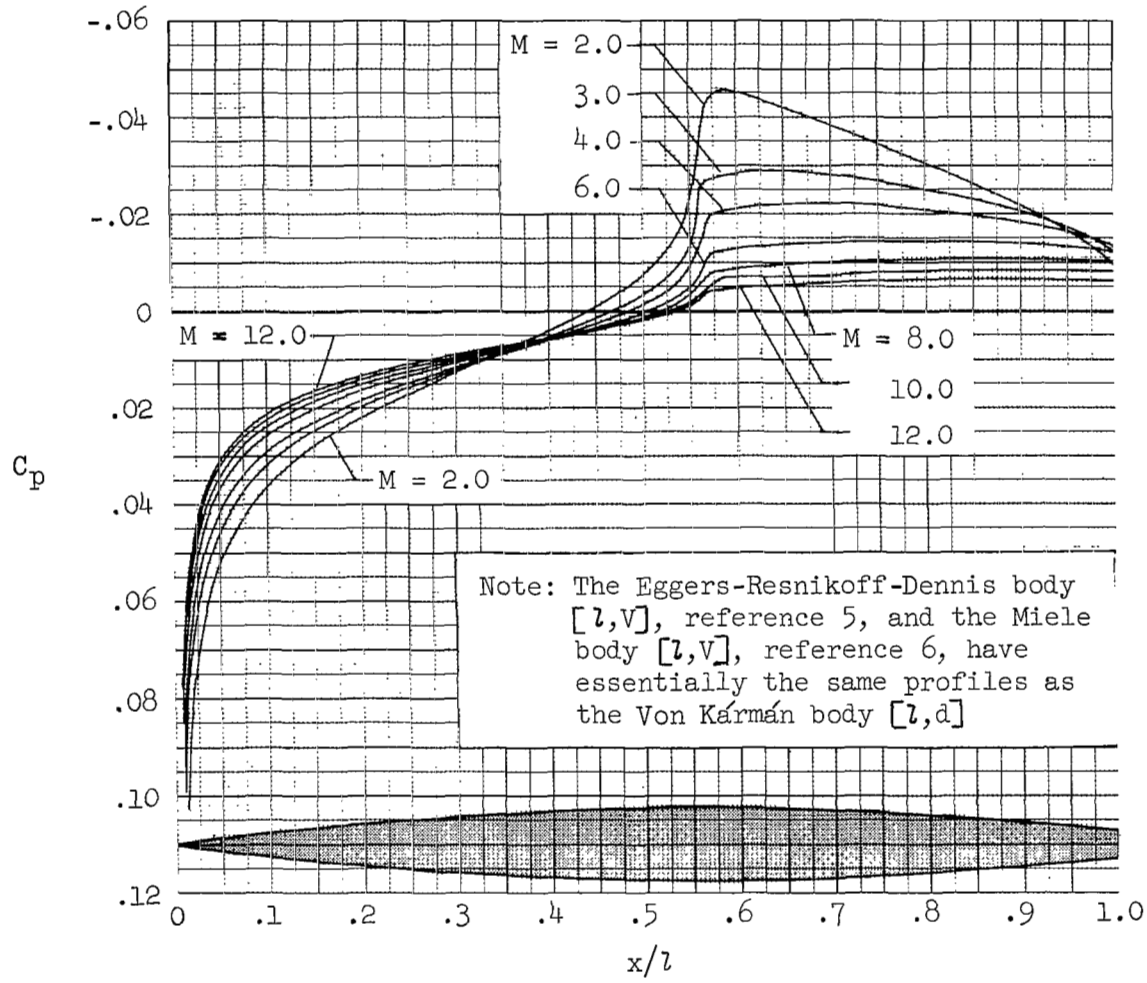

(n) Von Kármán [l,d], k = 0.1

Figure 7.- Continued.

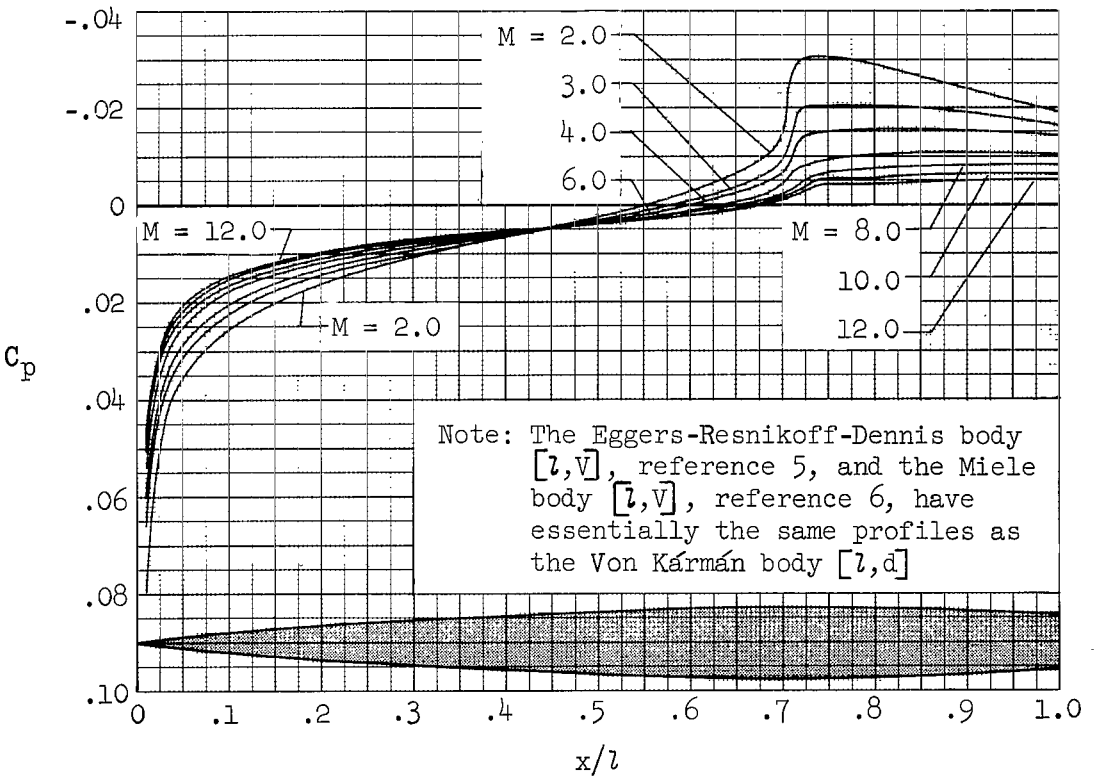

(o) Von Kármán [l,d], k = 0.3

Figure 7.- Continued.

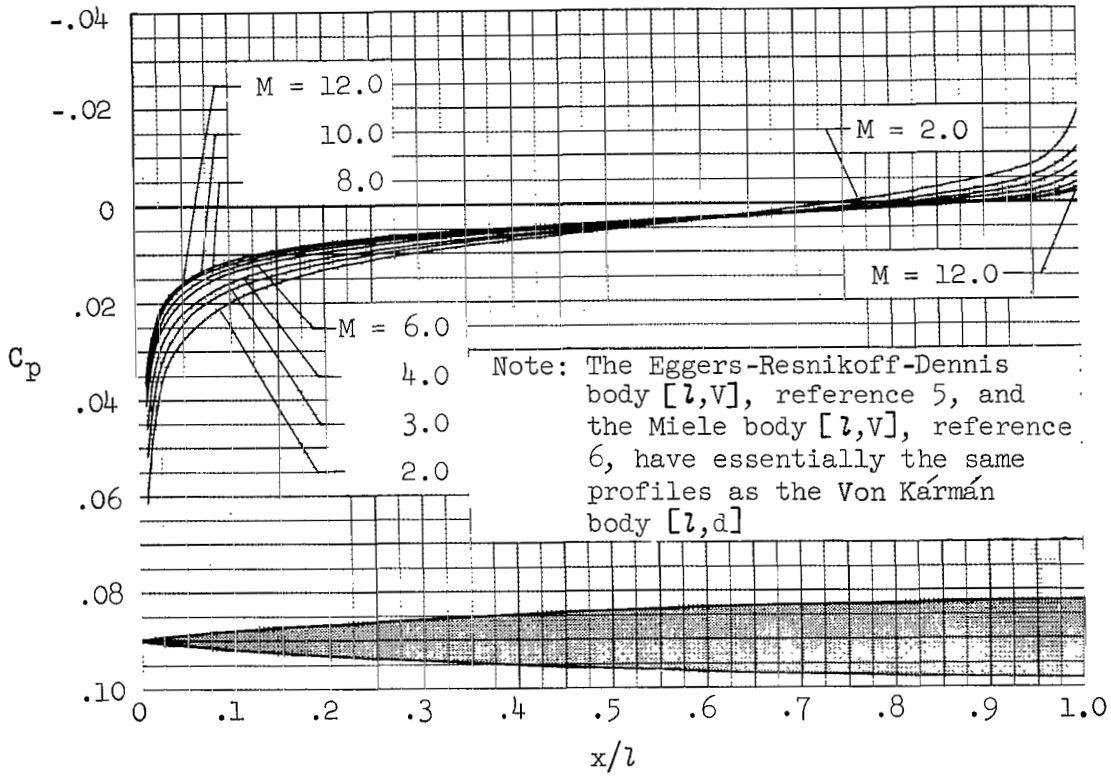

(p) Von Kármán [l,d], k = 0.5

Figure 7.- Continued.

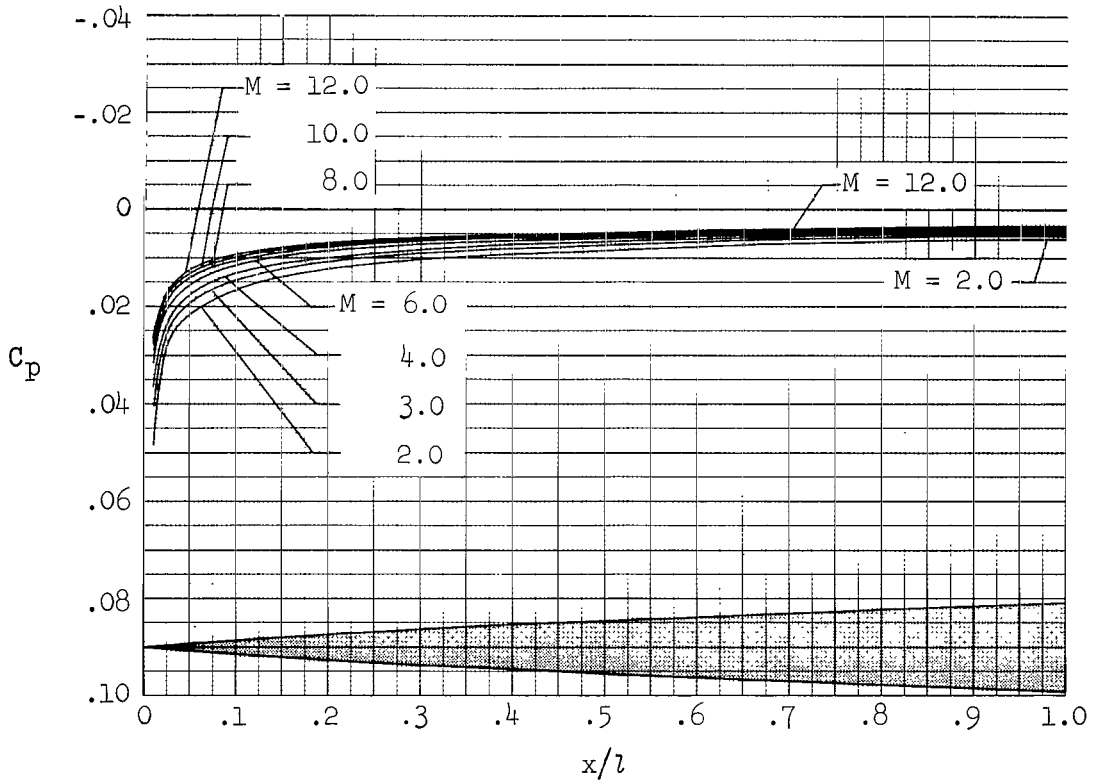

(q) Three-quarter power [l,d], k = 0.5

Figure 7.- Continued.

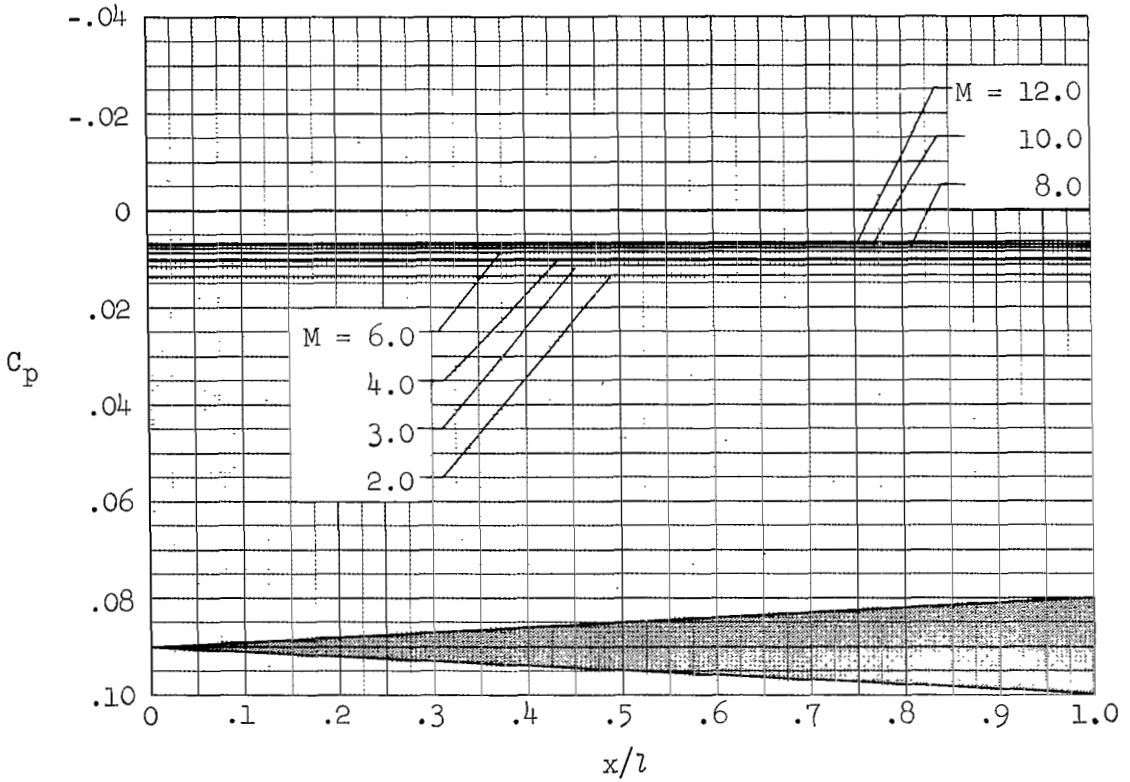

(r) Cone [Sw,d], k = 0.5

Figure 7.- Concluded.

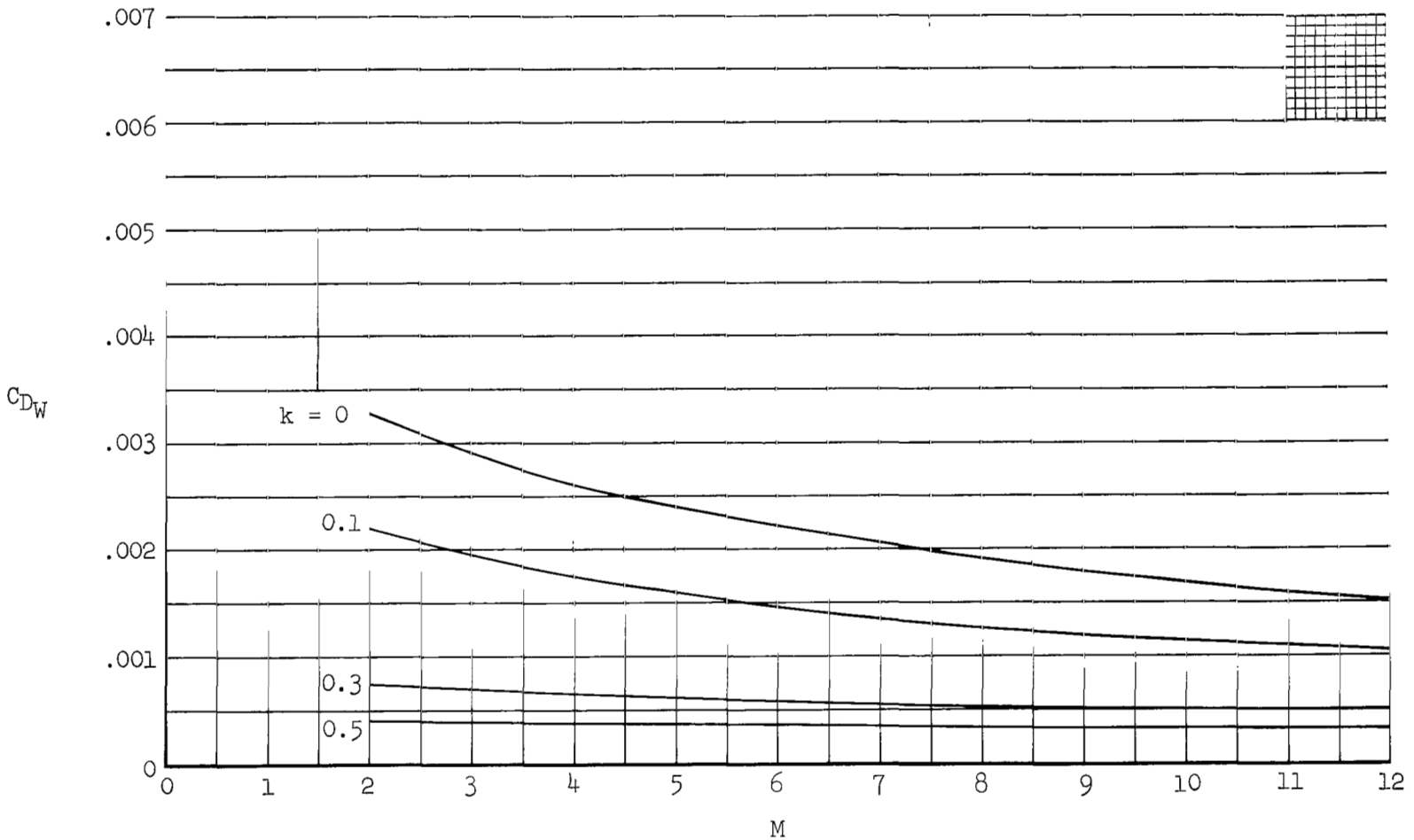

(a) Sears-Haack bodies [l,V]

Figure 8.- Effect of Mach number on the calculated wave-drag coefficients of the bodies, with body cutoff as a parameter.

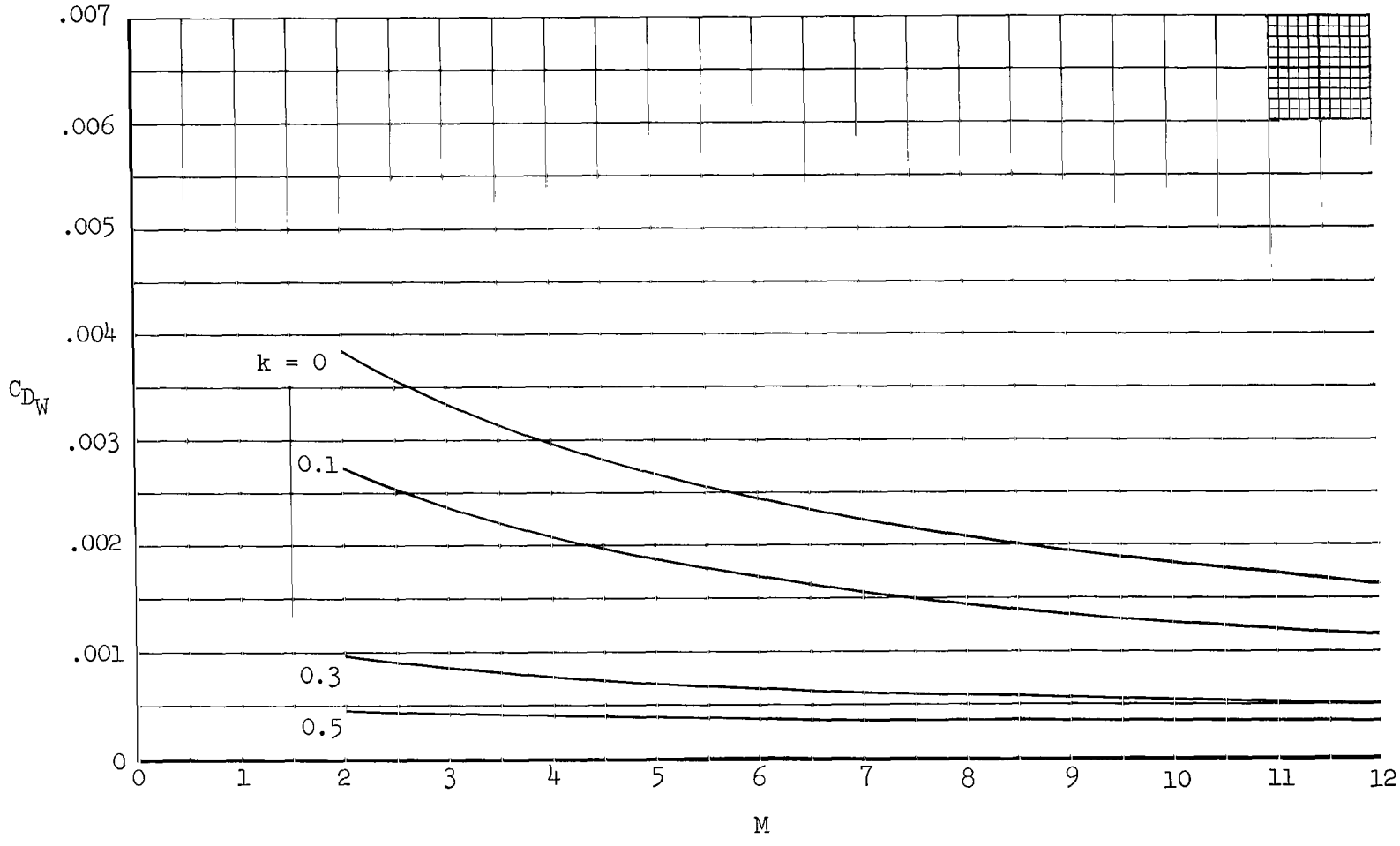

(b) Parabolic-arc bodies

Figure 8.- Continued.

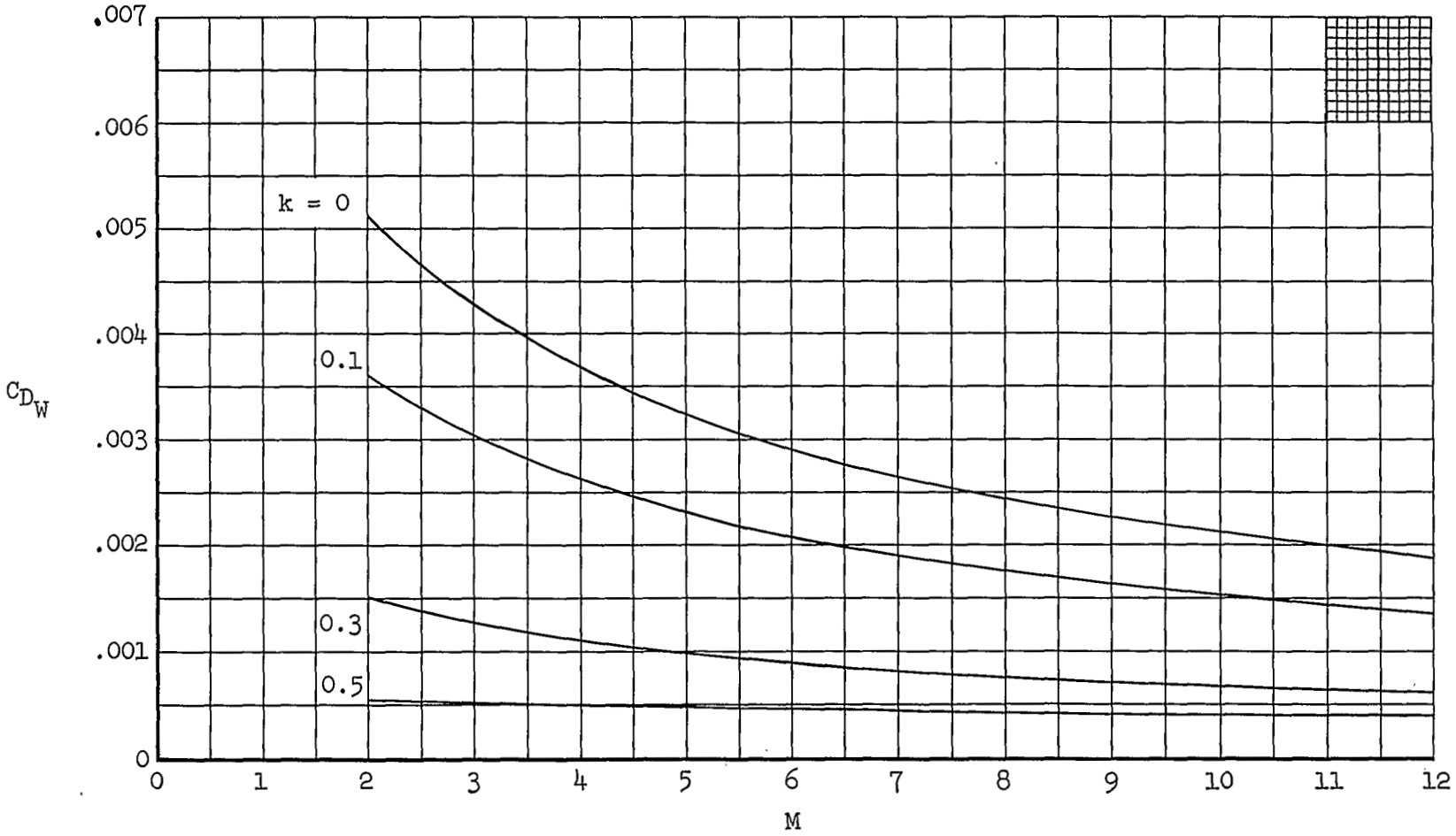

(c) Miele bodies [S_W,V]

Figure 8.- Continued.

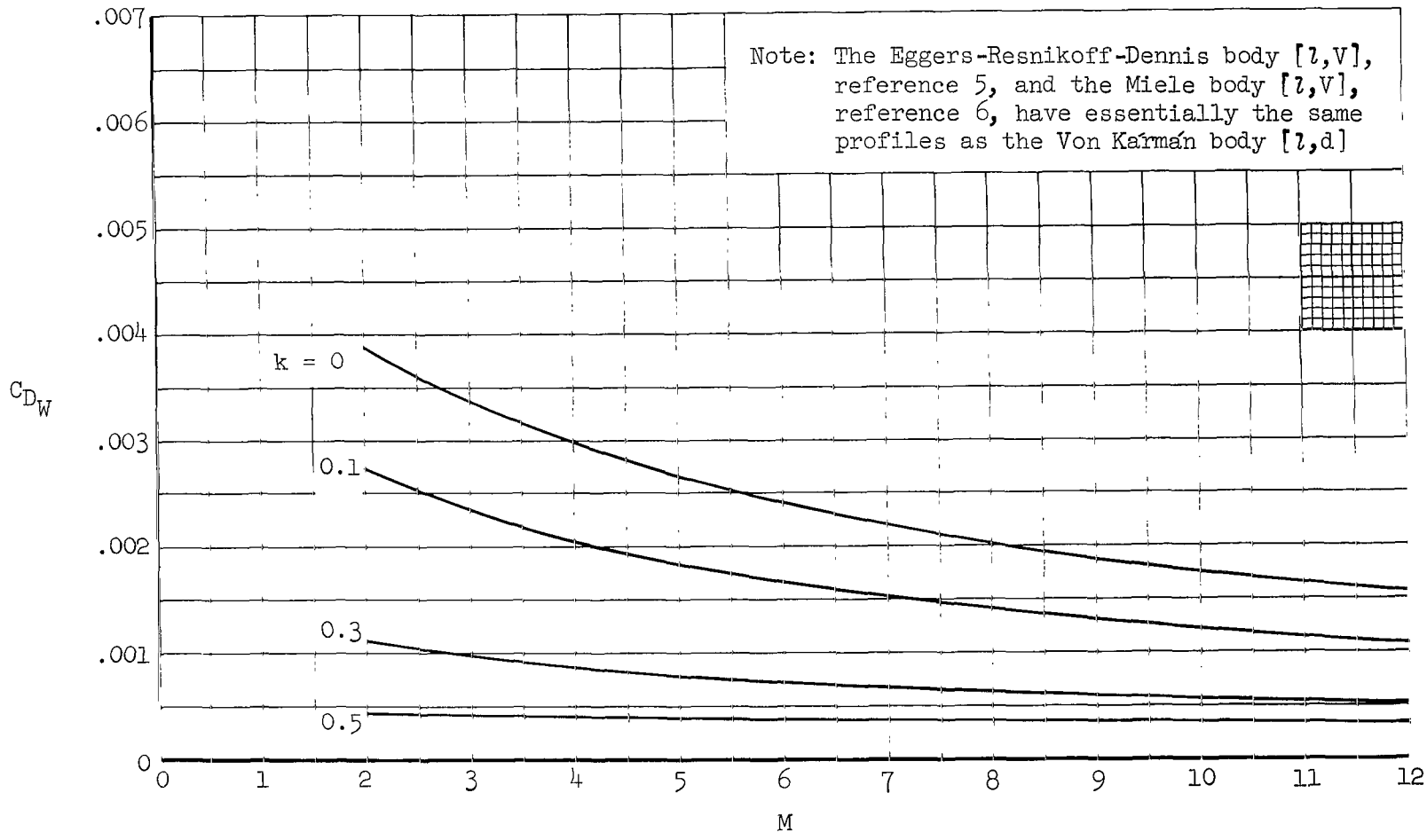

(d) Von Kármán bodies [l,d]

Figure 8.- Continued.

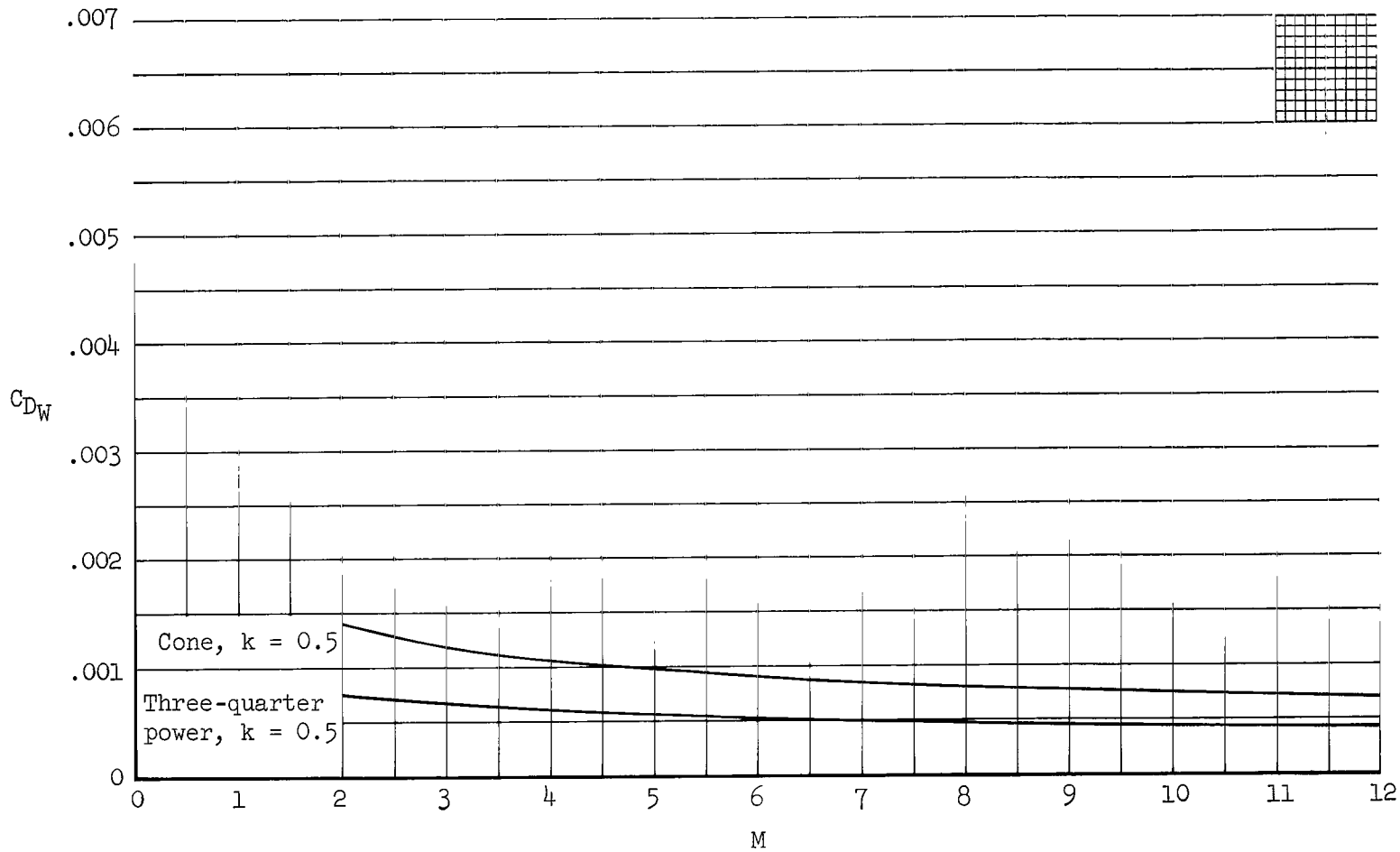

(e) Cone [S_W,d] and three-quarter power [l,d] bodies

Figure 8.- Concluded.

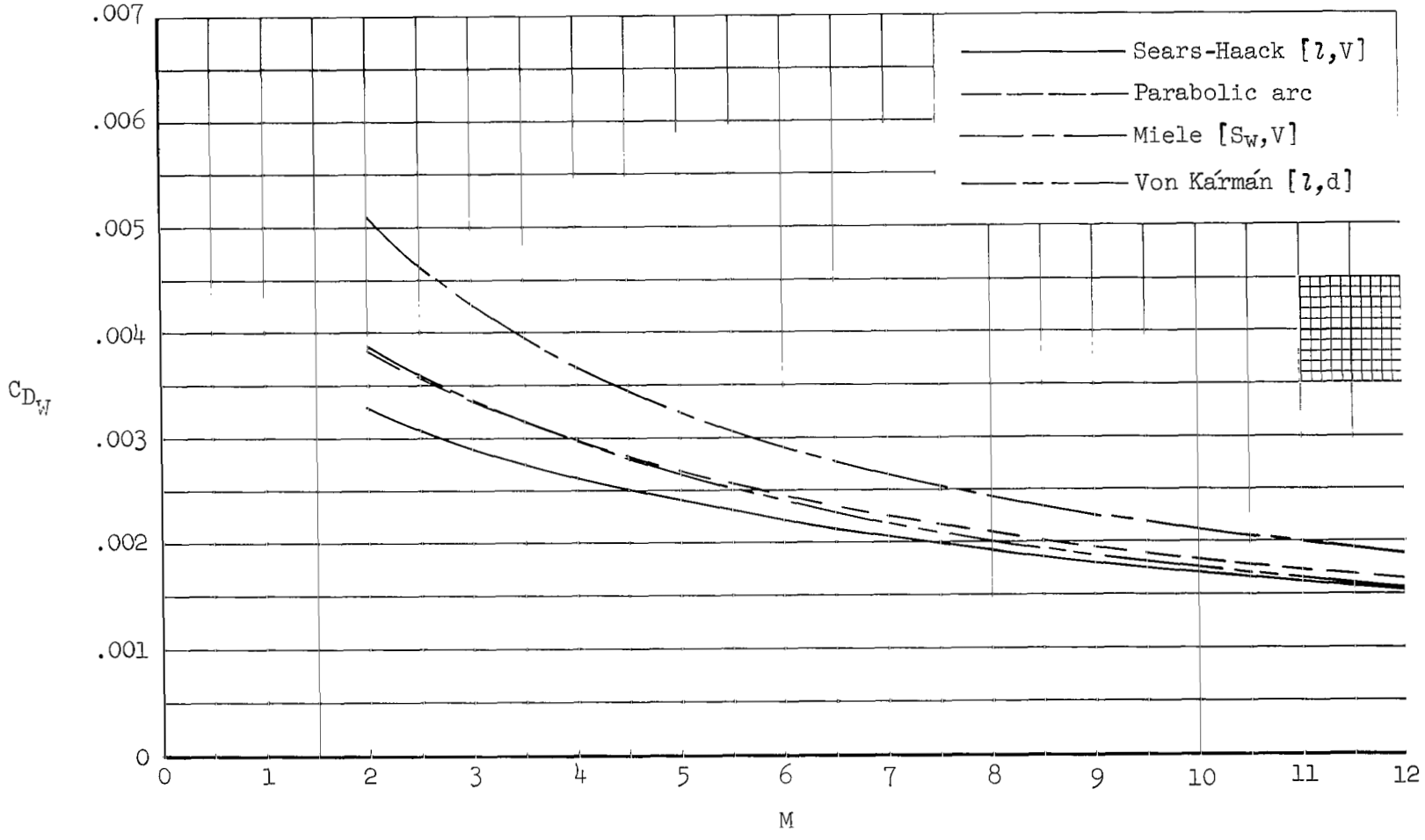

(a) k = 0

Figure 9.- Comparison of the calculated wave-drag coefficients of the bodies as a function of Mach number, for constant values of body cutoff.

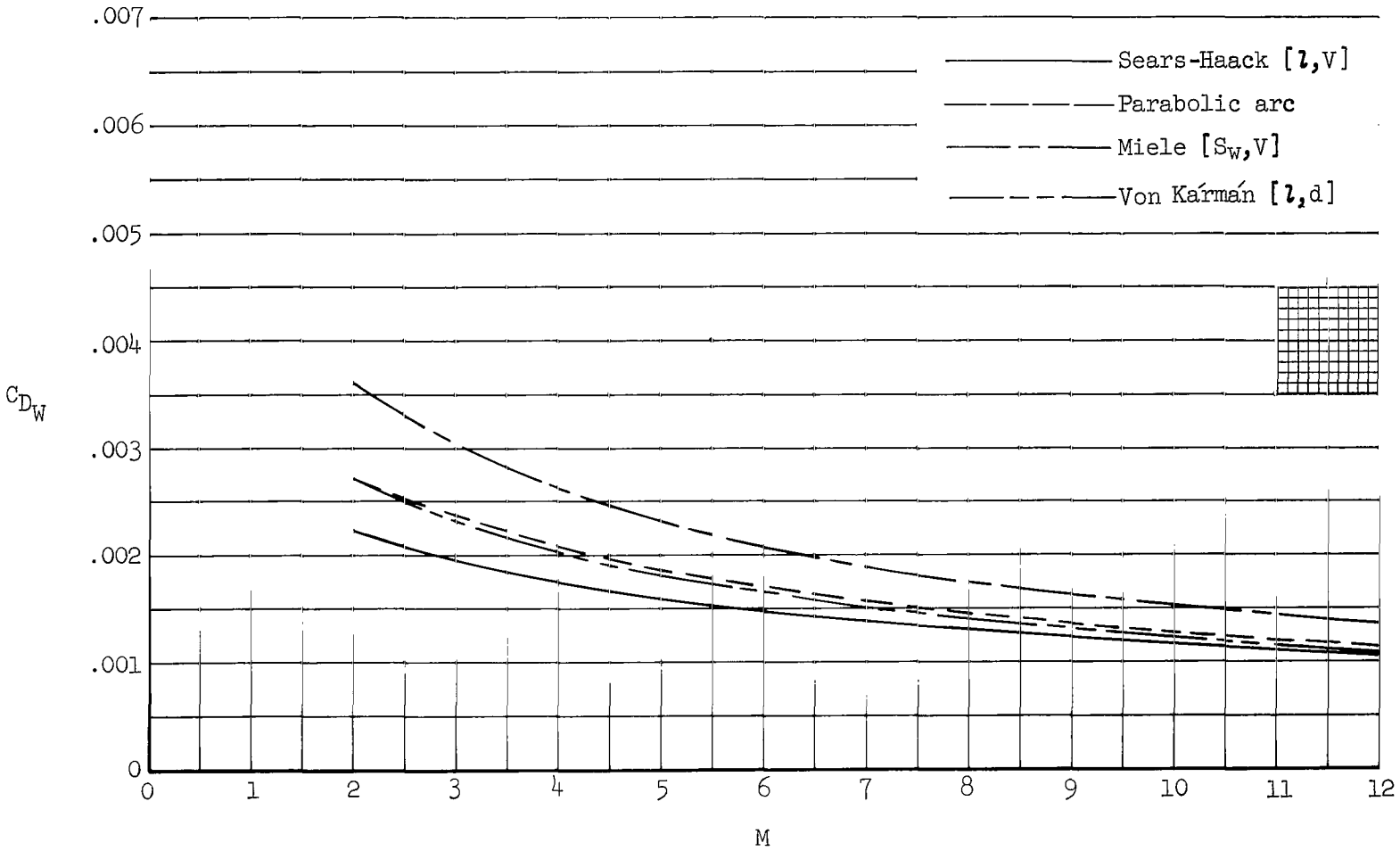

(b) k = 0.1

Figure 9.- Continued.

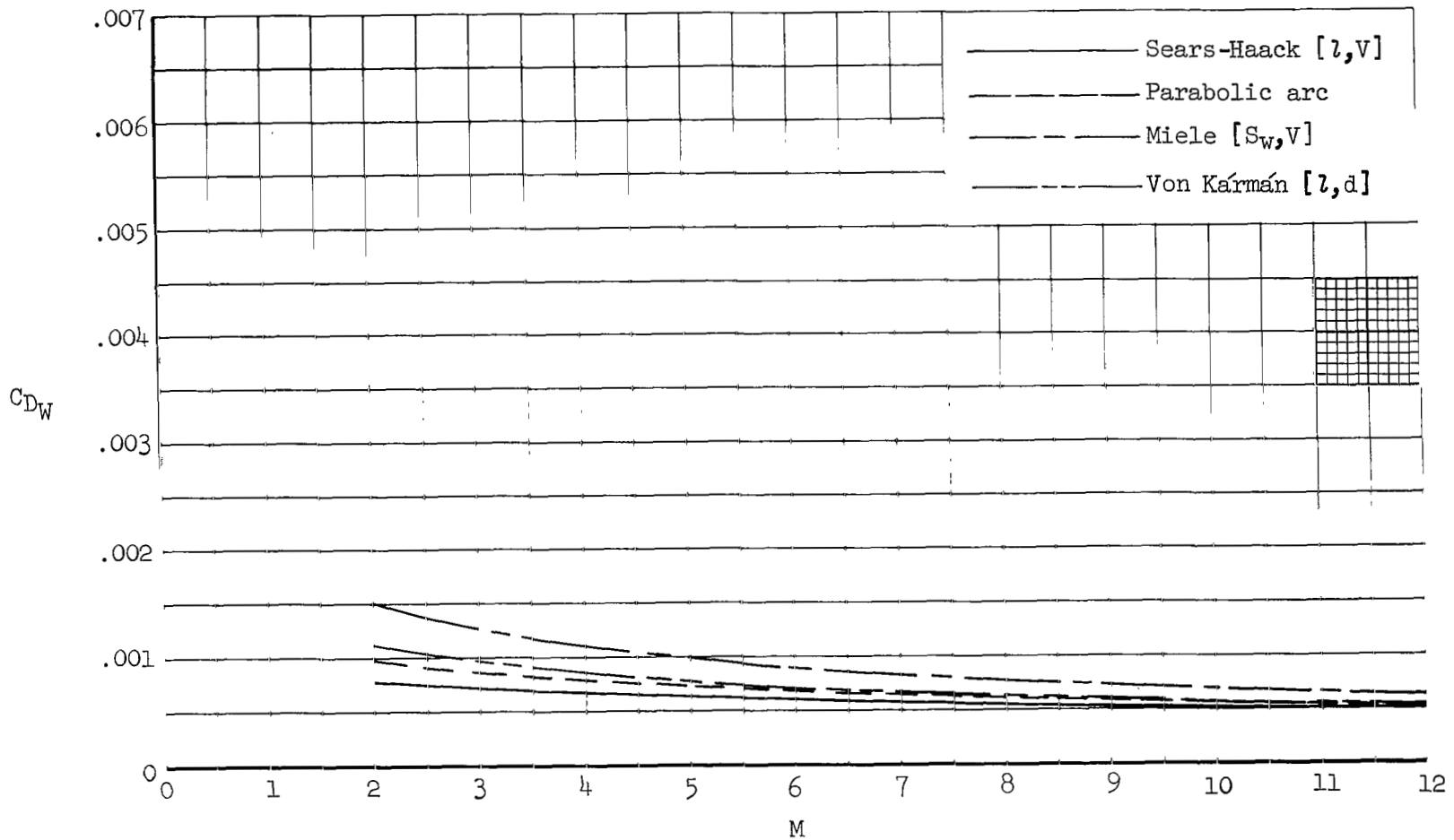

(c) k = 0.3

Figure 9.- Continued.

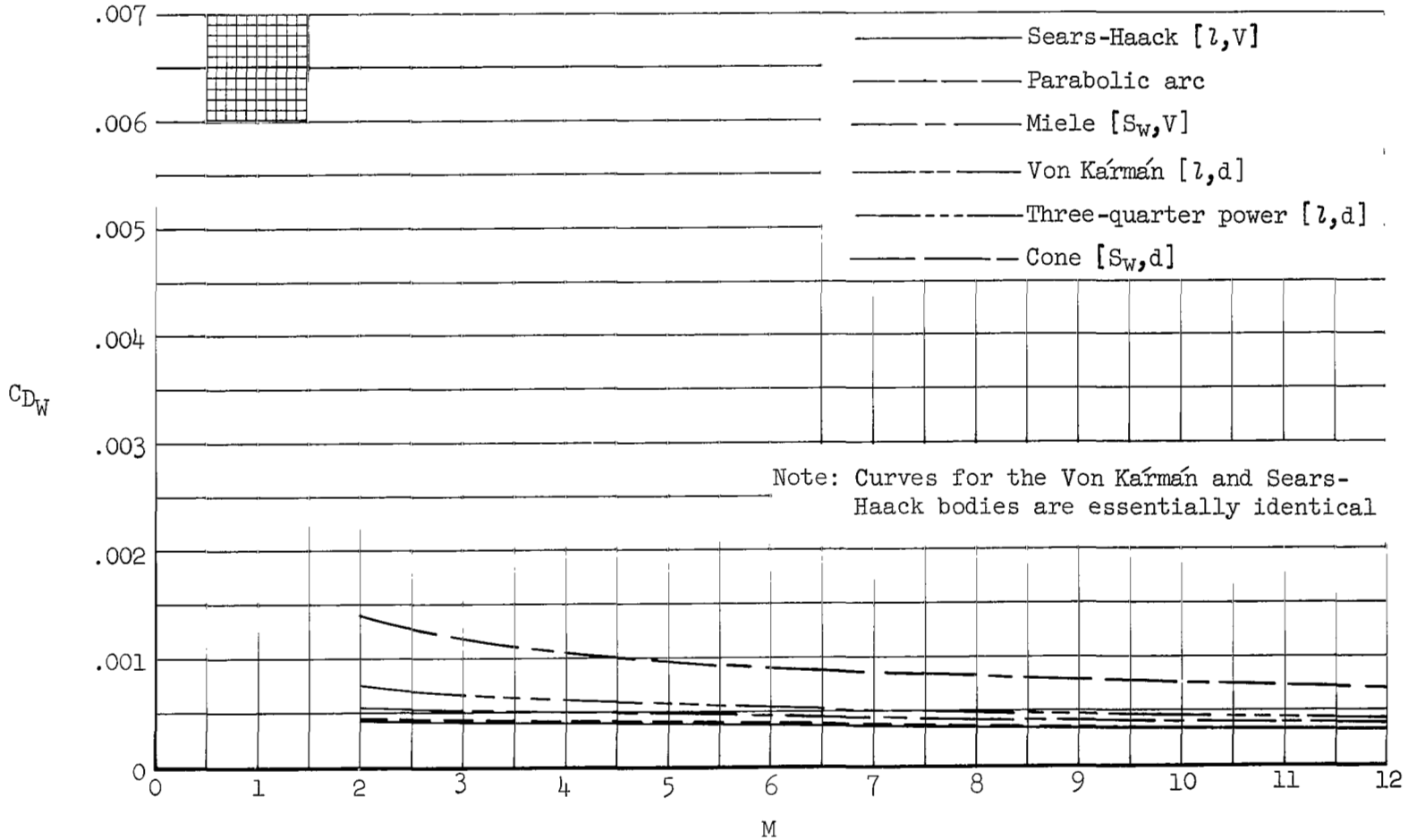

(d) k = 0.5

Figure 9.- Concluded.

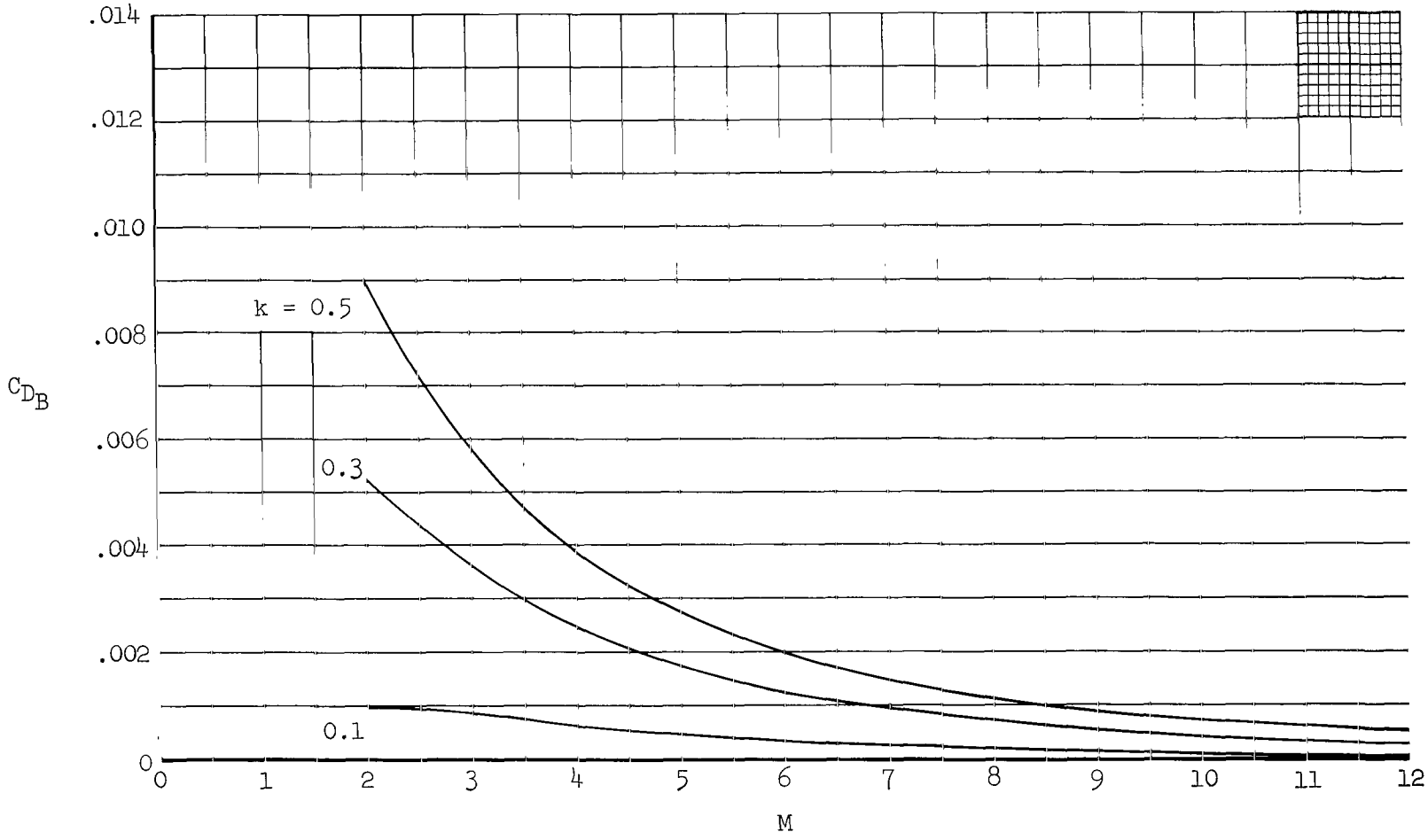

(a) Sears-Haack bodies [l,V]

Figure 10.- Effect of Mach number on the calculated base-drag coefficients of the bodies, with body cutoff as a parameter.

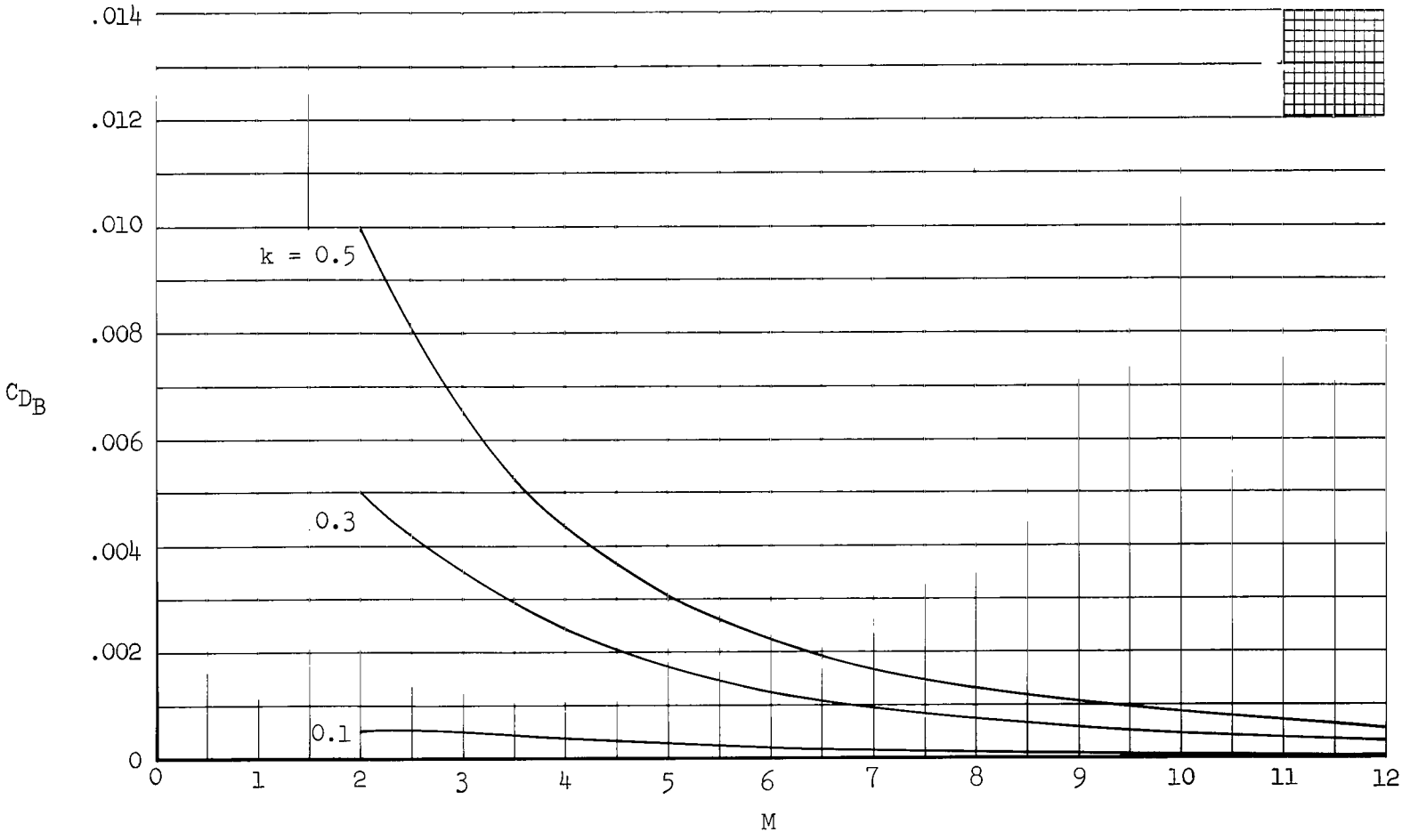

(b) Parabolic-arc bodies

Figure 10.- Continued.

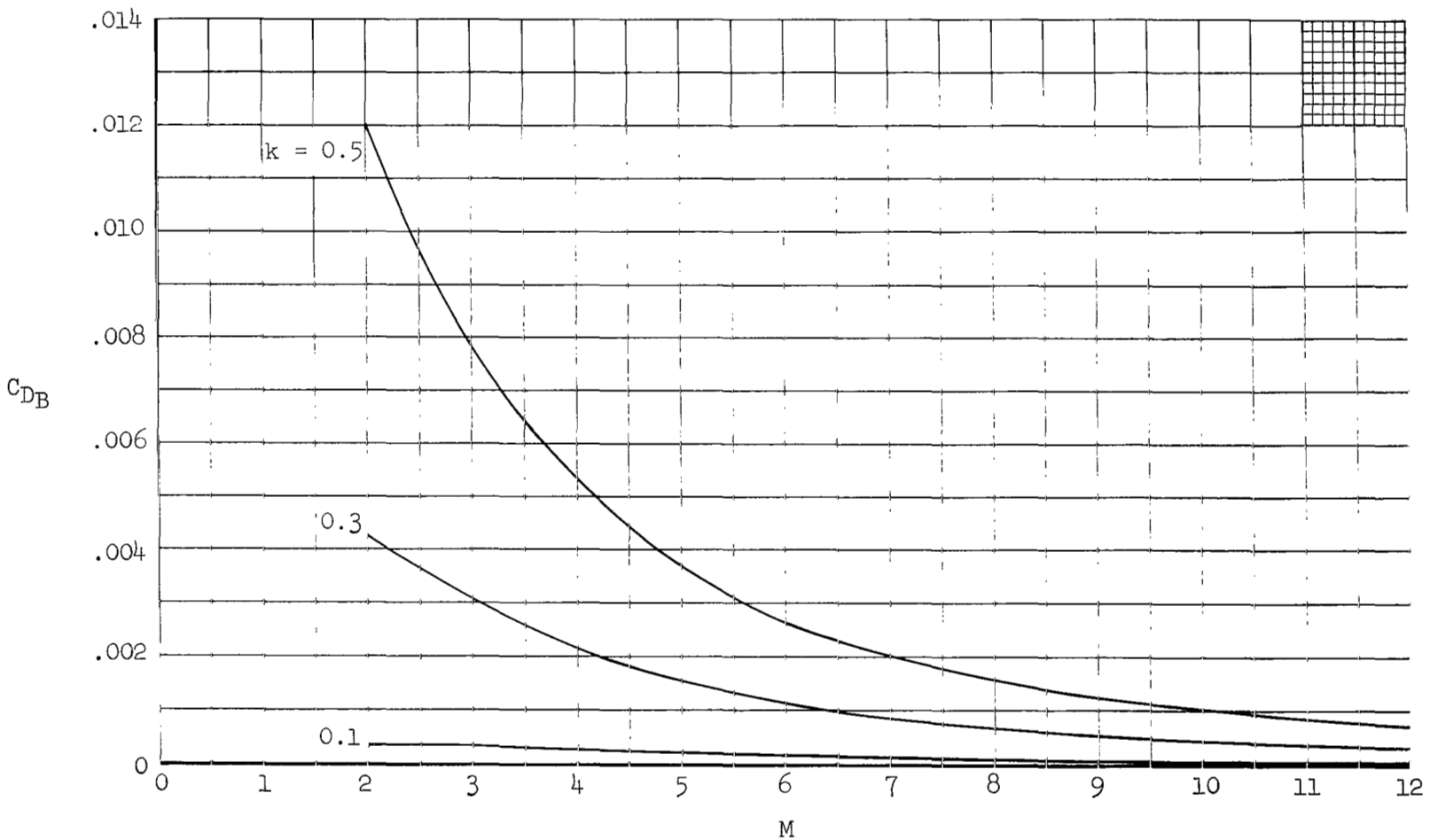

(c) Miele bodies [S_W,V]

Figure 10.- Continued.

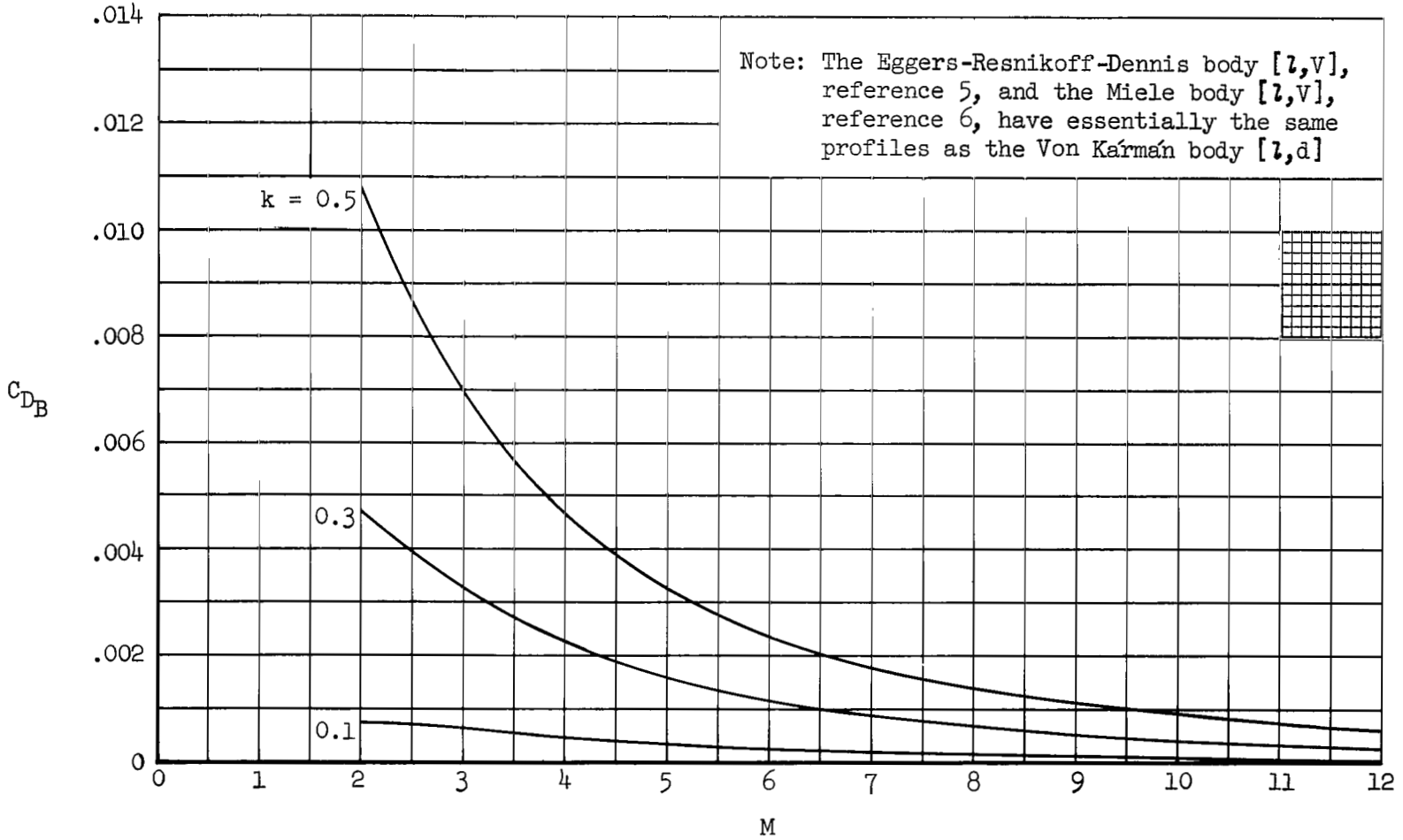

(d) Von Kármán bodies [1,d]

Figure 10.- Continued.

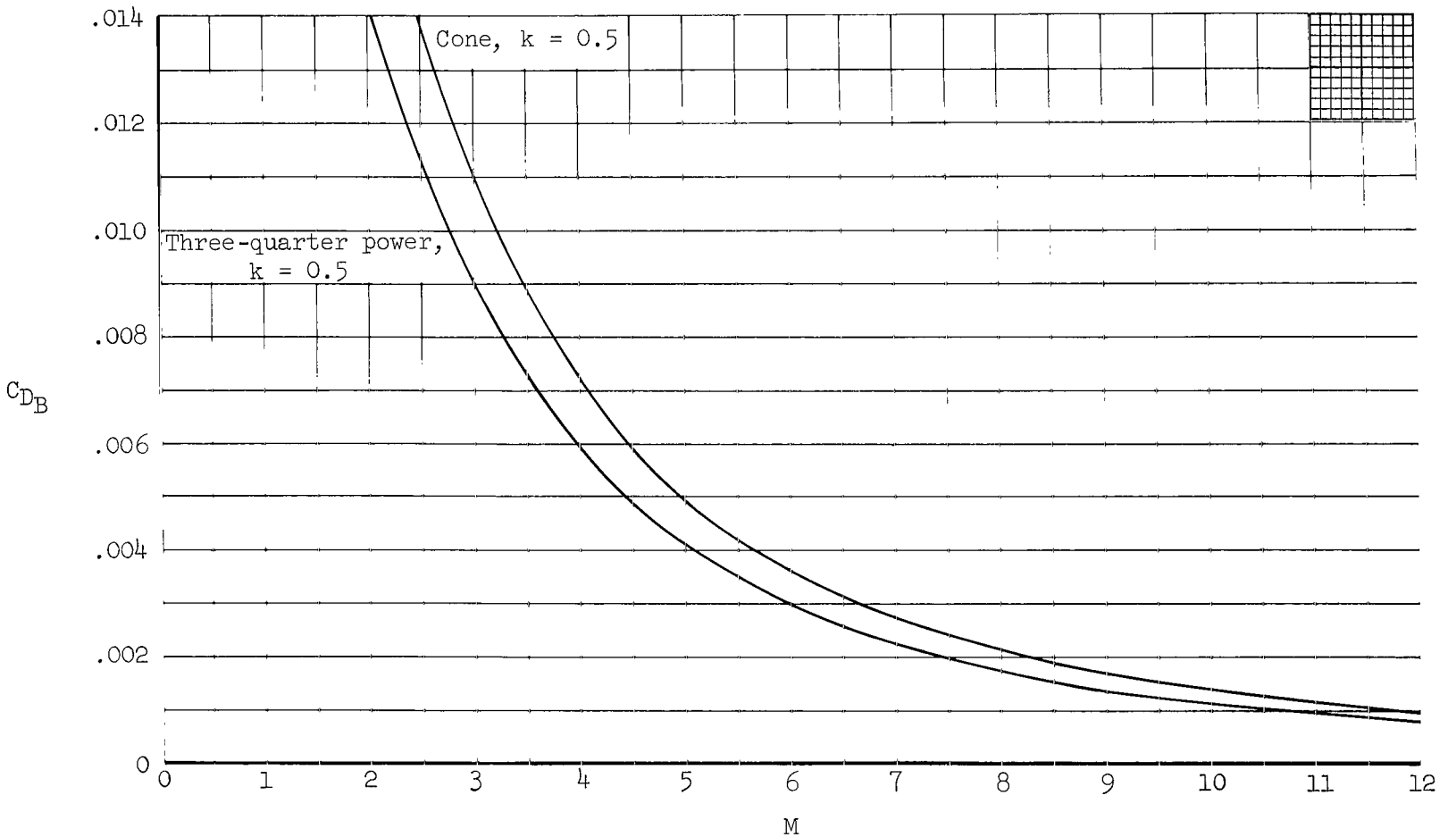

(e) Cone [S_w,d] and three-quarter power [l,d] bodies

Figure 10.- Concluded.

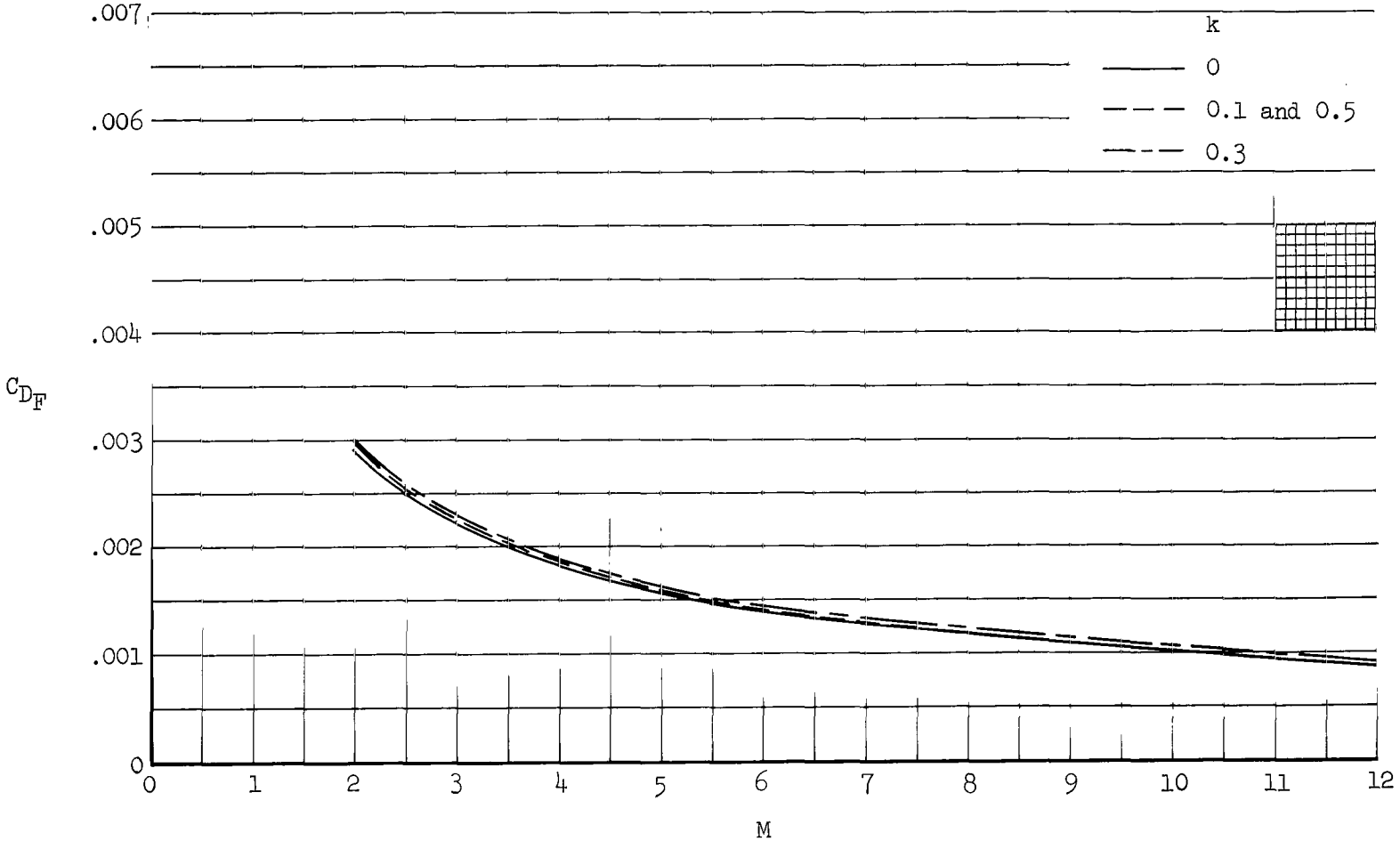

(a) Sears-Haack bodies [l,V]

Figure 11.- Effect of Mach number on the calculated skin-friction-drag coefficients of the bodies, with body cutoff as a parameter.

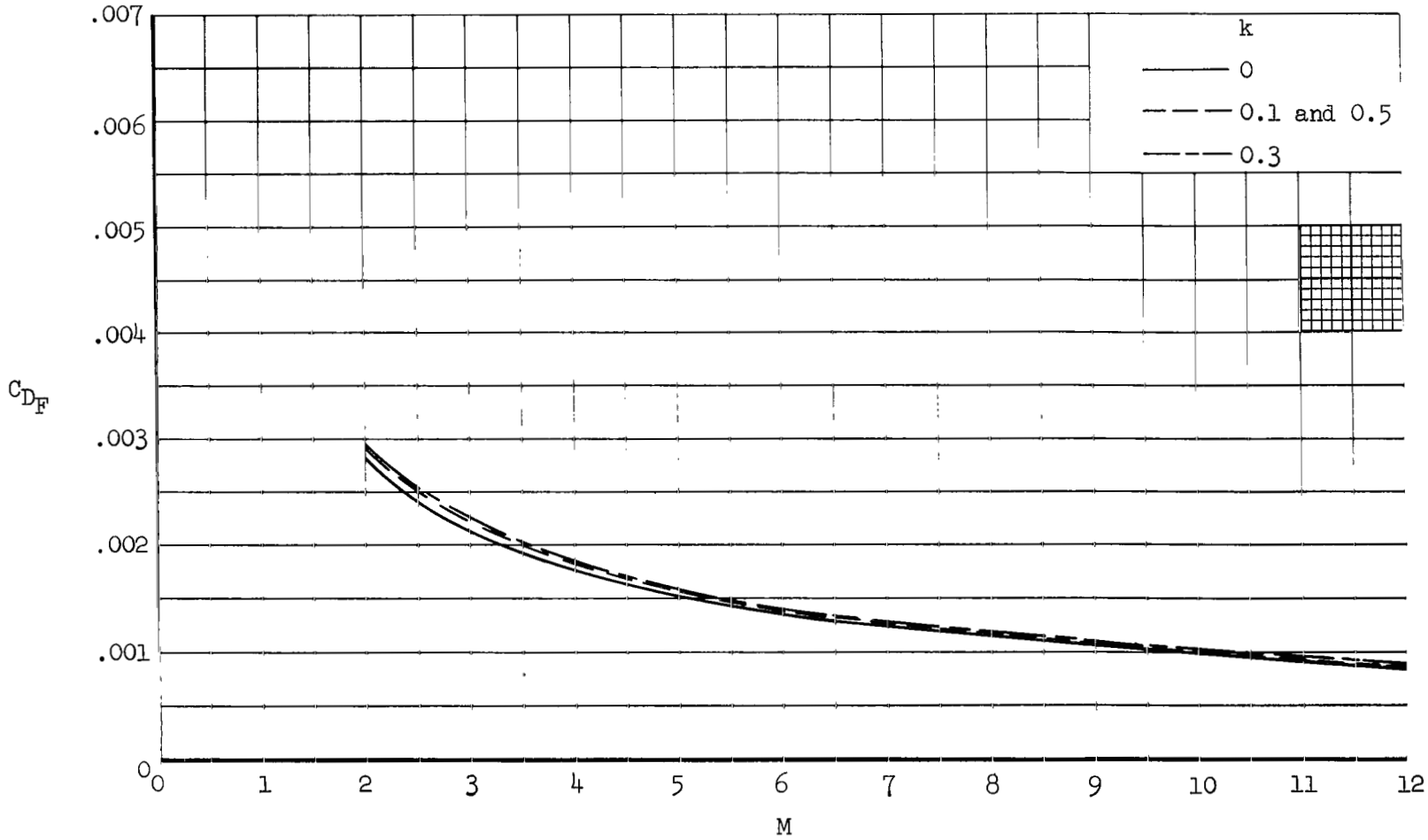

(b) Parabolic-arc bodies

Figure 11.- Continued.

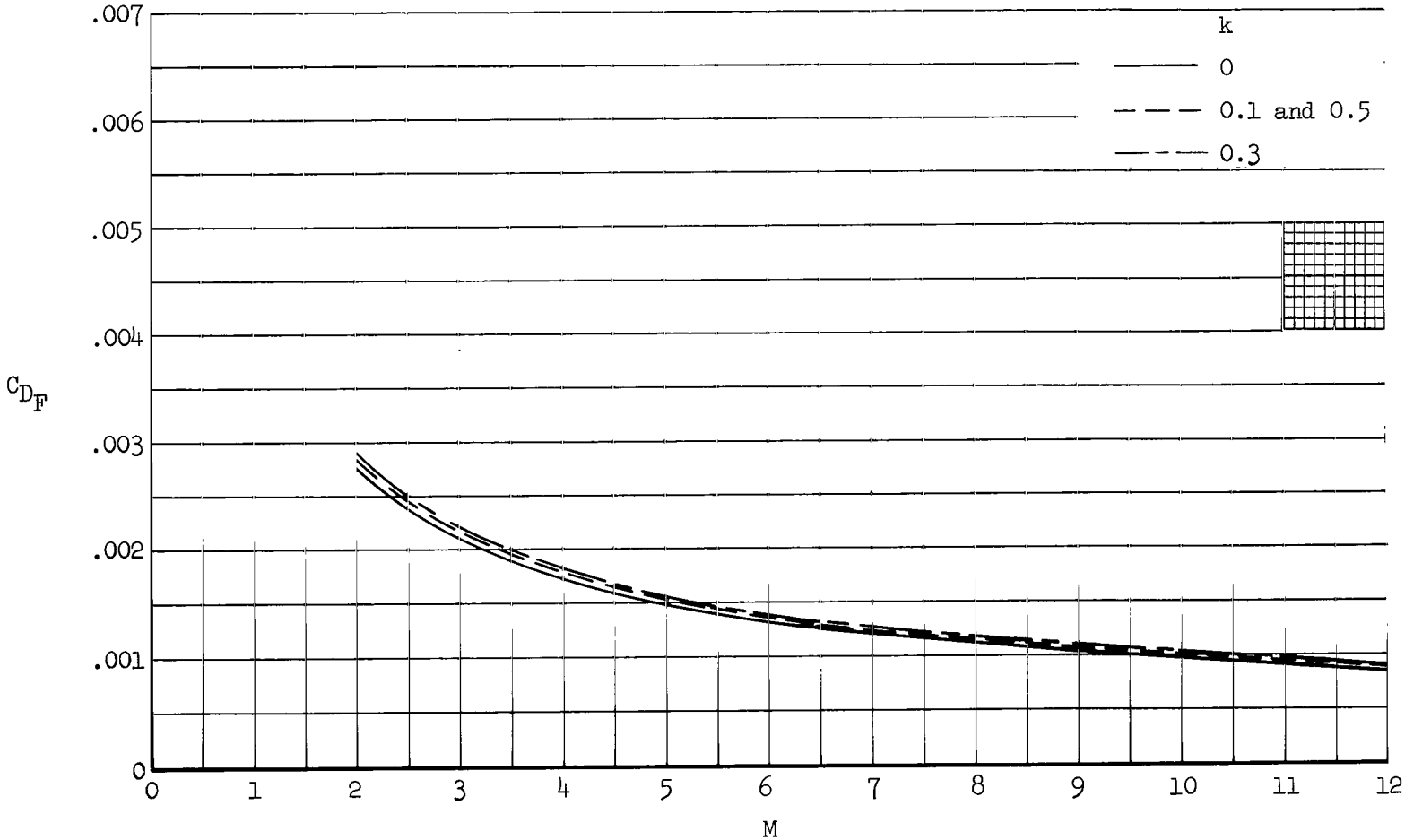

(c) Miele bodies [S_W,V]

Figure 11.- Continued.

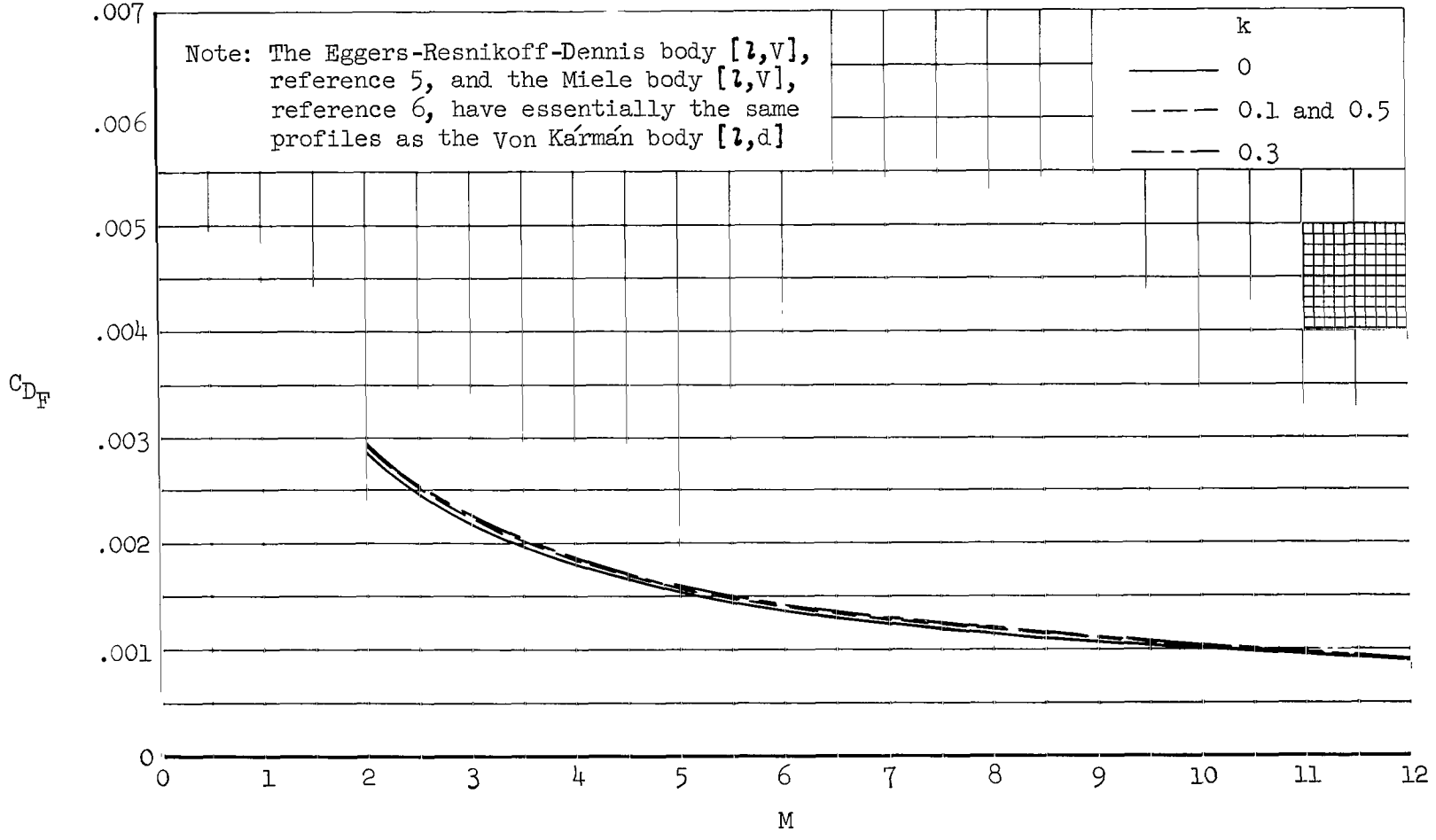

(d) Von Kármán bodies [2,d]

Figure 11.- Continued.

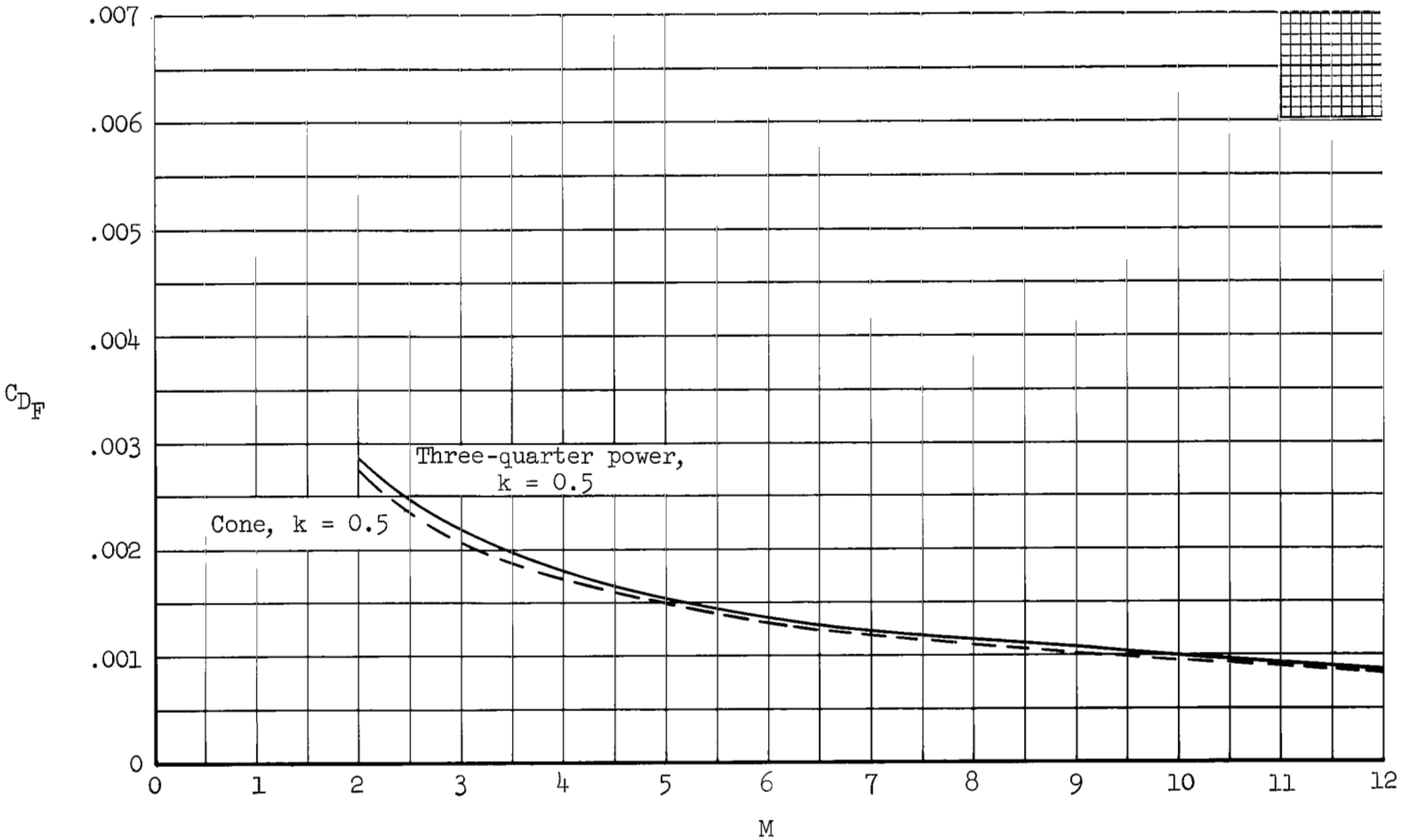

(e) Cone [S_w,d] and three-quarter power [l,d] bodies

Figure 11.- Concluded.

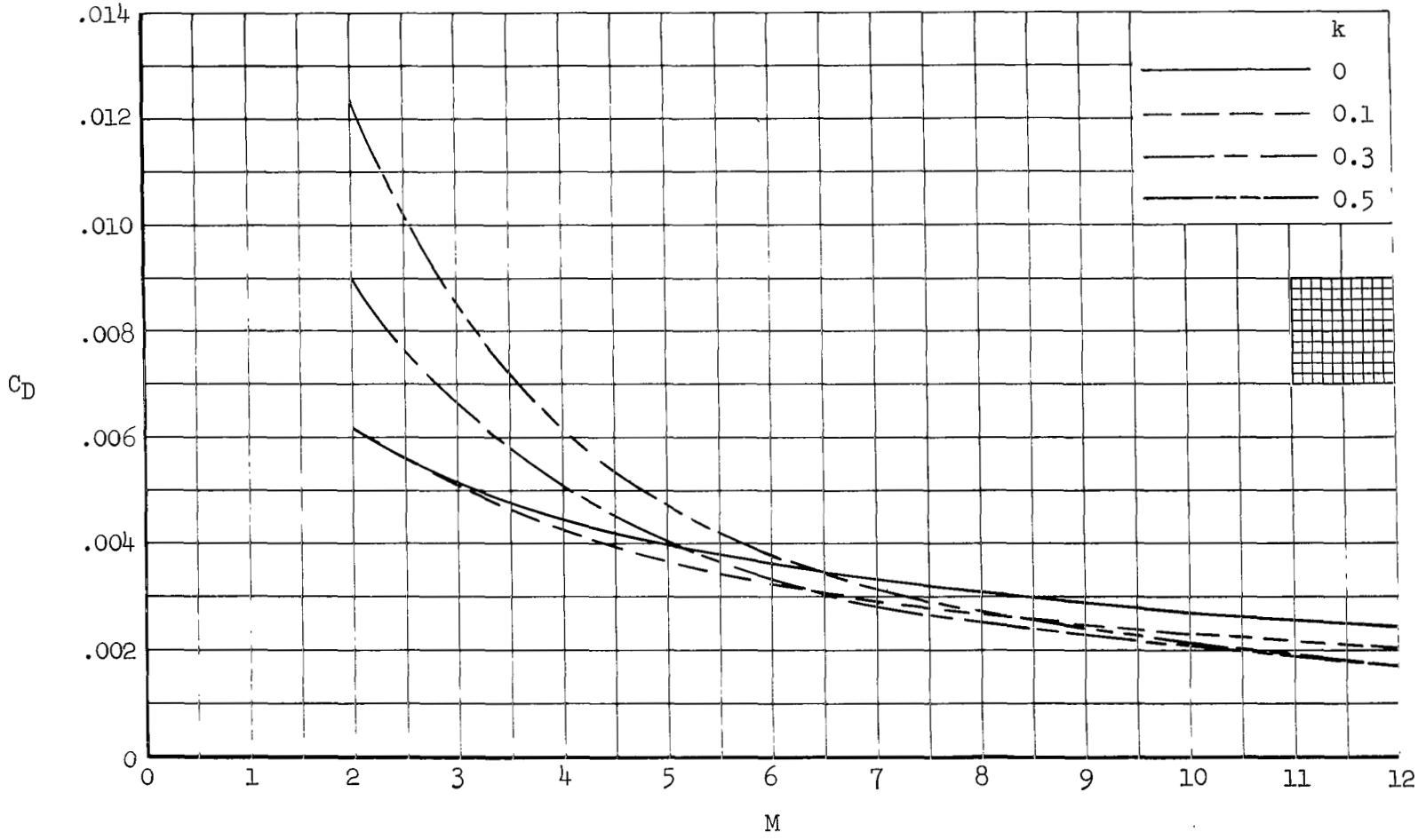

(a) Sears-Haack bodies [l,V]

Figure 12.- Effect of Mach number on the calculated total-drag coefficients of the bodies, with body cutoff as a parameter.

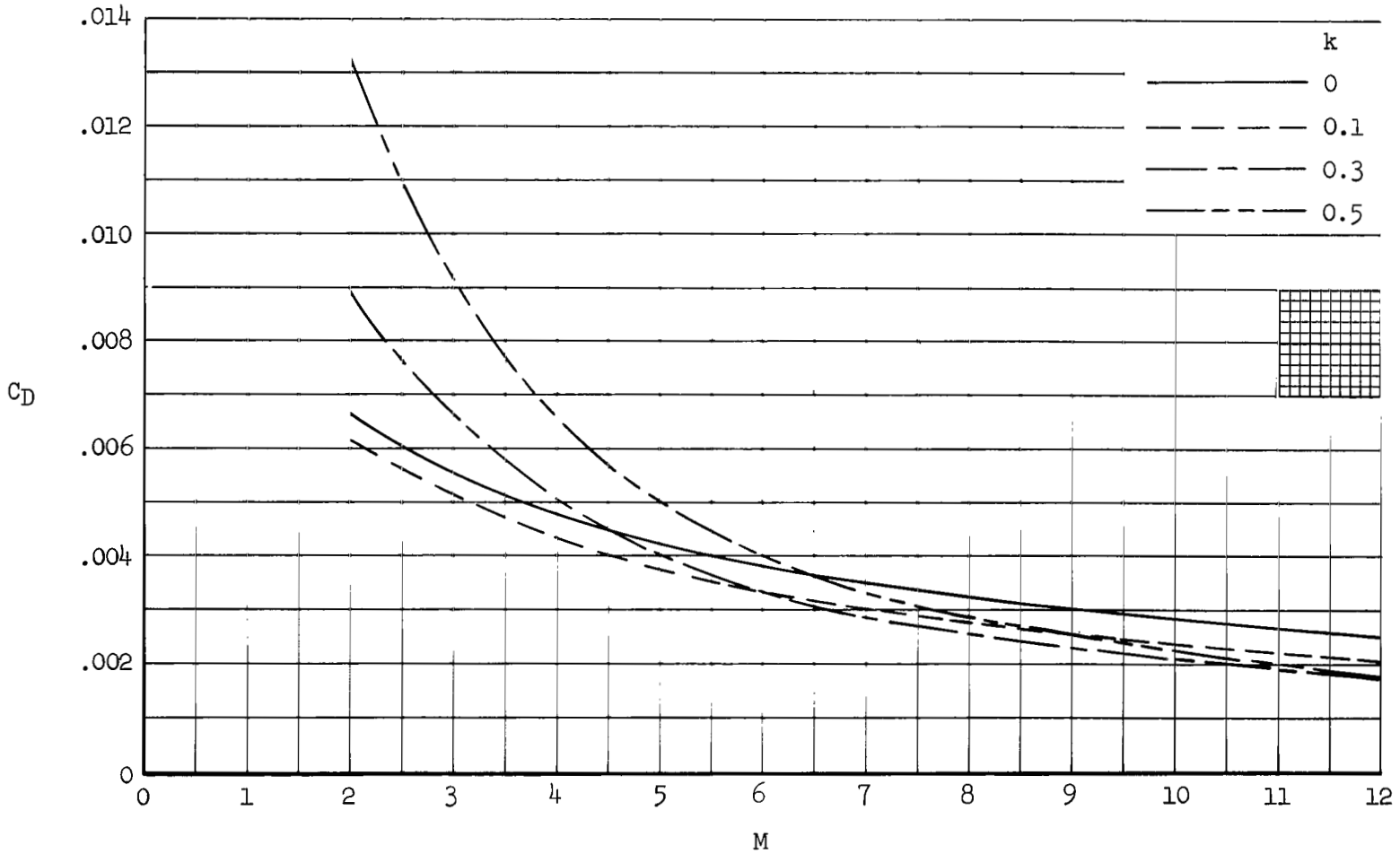

(b) Parabolic-arc bodies

Figure 12.- Continued.

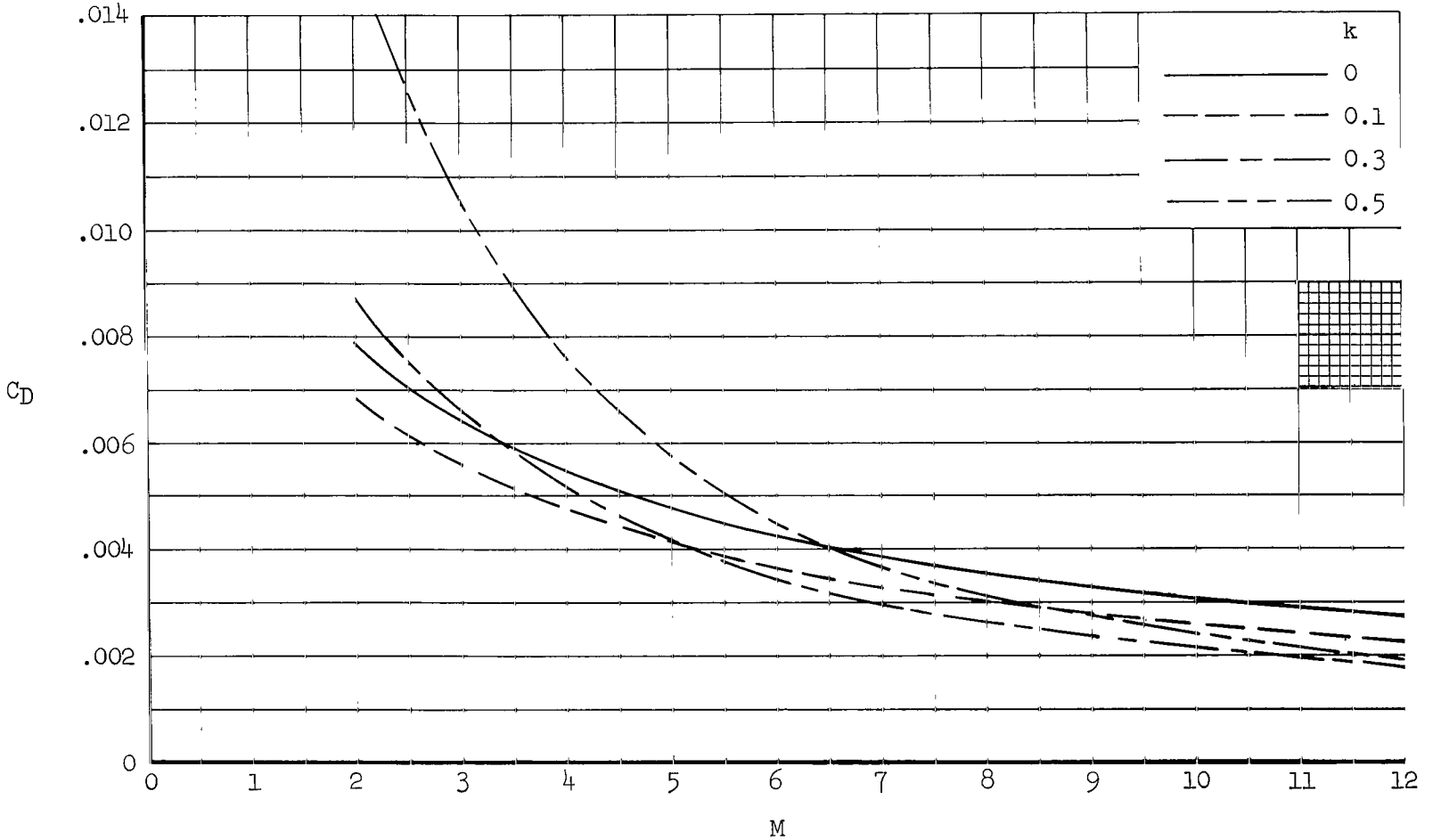

(c) Miele bodies [S_W,V]

Figure 12.- Continued.

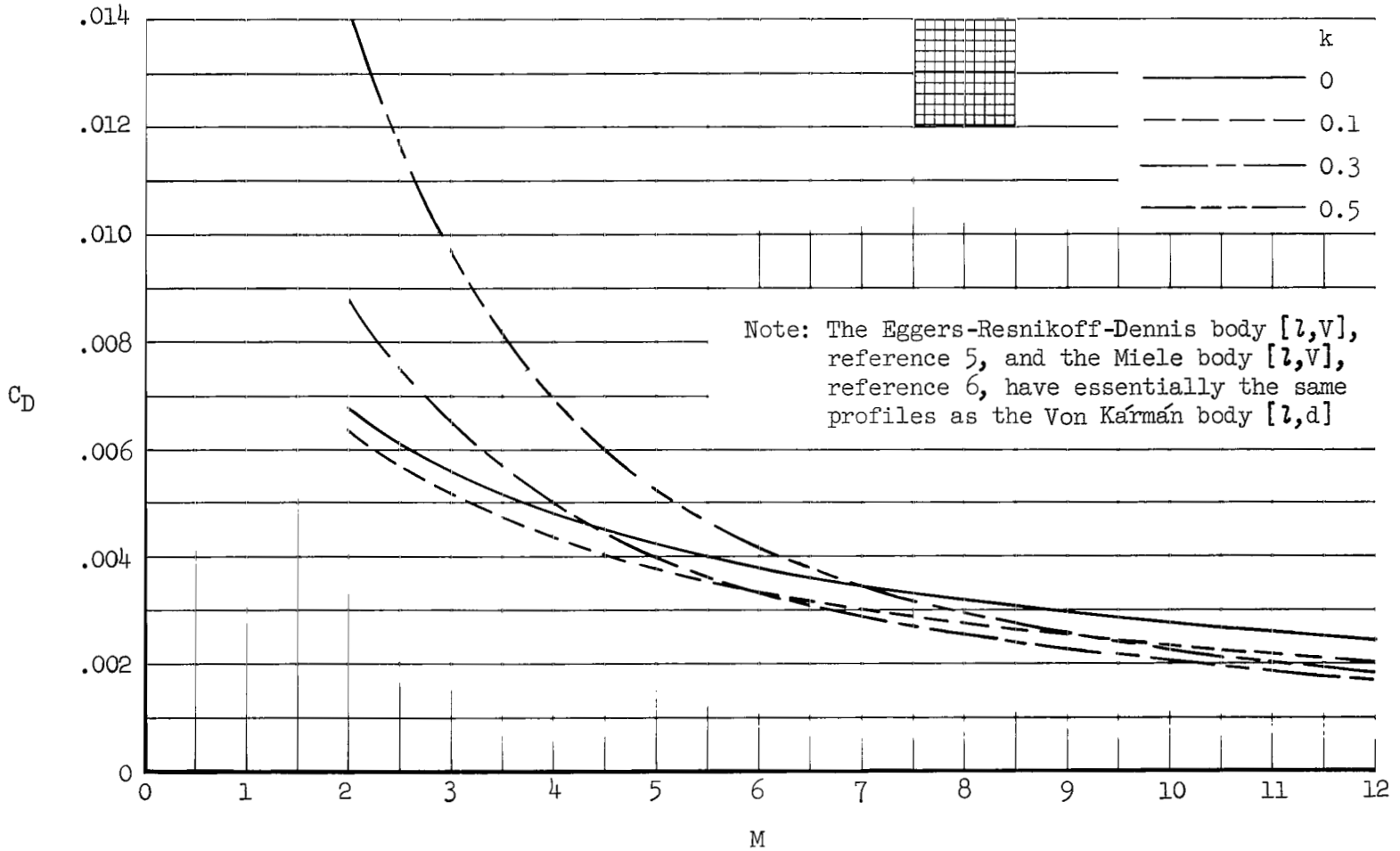

(d) Von Kármán bodies [ℓ,d]

Figure 12.- Continued.

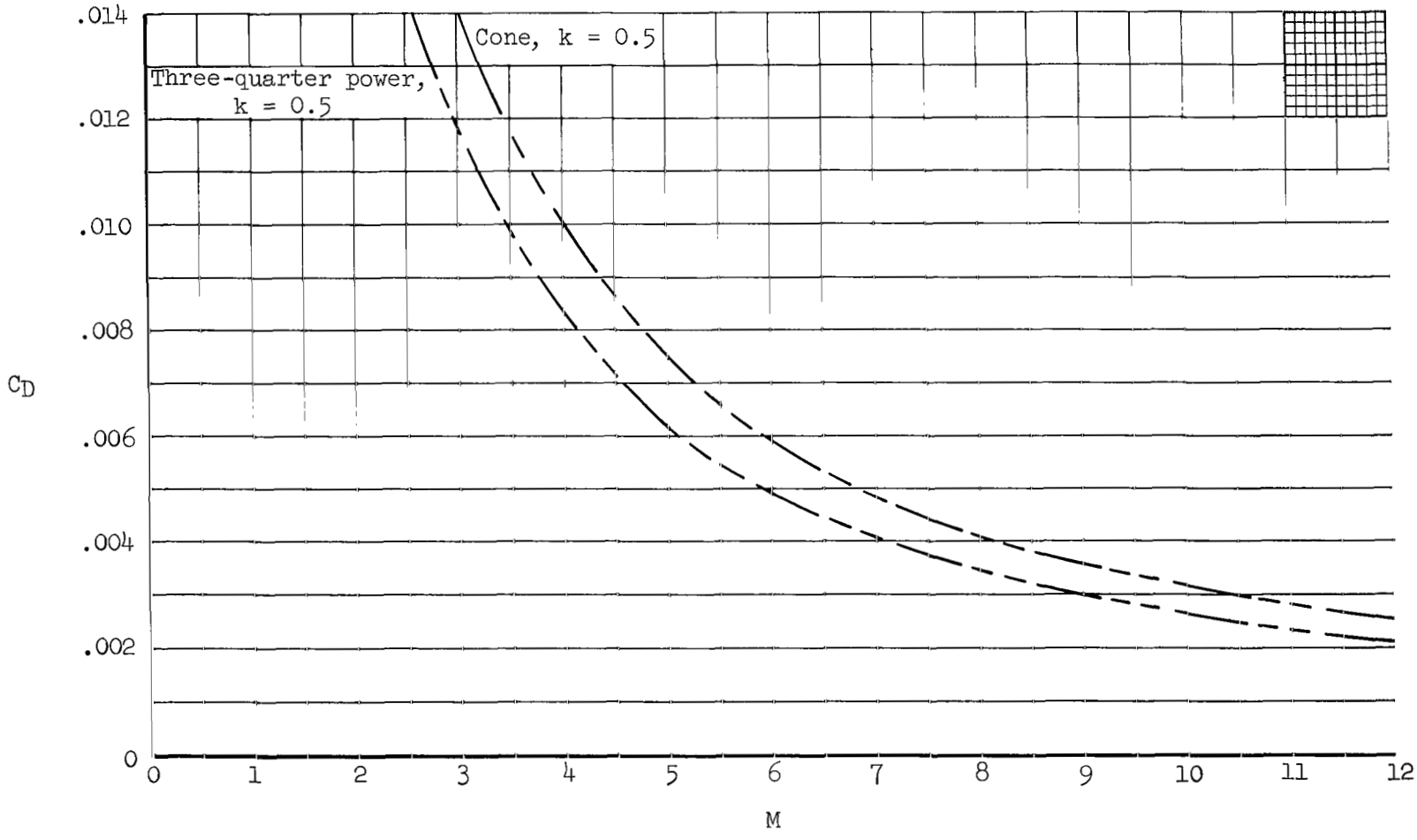

(e) Cone [S_w,d] and three-quarter power [l,d] bodies

Figure 12.- Concluded.

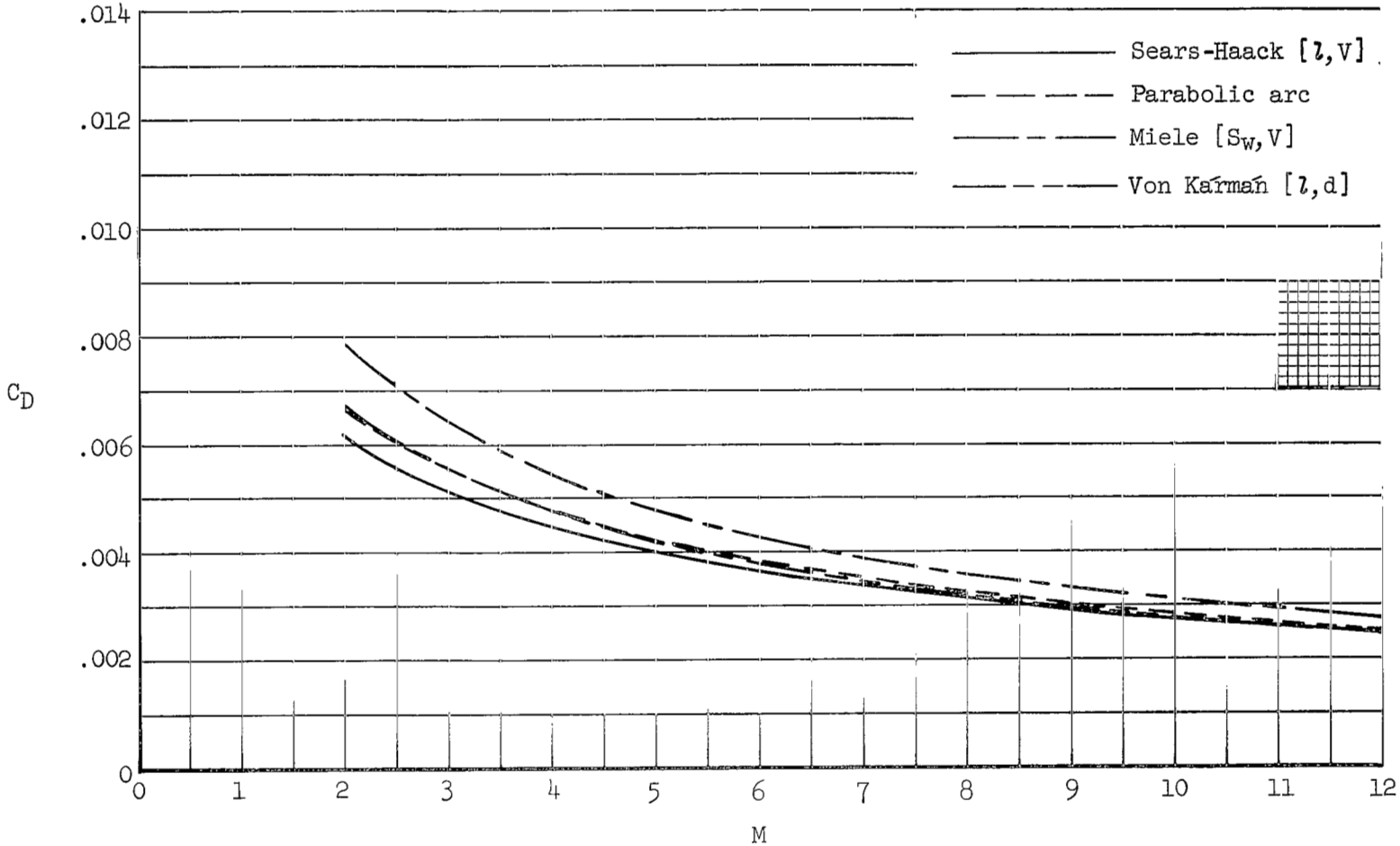

(a) k = 0

Figure 13.- Comparison of the calculated total-drag coefficients of the bodies as a function of Mach number, for constant values of body cutoff.

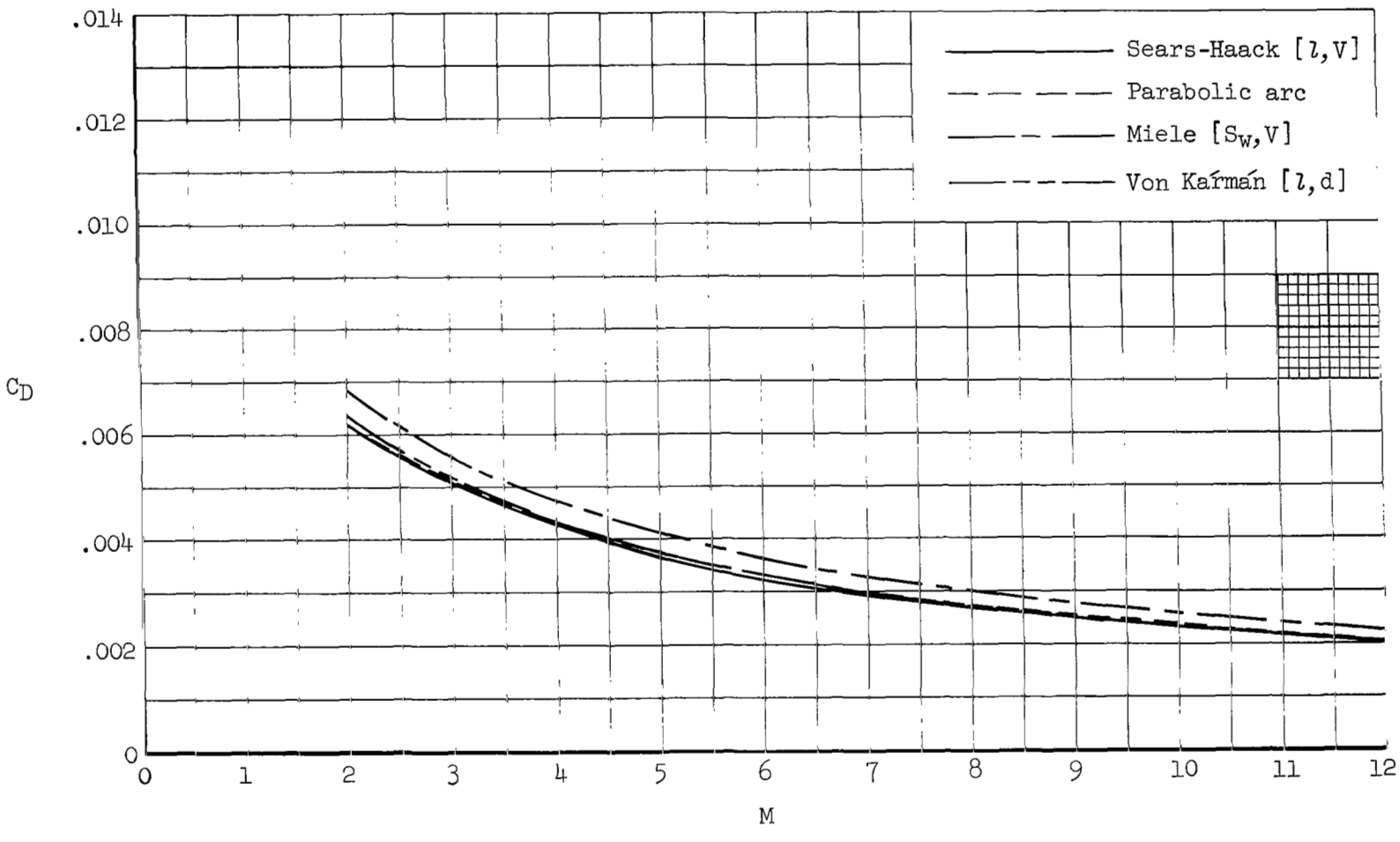

(b) k = 0.1

Figure 13.- Continued.

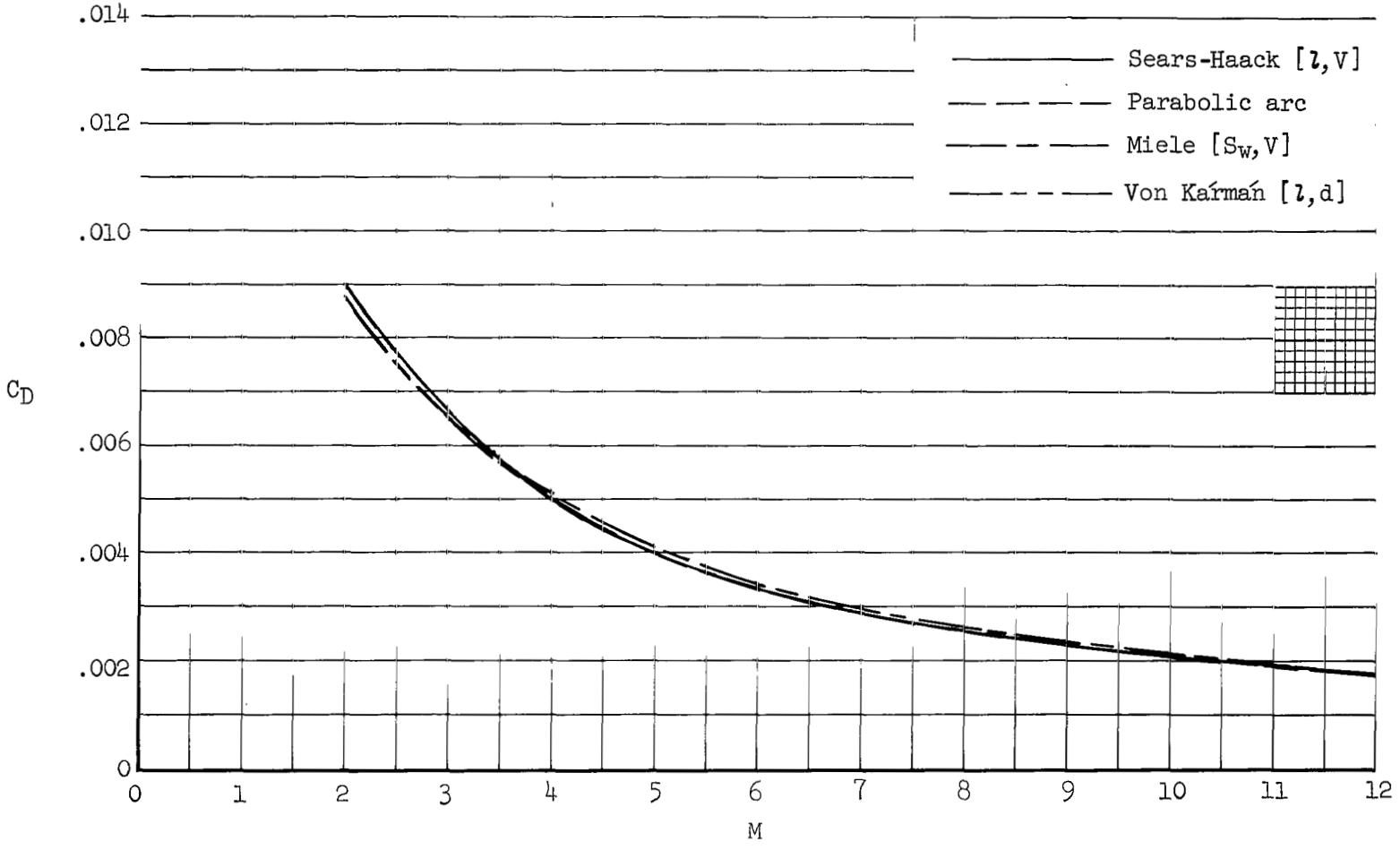

(c) k = 0.3

Figure 13.- Continued.

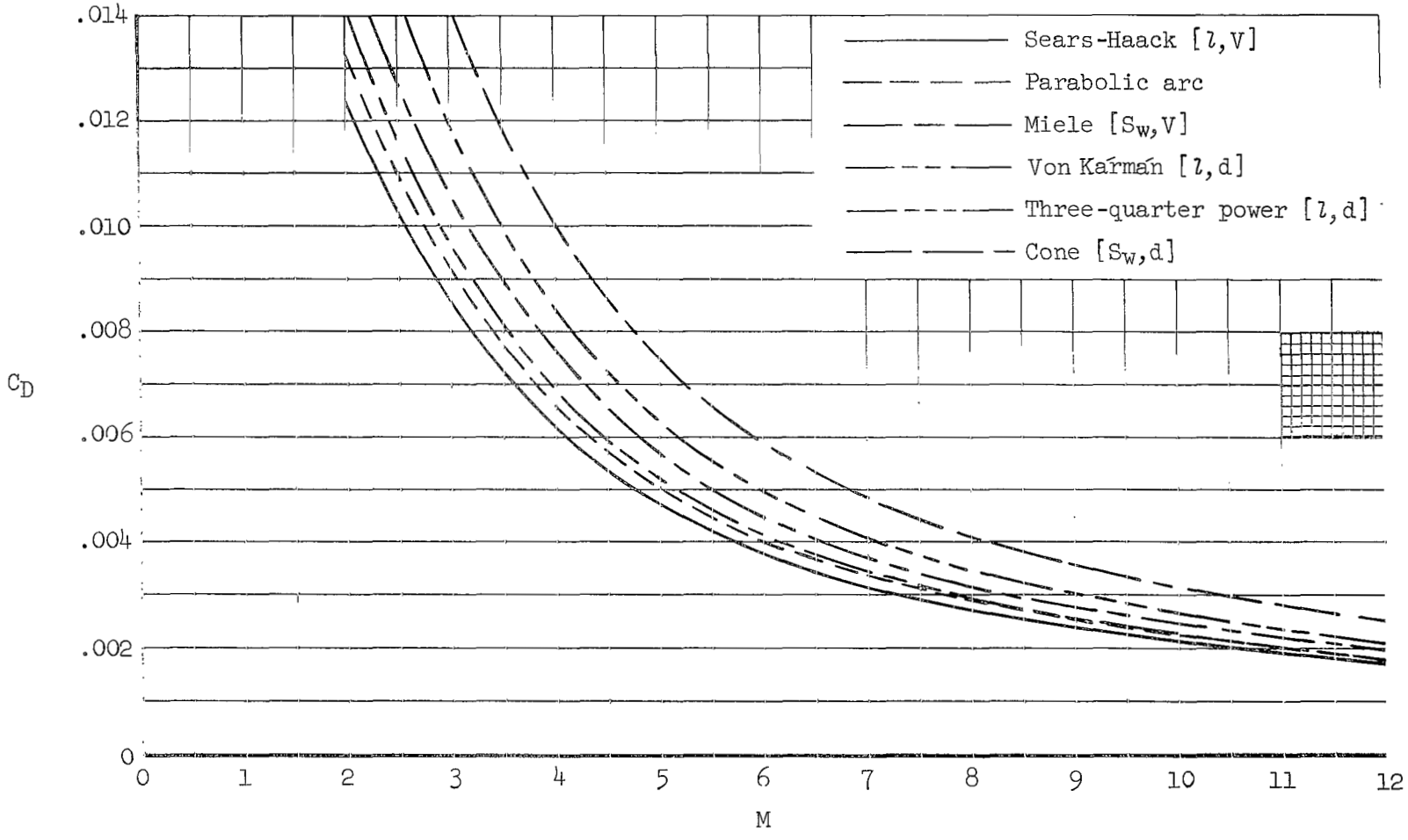

(d) k = 0.5

Figure 13.- Concluded.

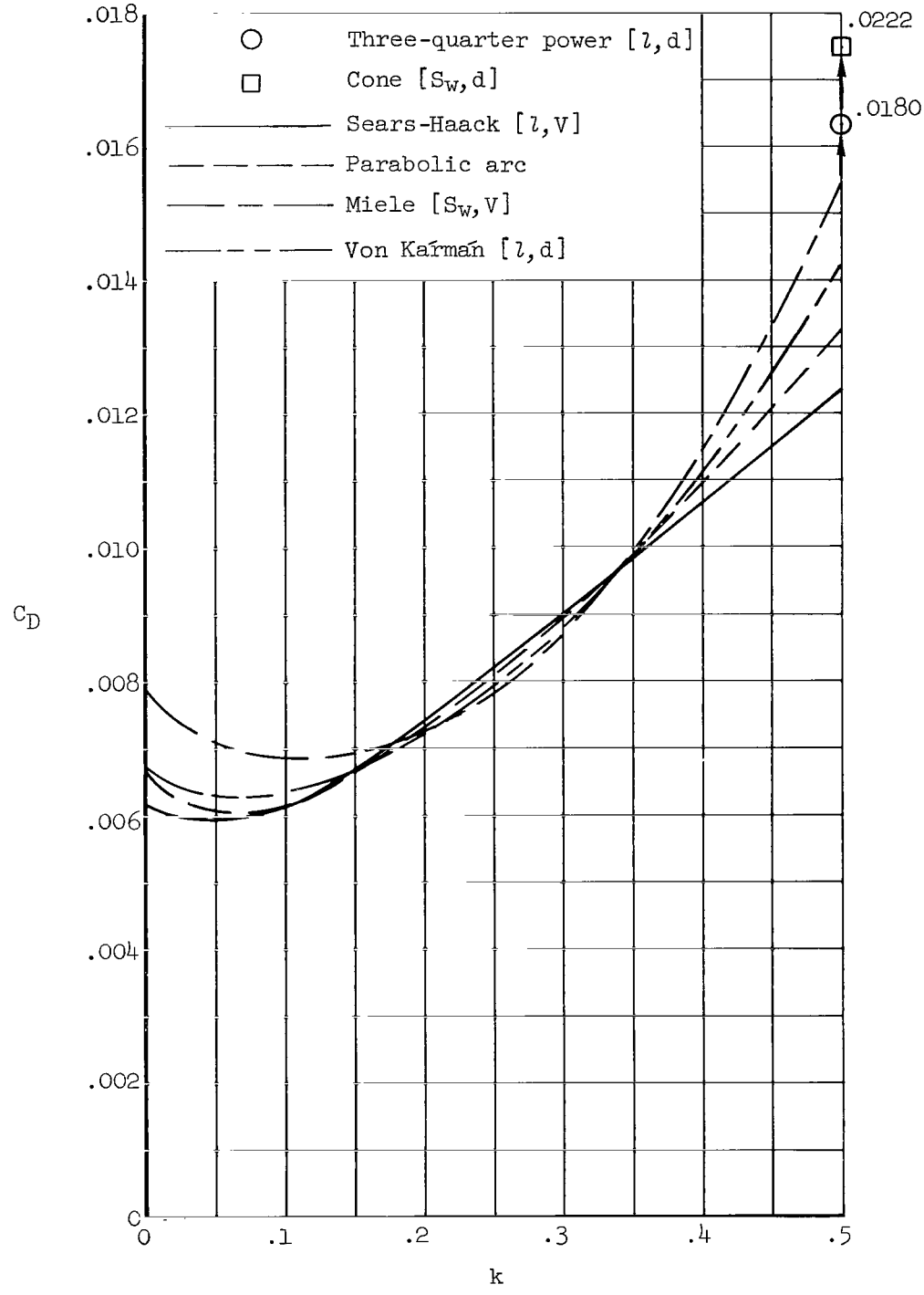

(a) M = 2.0

Figure 14.- Comparison of the calculated total-drag coefficients of the bodies as a function of body cutoff, for constant values of Mach number.

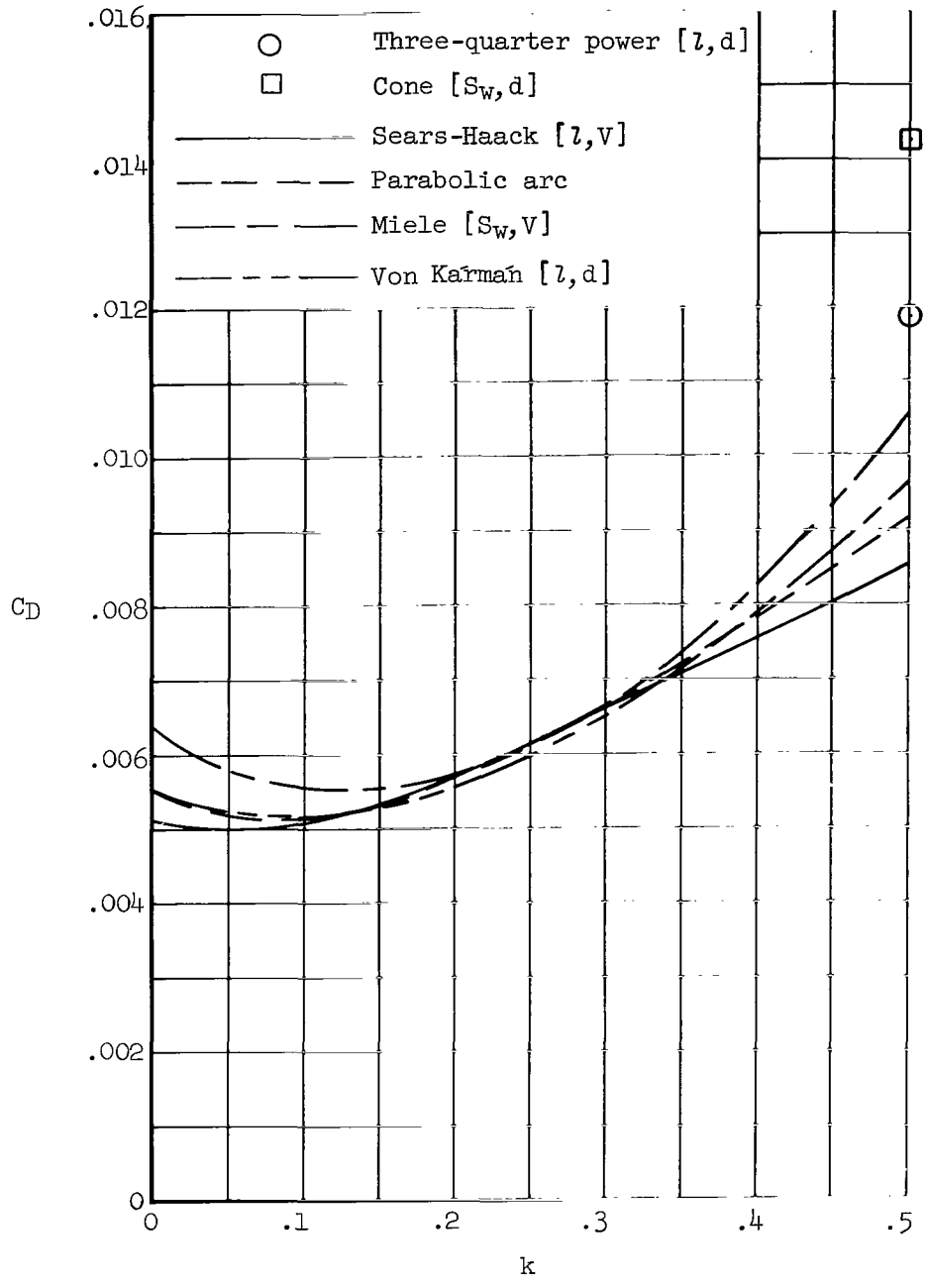

(b) M = 3.0

Figure 14.- Continued.

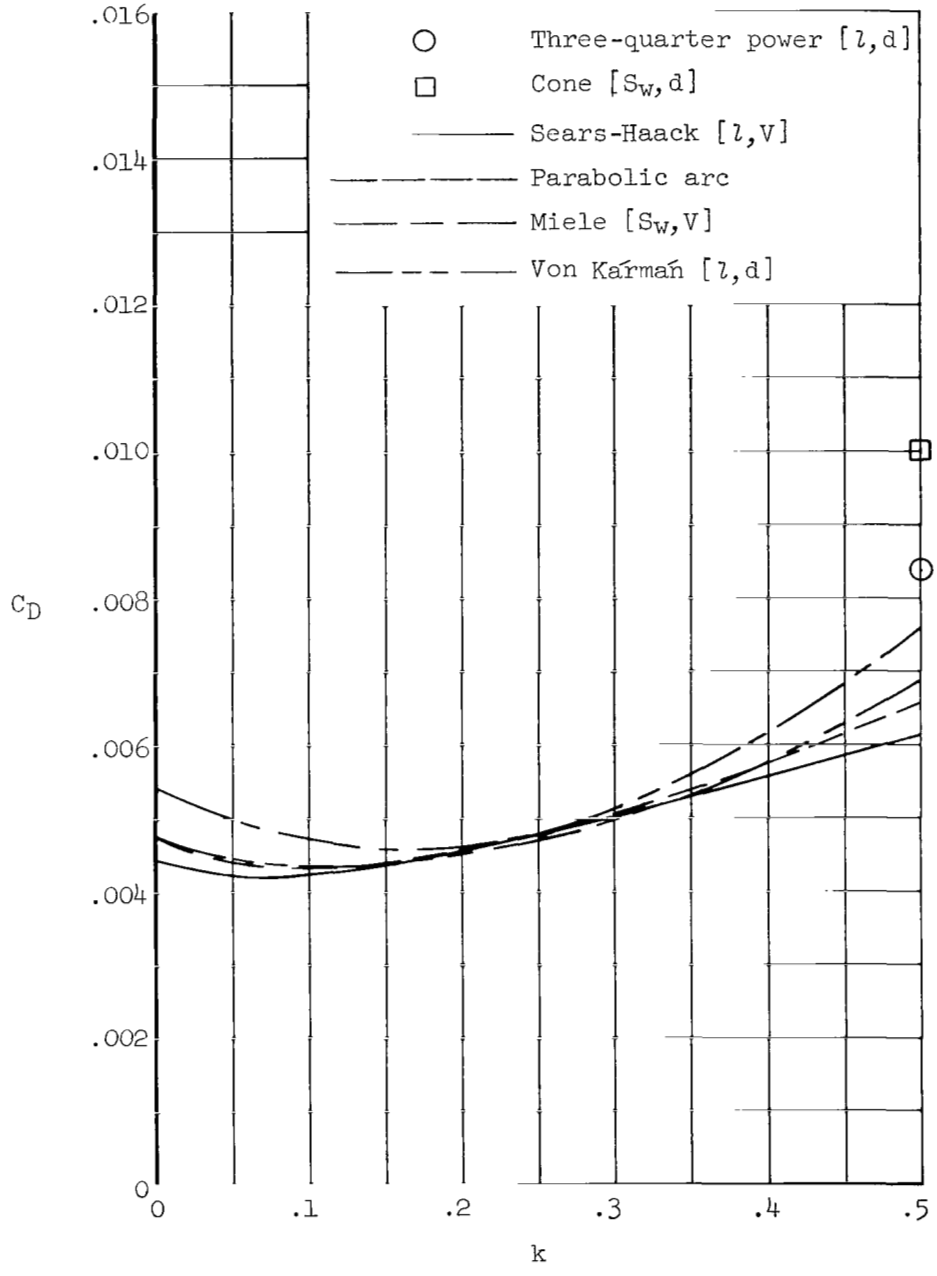

(c) M = 4.0

Figure 14.- Continued.

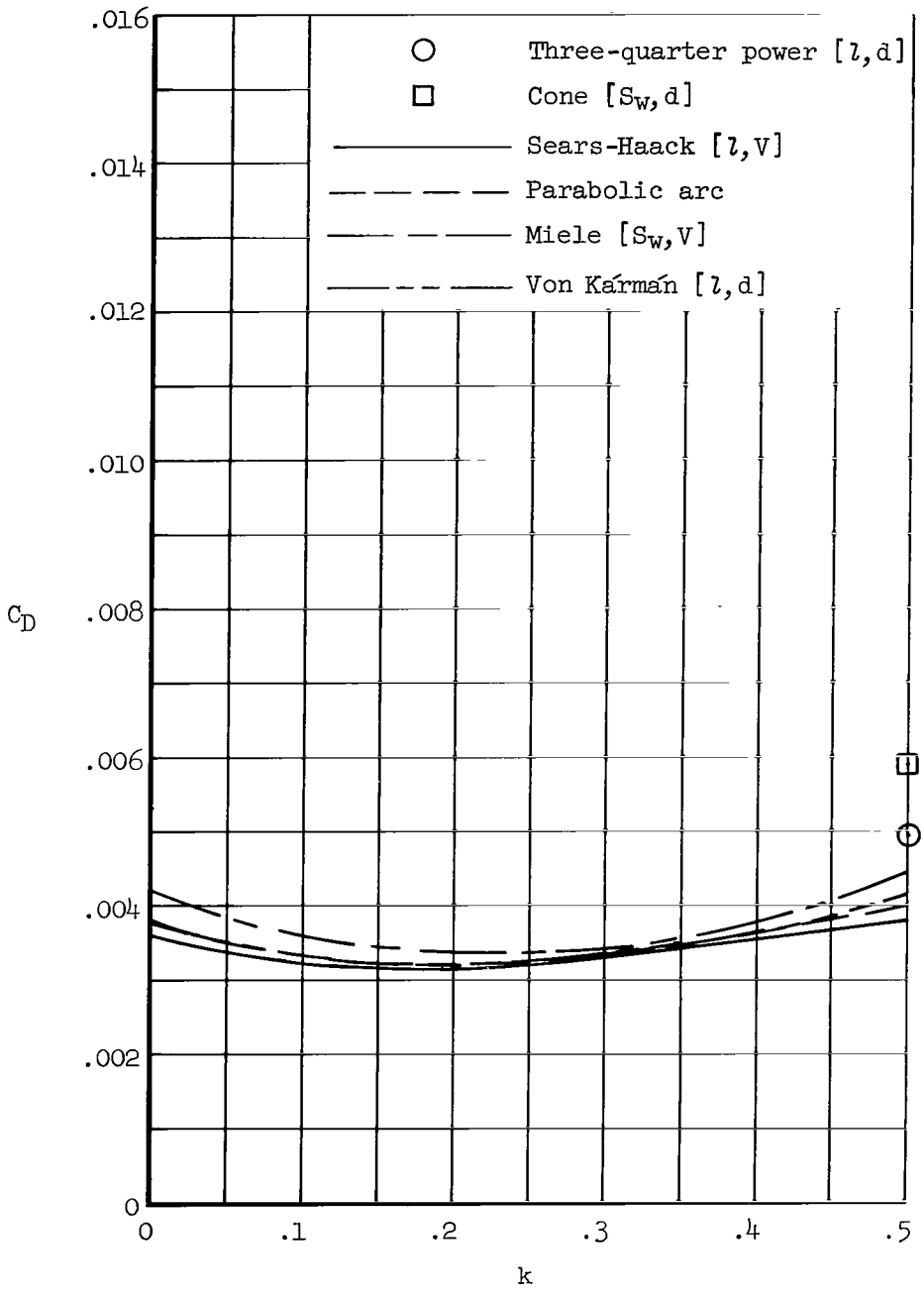

(d) M = 6.0

Figure 14.- Continued.

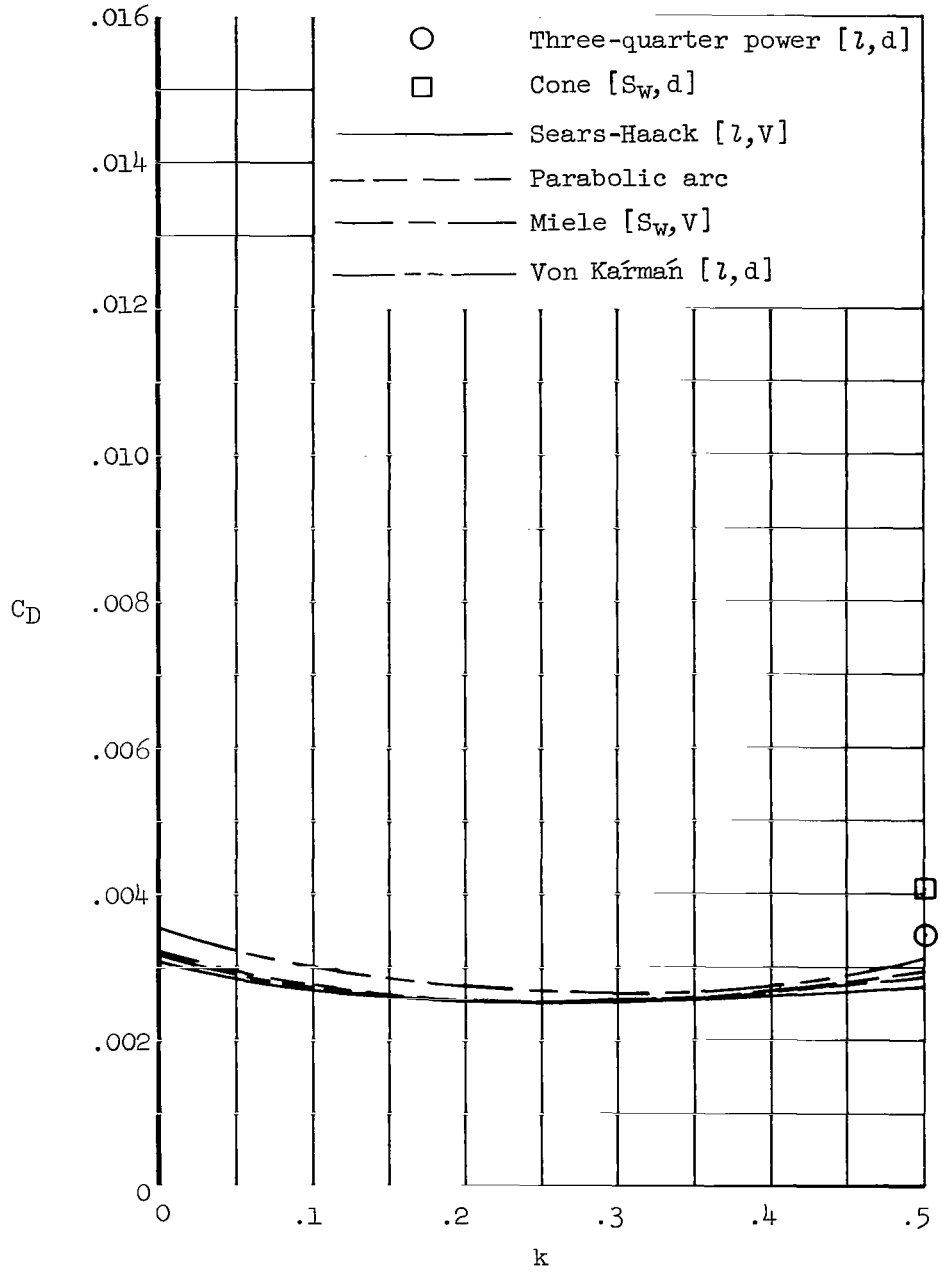

(e) M = 8.0

Figure 14.- Continued.

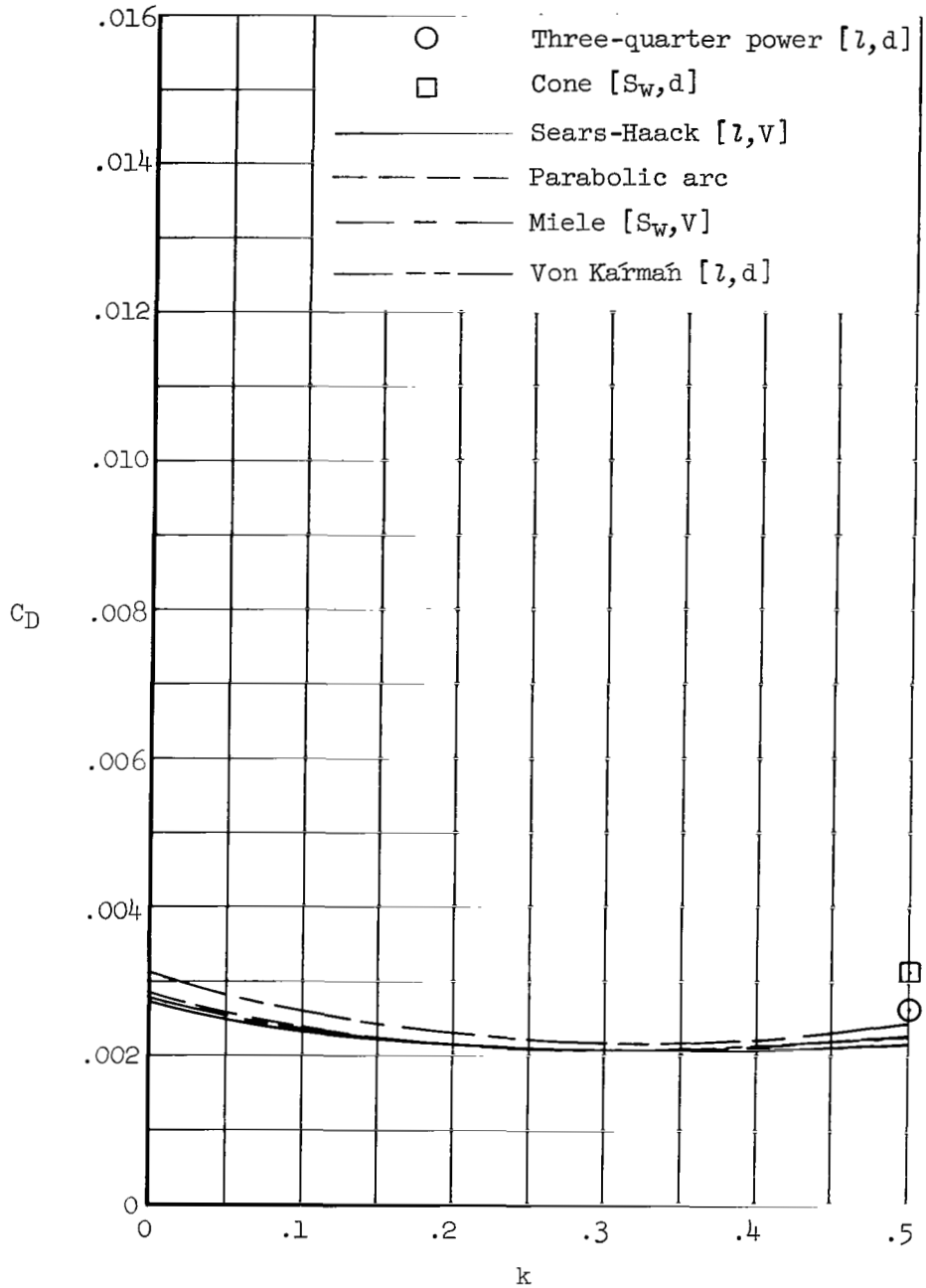

(f) M = 10.0

Figure 14.- Continued.

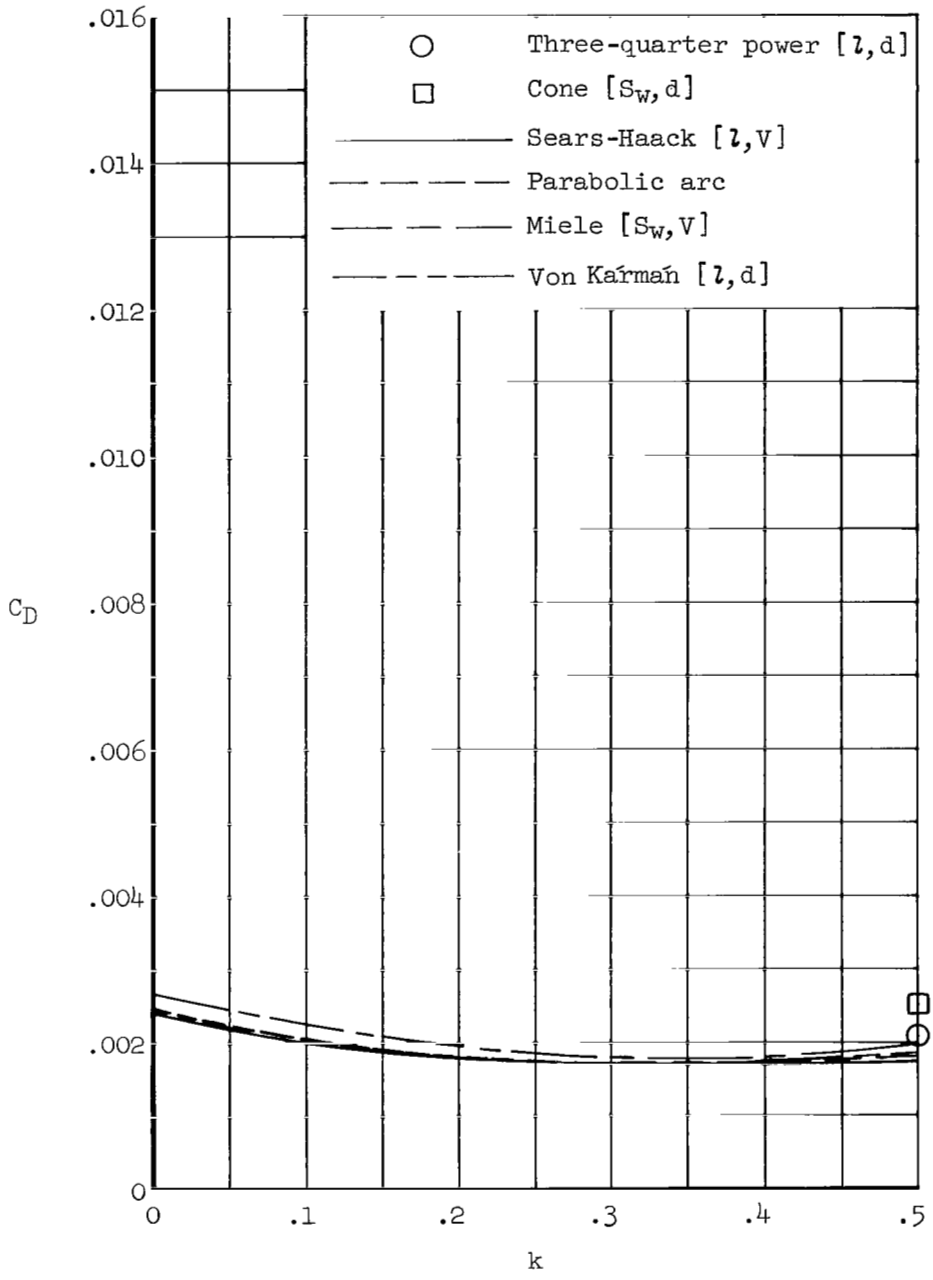

(g) M = 12.0

Figure 14.- Concluded.

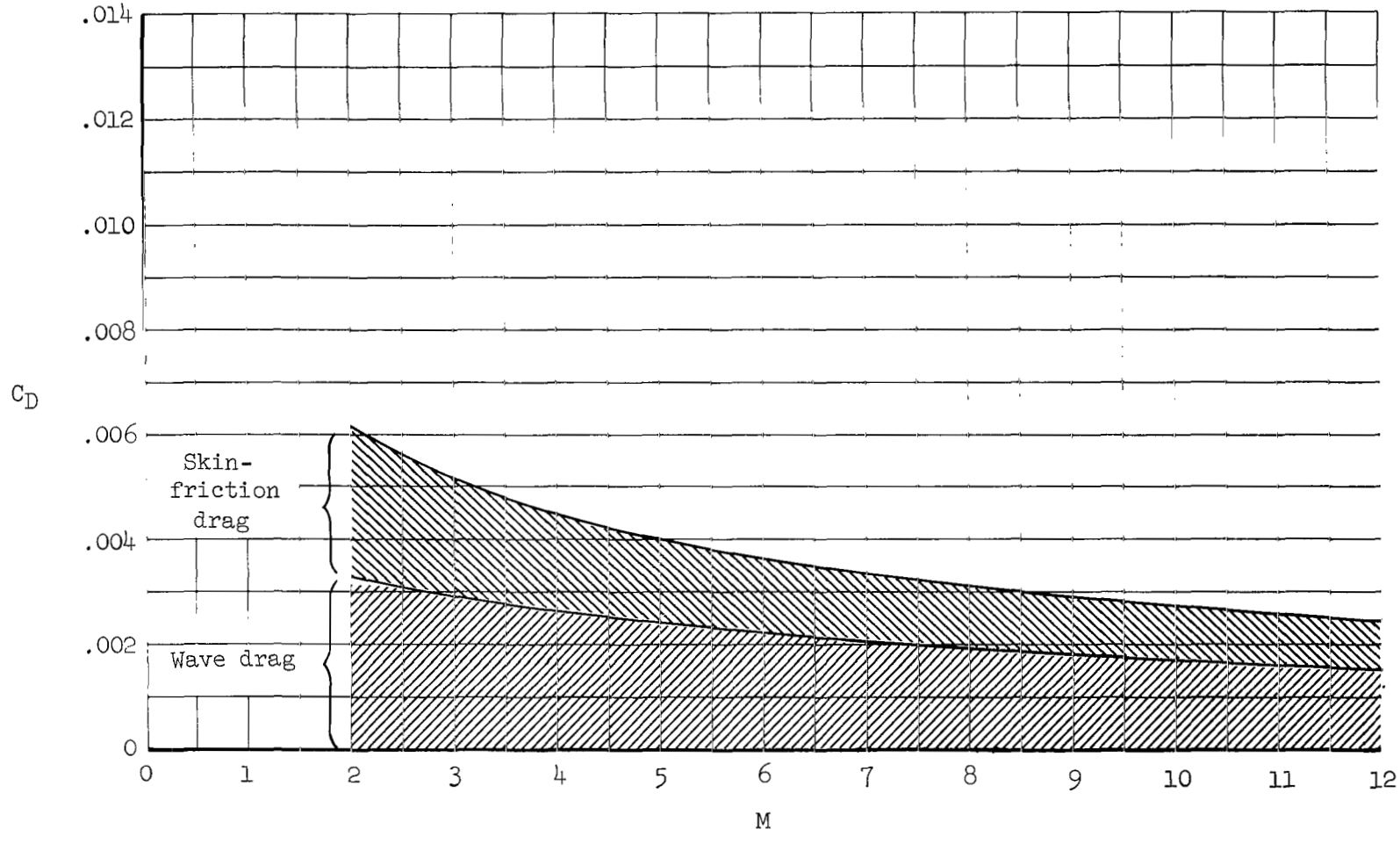

(a) Sears-Haack body [l,V], k = 0

Figure 15.- Comparison of the effects of Mach number on the components of the total drag coefficients of selected bodies.

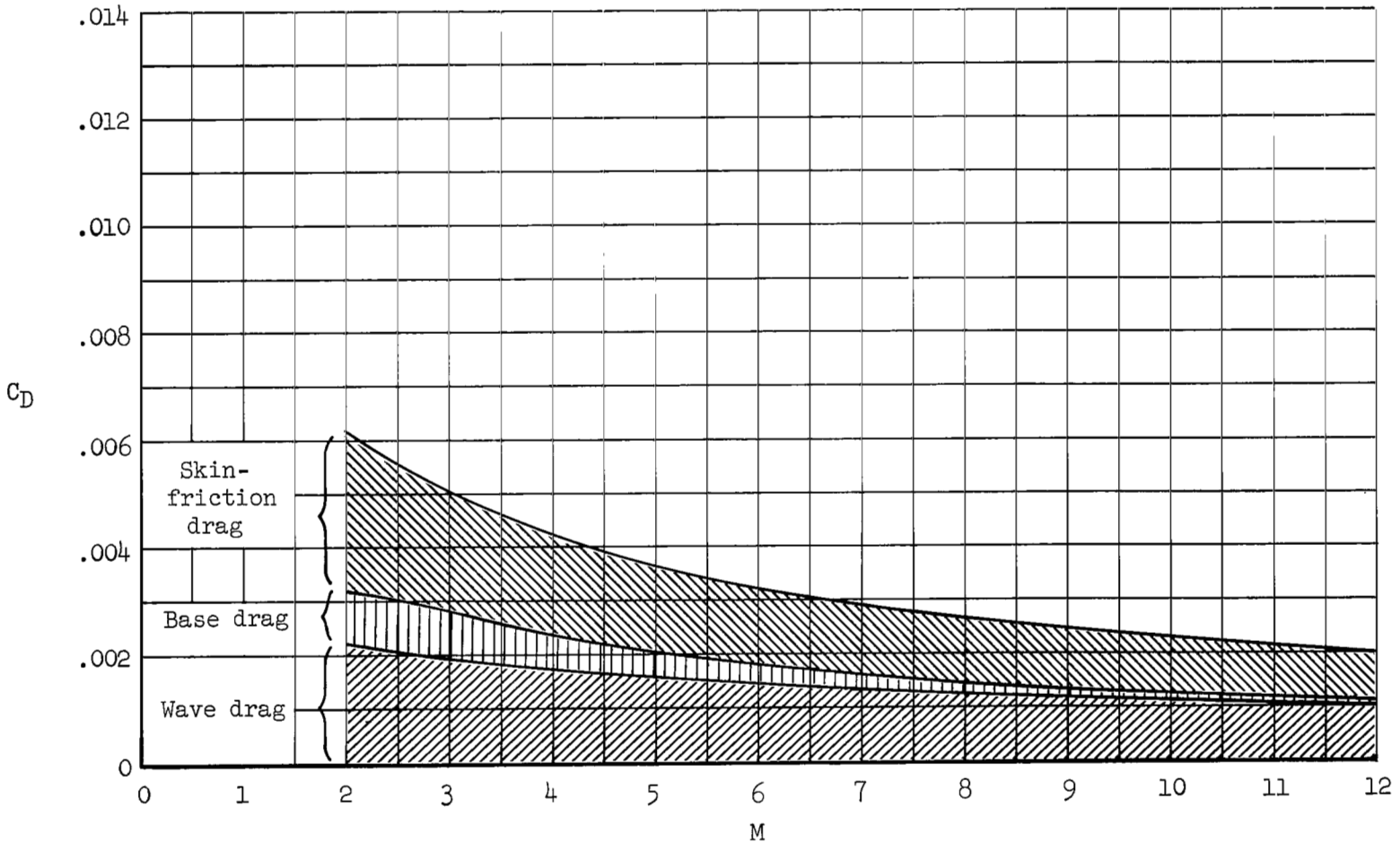

(b) Sears-Haack body [l,V], k = 0.1

Figure 15.- Continued.

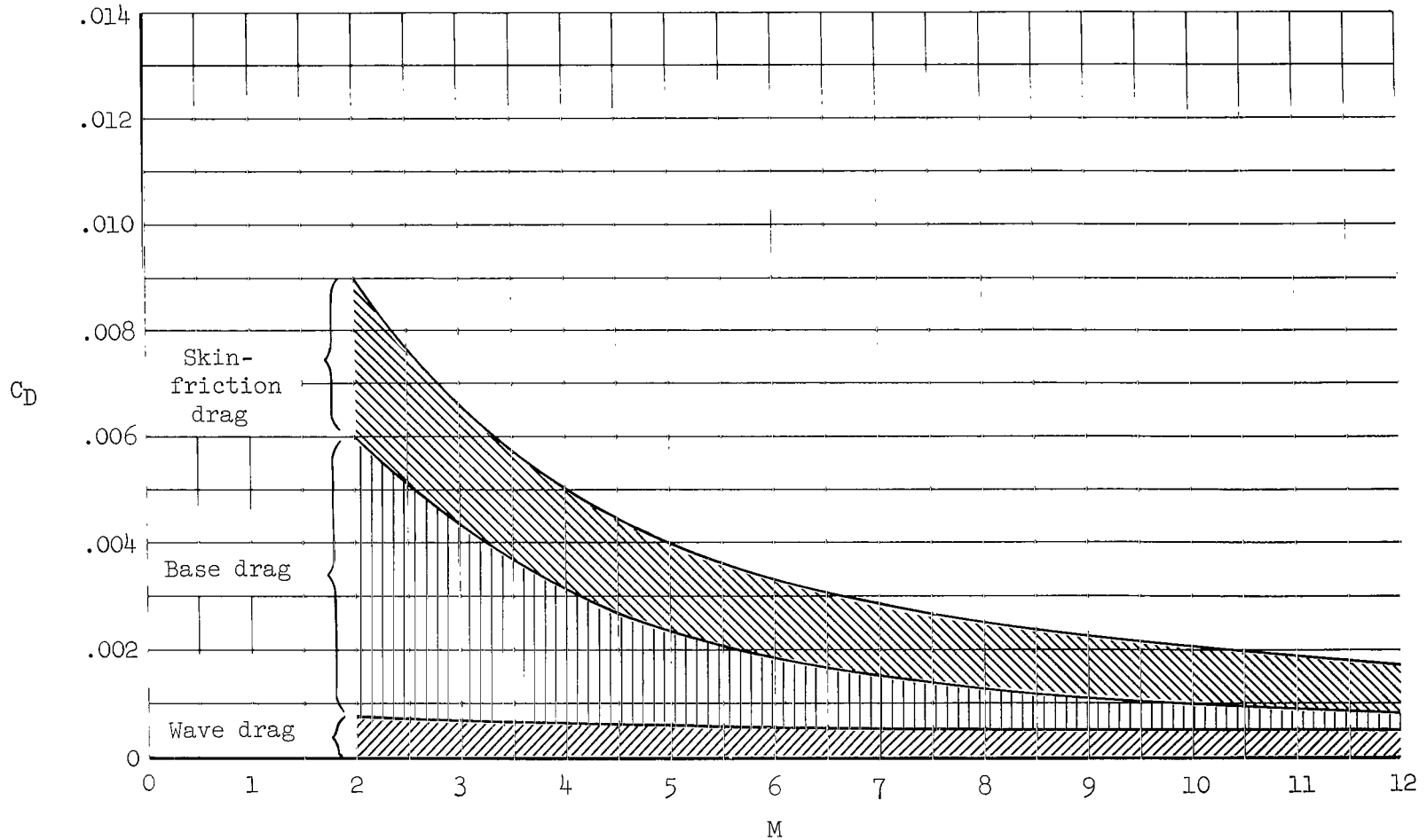

(c) Sears-Haack body [l,V], k = 0.3

Figure 15.- Continued.

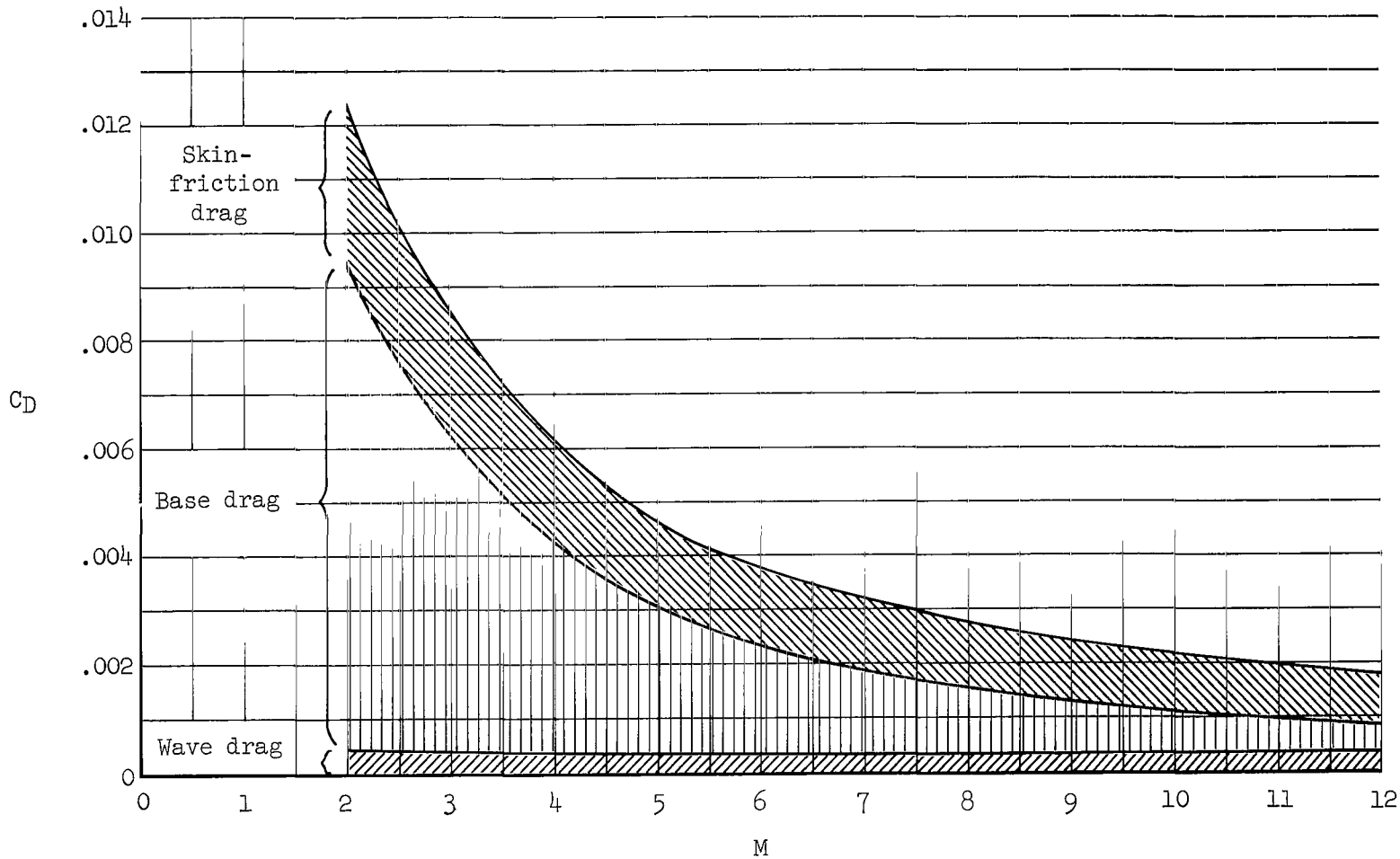

(d) Sears-Haack body [l,V], k = 0.5

Figure 15.- Continued.

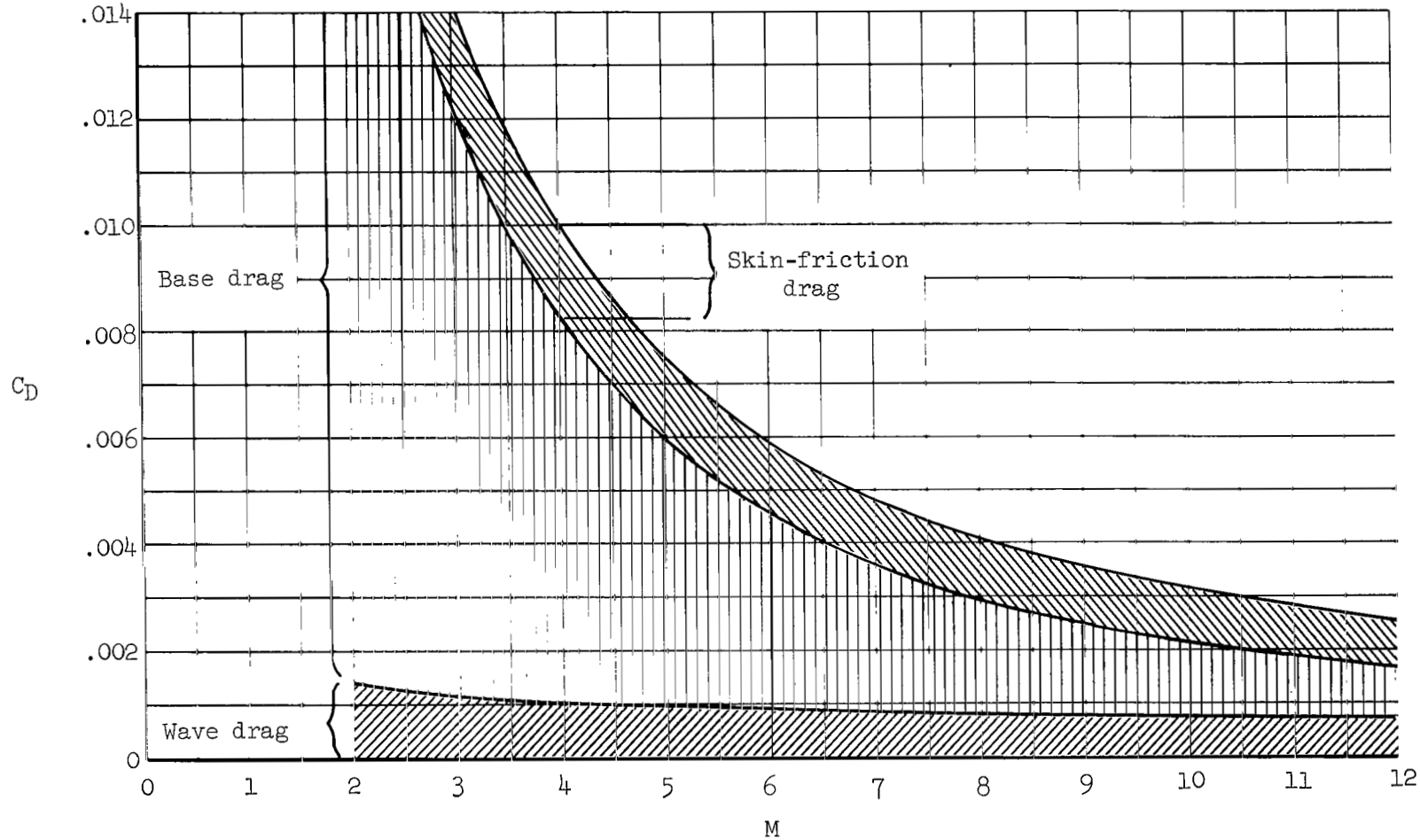

(e) Cone body [S_W,d], k = 0.5

Figure 15.- Concluded.

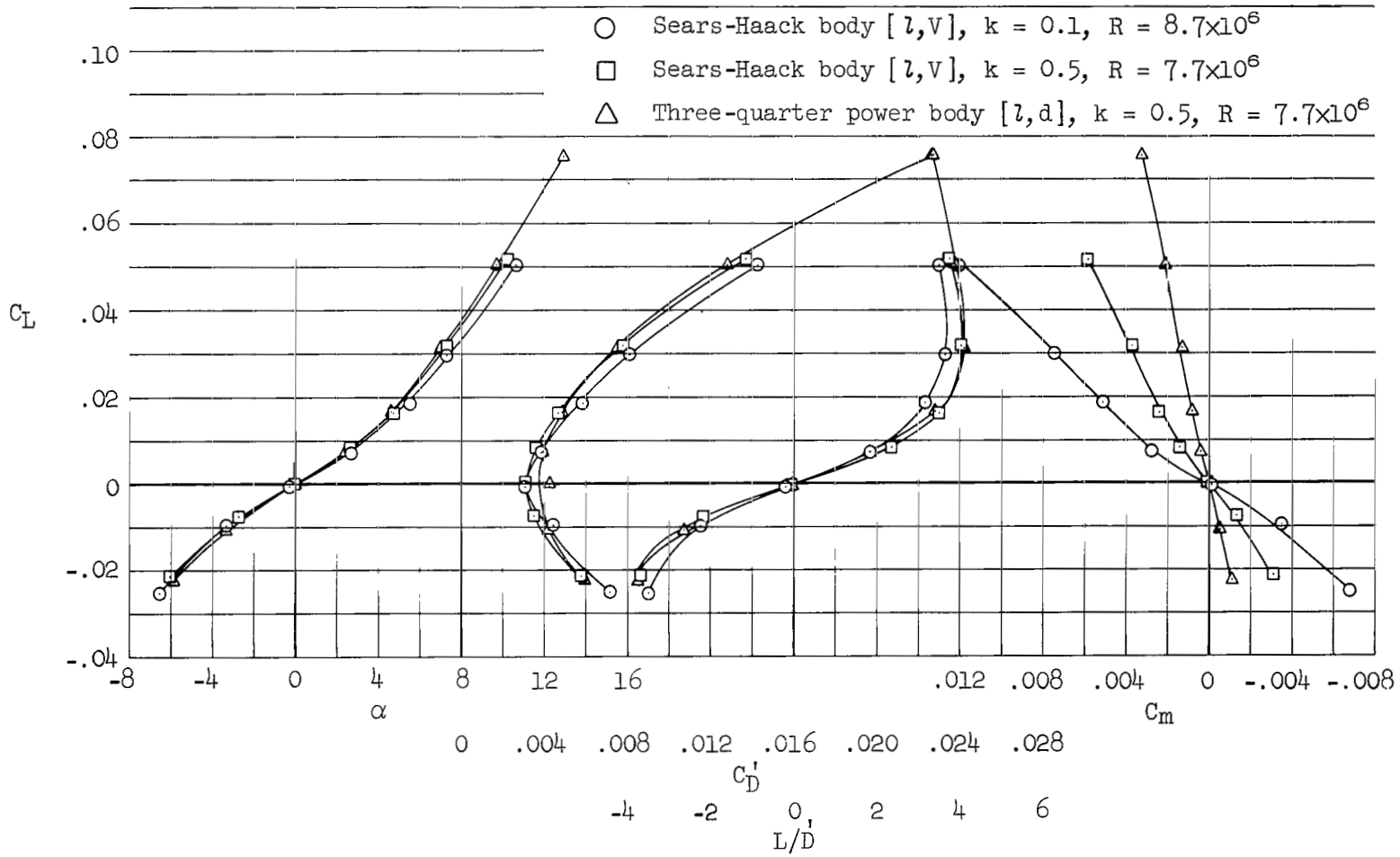

(a) M = 5.4; turbulent boundary-layer flow over base of models

Figure 16.- Aerodynamic characteristics of the selected bodies from tests in the Ames 3.5-Foot Hypersonic Wind Tunnel.

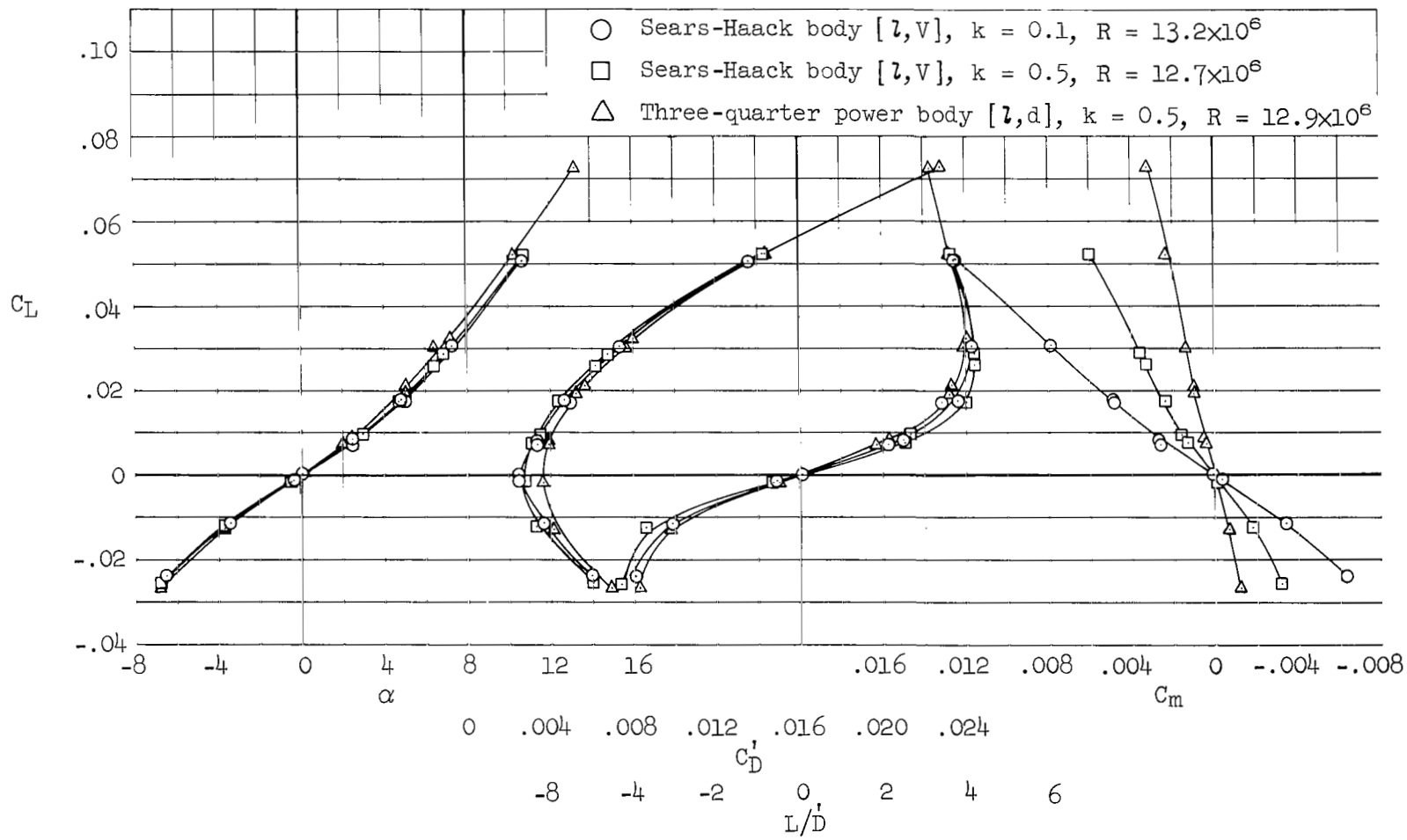

(b) M = 7.4; turbulent boundary-layer flow over base of models

Figure 16.- Continued.

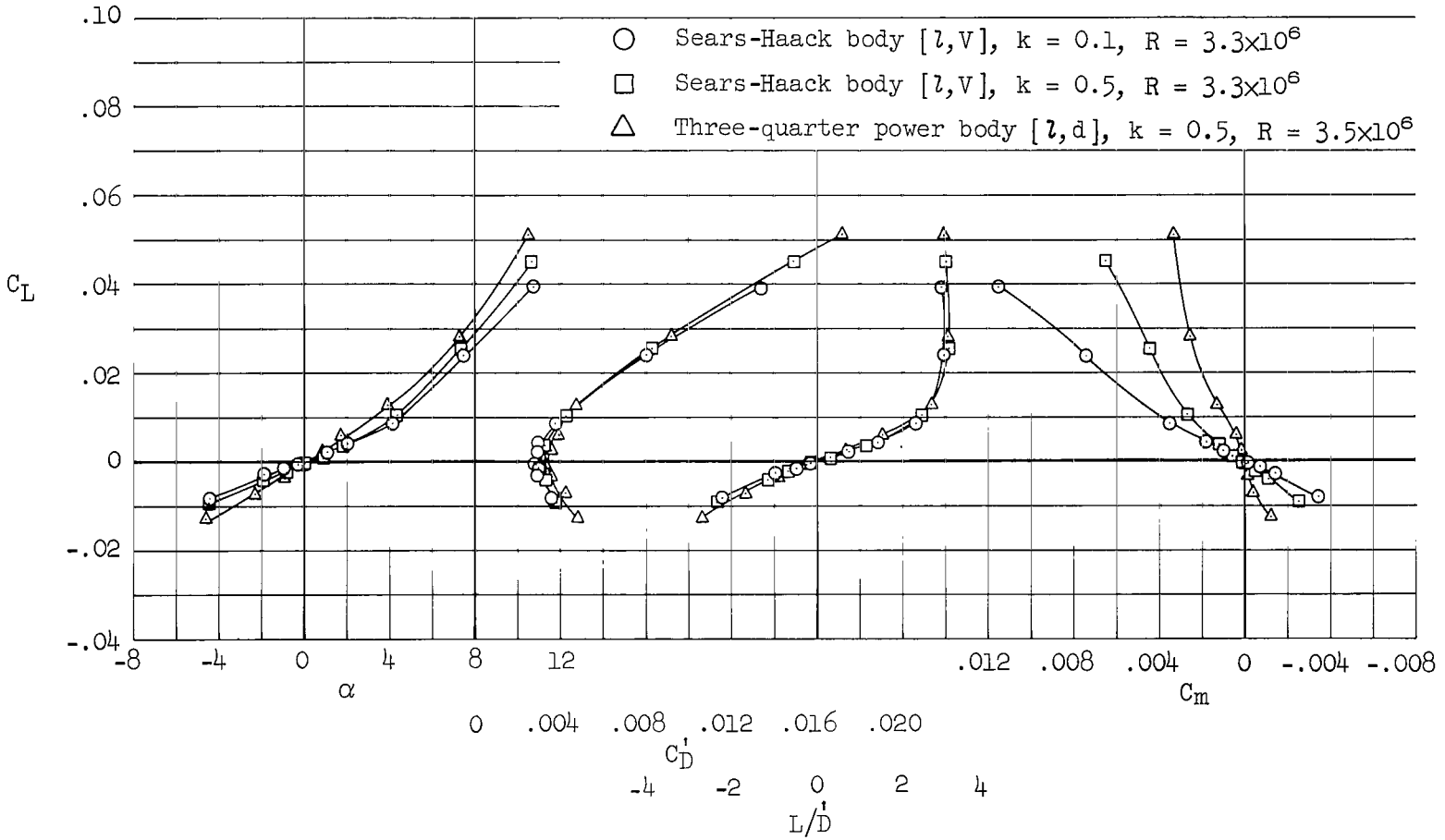

(c) M = 10.5; laminar boundary-layer flow over base of models

Figure 16.- Concluded.

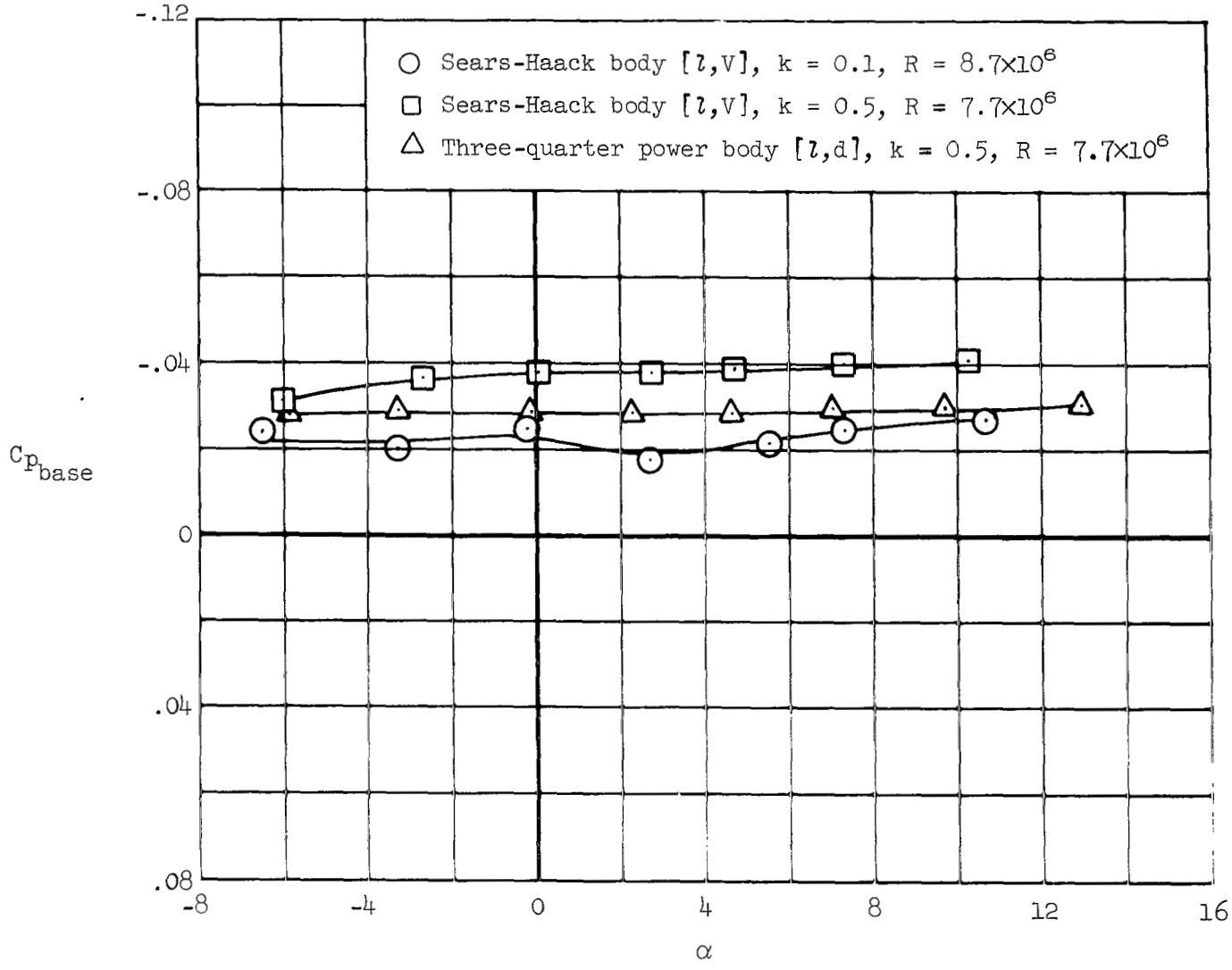

(a) M = 5.4; turbulent boundary-layer flow over base of models

Figure 17.- Experimental base-pressure coefficients for the selected bodies from tests in the Ames 3.5-Foot Hypersonic Wind Tunnel.

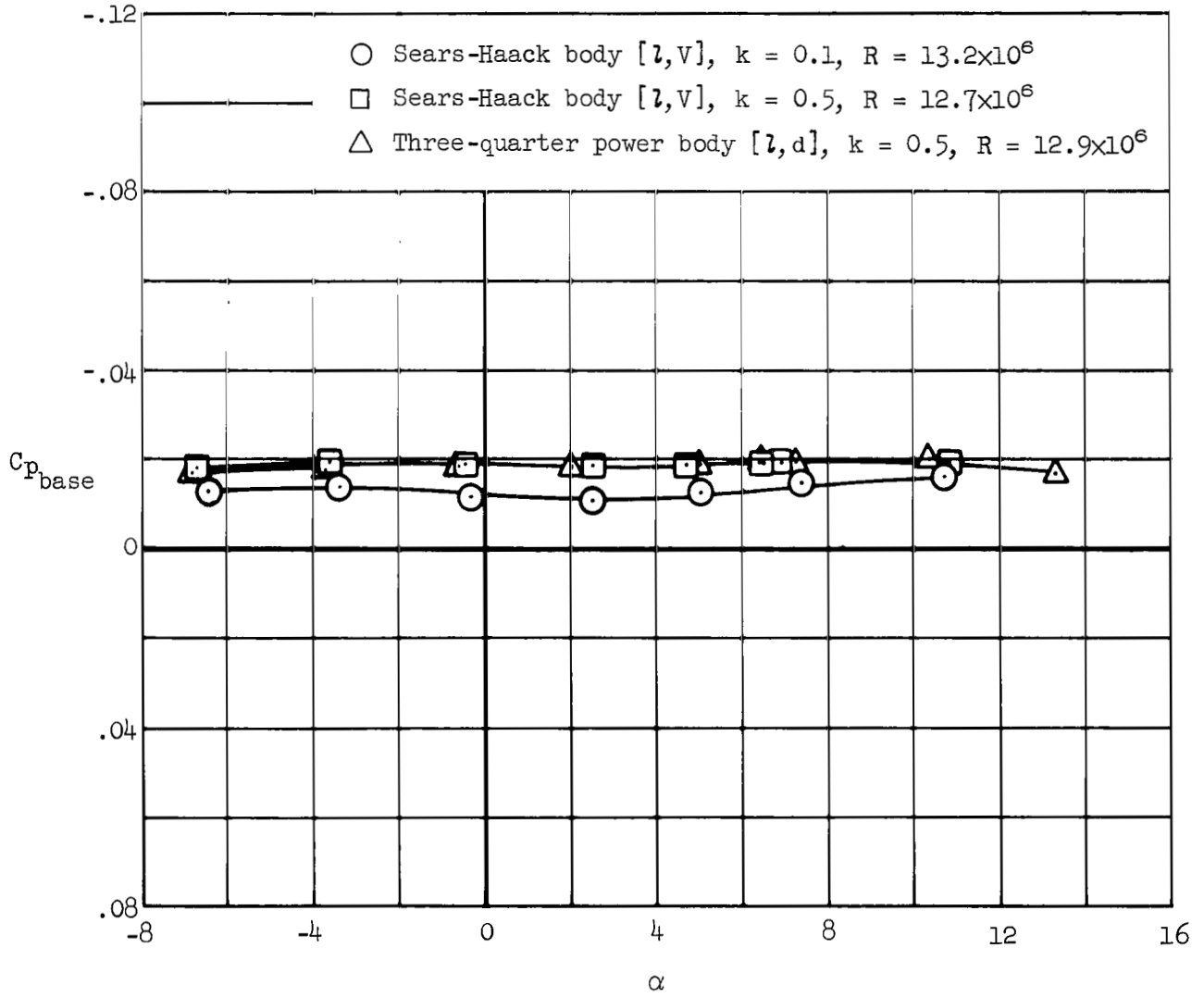

(b) M = 7.4; turbulent boundary-layer flow over base of models

Figure 17.- Continued.

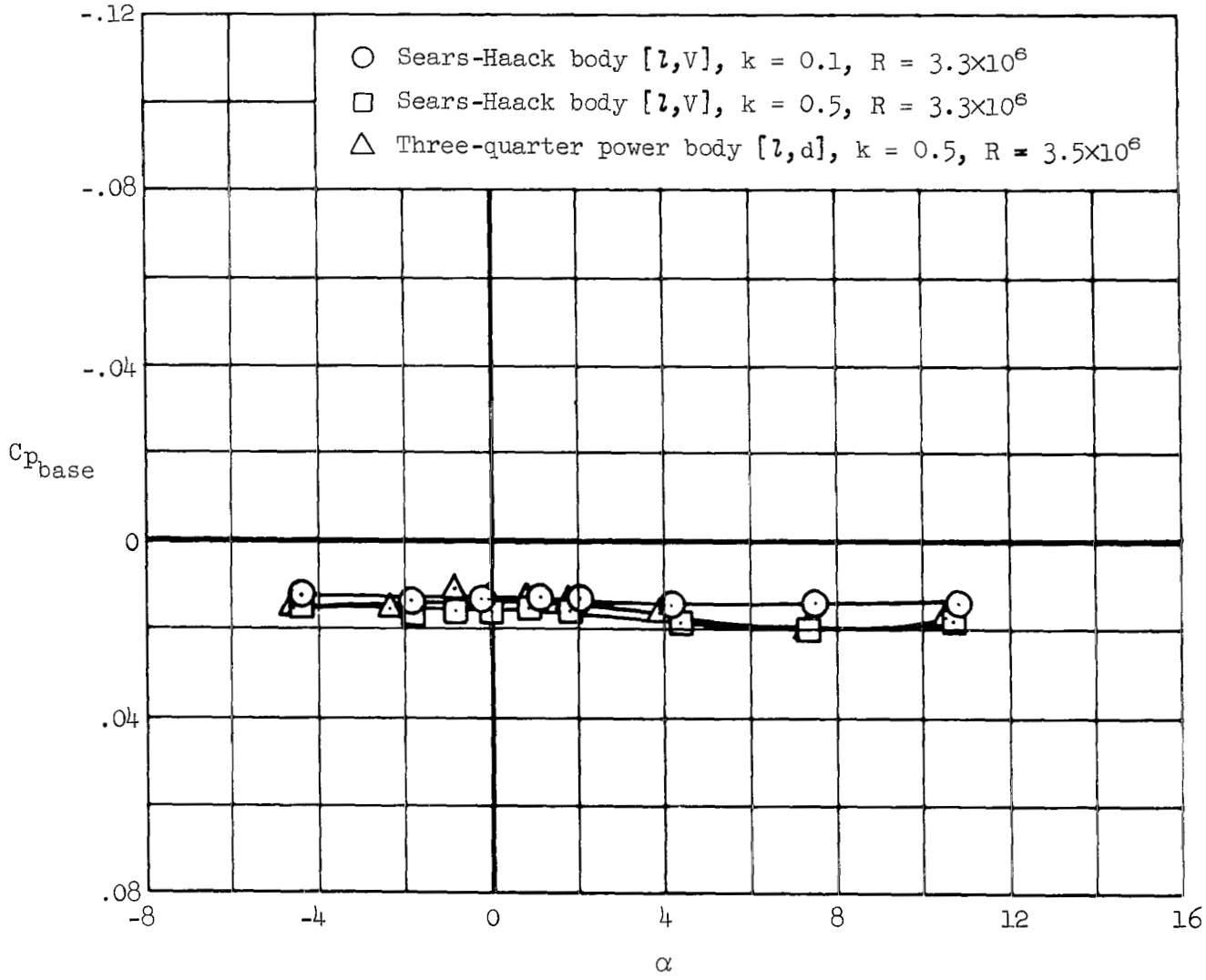

(c) M = 10.5; laminar boundary-layer flow over base of models

Figure 17.- Concluded.

"The aeronautical and space activities of the United States shall be conducted so as to contribute . . . to the expansion of human knowledge of phenomena in the atmosphere and space. The Administration shall provide for the widest practicable and appropriate dissemination of information concerning its activities and the results thereof."

—NATIONAL AERONAUTICS AND SPACE ACT OF 1958

NASA SCIENTIFIC AND TECHNICAL PUBLICATIONS

TECHNICAL REPORTS: Scientific and technical information considered important, complete, and a lasting contribution to existing knowledge.

TECHNICAL NOTES: Information less broad in scope but nevertheless of importance as a contribution to existing knowledge.

TECHNICAL MEMORANDUMS: Information receiving limited distribution because of preliminary data, security classification, or other reasons.

CONTRACTOR REPORTS: Scientific and technical information generated under a NASA contract or grant and considered an important contribution to existing knowledge.

TECHNICAL TRANSLATIONS: Information published in a foreign language considered to merit NASA distribution in English.

SPECIAL PUBLICATIONS: Information derived from or of value to NASA activities. Publications include conference proceedings, monographs, data compilations, handbooks, sourcebooks, and special bibliographies.

TECHNOLOGY UTILIZATION PUBLICATIONS: Information on technology used by NASA that may be of particular interest in commercial and other non-aerospace applications. Publications include Tech Briefs, Technology Utilization Reports and Technology Surveys.

Details on the availability of these publications may be obtained from:

SCIENTIFIC AND TECHNICAL INFORMATION OFFICE

NATIONAL AERONAUTICS AND SPACE ADMINISTRATION

Washington, D.C. 20546